

The role of calcium signaling in plants: from Arabidopsis to barley

Dissertation

zur Erlangung des Doktorgrades (Dr. rer. nat.)

der

Mathematisch-Naturwissenschaftlichen Fakultät

der

Rheinischen Friedrich-Wilhelms-Universität Bonn

vorgelegt von

Maya Giridhar

aus

Bangalore, Indien

Bonn, 2021

Angefertigt mit Genehmigung der Mathematisch-Naturwissenschaftlichen
Fakultät der Rheinischen Friedrich-Wilhelms-Universität Bonn

Gutachter/in: 1. Prof. Dr. Ute C. Vothknecht
 2. Prof. Dr. Andreas Meyer
 3. Prof. Dr. Jörg Höfeld
 4. Prof. Dr. Ian C. Brock

Tag der Promotion: 07.10.2021

Erscheinungsjahr: 2021

Contents

Contents	2
List of figures	6
List of tables.....	8
Abbreviations	9
1. Introduction.....	10
1.1 Abiotic stress induced Ca ²⁺ measurement in plants.....	11
1.1.1 Salinity stress and Ca ²⁺ signaling	11
1.1.2 Oxidative stress and Ca ²⁺ signaling	13
1.2 The source of Ca ²⁺ in abiotic stress response	14
1.3 Barley as a model crop for Ca ²⁺ signaling	16
1.4 Calcium signaling in plant mitochondria.....	17
1.5 Aim of this work	21
2.1 Materials	22
2.1.1 Chemicals.....	22
2.1.2 Buffers, enzymes and kits	23
2.1.3 Plasmid DNA vectors	24
2.1.4 Constructs	24
2.1.5 Bacterial strains.....	25
2.1.6 T-DNA insertion lines.....	25
2.1.7 Primers	25
2.1.8 Antibodies	27
2.2 Methods.....	28
2.2.1 Molecular and cell biological methods	28
2.2.1.1 Plant material and growth conditions	28

2.2.1.2 Luminescence imaging of aequorin	28
2.2.1.3 Ca ²⁺ measurements in barley and Arabidopsis	29
2.2.1.4 Sample preparation for RNA isolation and sequencing.....	30
2.2.1.5 Polymerase chain reaction	31
2.2.1.6 Cloning strategy	32
2.2.1.7 Isolation of genomic DNA from Arabidopsis.....	32
2.2.1.8 Self-assembly GFP (saGFP) assay.....	33
2.2.2 Biochemical methods.....	33
2.2.2.1 Isolation of mitochondria and mitoplast	33
2.2.2.2 Expression and purification of recombinant proteins	34
2.2.2.3 SDS-PAGE and western blot analysis	34
2.2.2.4 Blue Native PAGE.....	35
2.2.2.5 Affinity chromatography on CaM-agarose.....	35
2.2.3 Bioinformatics.....	36
3. Results.....	38
3.1 Ca ²⁺ signaling in barley	38
3.1.1 Ca ²⁺ response measured in the whole seedlings of barley-Aeq.....	39
3.1.1.1 Measurements using a Photek system.....	39
3.1.1.2 Measurements using a luminometer	41
3.1.2 NaCl induced Ca ²⁺ response	42
3.1.2.1 Ca ²⁺ response to different NaCl concentrations.....	43
3.1.2.2 NaCl induced Ca ²⁺ response in five, seven, and eleven- days-old barley leaf	44
3.1.2.3 Ca ²⁺ response after pre-treatment with Ca ²⁺ channels and Ca ²⁺ -ATPases inhibitors	45
3.1.3 H ₂ O ₂ induced Ca ²⁺ responses	47

3.1.3.1 Ca ²⁺ response to different H ₂ O ₂ concentrations.....	47
3.1.3.2. H ₂ O ₂ induced Ca ²⁺ response in five, seven, and eleven- days-old barley leaf	48
3.1.3.3 Ca ²⁺ response after pre-treatment with Ca ²⁺ channels and Ca ²⁺ -ATPases inhibitors	50
3.1.4 Barley transcriptome analysis upon oxidative stress	52
3.2 Analysis of RISP in Arabidopsis	55
3.2.1 Sequence analysis of RISP1 and RISP2	55
3.2.2 Production of specific antibody against RISP	58
3.2.3 RISP2 is a CaM-binding protein.....	59
3.2.4 Topology of RISP	60
3.2.4.1 Localization of the C-terminus of RISP2.....	61
3.2.4.2 Localization of the N-terminus of RISP2	62
3.2.5 Mitochondrial complex analysis in wild type and <i>risp2</i> knockout.....	64
4. Discussion.....	65
4.1 Ca ²⁺ signaling in barley	65
4.1.1 Functionality of the barley-Aeq line	65
4.1.2 NaCl induced Ca ²⁺ response	67
4.1.3 H ₂ O ₂ induced Ca ²⁺ response	69
4.1.4 RNA-Seq analysis	70
4.2 Analysis of RISP in Arabidopsis	72
5. Summary.....	77
Zusammenfassung.....	78
Appendices.....	79
Appendix I: Protein sequences of RISP subjected to MSA.....	79
Appendix II: Transmembrane domain prediction of RISP1	82

Appendix III: Transmembrane domain prediction of RISP2..... 83

Appendix IV: Sequence alignment between chloroplast and mitochondrial RISP 84

References..... 85

Acknowledgment 99

Scientific Publications 100

List of figures

Figure 1. Phenotype and expression of Apoaequorin in the barley wild type and barley-Aeq lines	38
Figure 2. Aequorin-based luminescence in barley-Aeq in response to H ₂ O treatment measured in the Photek.....	40
Figure 3. Aequorin-based luminescence in barley-Aeq in response to NaCl and H ₂ O ₂ treatment measured in the Photek	41
Figure 4. Aequorin-based luminescence in barley-Aeq and Arabidopsis-Aeq in response to NaCl and H ₂ O ₂ treatment measured in the luminometer	42
Figure 5. Aequorin-based luminescence in barley-Aeq and Arabidopsis-Aeq measured in response to NaCl treatment in the luminometer	43
Figure 6. Aequorin-based luminescence in different ages and sections of the barley-Aeq leaf in response to NaCl treatment measured in the luminometer	44
Figure 7. Effect of the inhibitor LaCl ₃ on the NaCl induced [Ca ²⁺] _{cyt} measured in the luminometer	45
Figure 8. Effect of the inhibitor Thapsigargin on the NaCl induced [Ca ²⁺] _{cyt} measured in the luminometer	46
Figure 9. Effect of the inhibitor combination of LaCl ₃ and Thapsigargin on the NaCl induced [Ca ²⁺] _{cyt} signature measured in the luminometer.....	47
Figure 10. Aequorin-based luminescence in barley-Aeq and Arabidopsis-Aeq tissues measured in response to H ₂ O ₂ treatment in the luminometer	48
Figure 11. Aequorin-based luminescence in different ages and sections of the barley-Aeq leaf in response to H ₂ O ₂ treatment measured in the luminometer	49
Figure 12. Effect of the inhibitor LaCl ₃ on the H ₂ O ₂ induced [Ca ²⁺] _{cyt} signature measured in the luminometer	50
Figure 13. Effect of the inhibitor Thapsigargin on the H ₂ O ₂ induced [Ca ²⁺] _{cyt} signature measured in the luminometer	51
Figure 14. Effect of the inhibitor combination of LaCl ₃ and Thapsigargin on the H ₂ O ₂ induced [Ca ²⁺] _{cyt} signature measured in the luminometer.....	51

Figure 15. Venn diagram describing overlaps among differentially expressed genes (DEGs) in the shoots of barley upon different treatments.....	52
Figure 16. Venn diagram describing overlaps among differentially expressed genes (DEGs) in the roots of barley upon different treatments	54
Figure 17. Gene assembly and protein sequence alignment of RISP1 and RISP2	56
Figure 18. Alignment of the amino acid sequence of RISP from different organisms.....	57
Figure 19. Analysis of the RISP2 CaM-binding domain	58
Figure 20. Immunodetection of wild type and <i>risp2 ko</i> mitochondrial extracts	59
Figure 21. CaM-agarose affinity chromatography of Arabidopsis mitochondrial proteins.....	60
Figure 22. Topology model of RISP2.....	61
Figure 23. Analysis of the localization of C-terminus of RISP2	62
Figure 24. Immunodetection-based localization of the N-terminus of RISP.....	63
Figure 25. BN-PAGE analysis of mitochondria isolated from wild type and <i>risp2 ko</i> #19	64

List of tables

Table 1: List of special chemicals used in this study.	22
Table 2: List of Buffers, enzymes, and kits used in this study.....	23
Table 3: List of Vectors used in this study.....	24
Table 4: List of constructs used in this study.....	24
Table 5: List of bacterial strains used in this study.....	25
Table 6: List of T-DNA insertion mutant lines used in this study.....	25
Table 7: List of primers used in this study.....	25
Table 8: Table indicating the four different treatments that were applied to the shoots and roots of five-days-old barely.....	30
Table 9: Components of a PCR reaction.....	31
Table 10: Optimized PCR settings.....	31
Table 11: Summary of differentially expressed genes in barley shoots.	53
Table 12: Summary of differentially expressed genes in barley roots.....	54

Abbreviations

°C	Degree Celsius	GFP	Green fluorescent protein
μ	Micro	H ₂ O ₂	Hydrogen peroxide
AAs	Amino acids	Kb	Kilobase
BN	Blue native	kDa	Kilo dalton
[Ca ²⁺] _{cyt}	Cytosolic Ca ²⁺ concentration	LaCl ₃	Lanthanum chloride
CaM	Calmodulin	M	Molar
CML	Calmodulin like protein	MS	Murashige–Skoog–Medium
CPK	Calcium dependent protein kinase	NaCl	Sodium chloride
CBL	Calcineurin B like protein	PAGE	Poly acrylamide gel electrophoresis
H ₂ O	Water	PVDF	Poly vinyliden fluorine
DEGs	Differentially expressed genes	RISP	Rieske iron sulphur protein
dNTP	Deoxynucleotides	saGFP	Self-assembly GFP
EDTA	Ethylenediaminetetraacetic acid	SDS	Sodium dodecyl sulfate
EF	Elongation factor	SE	Standard Error
EGTA	Ethylene glycol tetraacetic acid	Tpg	Thapsigargin
		T-DNA	Transfer DNA used for insertional mutagenesis

1. Introduction

The environment we live in is perpetually faced by various ecological processes, natural disasters, and human and animal interferences. Plants being sessile organisms, adapt to such changes in the environment via certain signal transduction pathways. One of the first response mechanisms involves the detection of external stimuli by the cellular receptors followed by rapid and transient increases in cytosolic Ca^{2+} concentration (McAinsh & Hetherington, 1998). It has been discovered that temporally and spatially determined shifts in cytosolic or organellar Ca^{2+} concentration occur at some point in several biological processes within the cell (Dodd et al., 2010; Kudla et al., 2010; Stael et al., 2012). Calcium ions act as an important intracellular secondary messenger (Rudd & Franklin-Tong, 1999) which activate various signaling networks, that comprise a set of Ca^{2+} sensor proteins such as Calmodulin (CaM), CaM-like proteins (CML), Calcineurin B-like proteins (CBL), and Calcium-dependent protein kinases (CDPK) (DeFalco et al., 2010). However, not many studies have revealed the exact role Ca^{2+} plays in these processes.

After the initial identification of stimulus-specific changes in the cytosolic calcium concentration ($[\text{Ca}^{2+}]_{\text{cyt}}$) (Fricker et al., 1991), a growing number of processes involving Ca^{2+} signaling have been identified such as plant growth, including cell division and organ formation (Zhang et al., 2014). A wider range of downstream responses that these Ca^{2+} signals control have been described in other studies as well (Batistič & Kudla, 2012; McAinsh & Hetherington, 1998). The significance of decoding Ca^{2+} signals has grown in value, and several families of Ca^{2+} sensing proteins have been described and characterized (Hashimoto & Kudla, 2011). These findings led to the development of the “ Ca^{2+} signature” principle, which states that Ca^{2+} transients caused by different stimuli reflect stimulus-specific patterns. Ca^{2+} signatures are generated as a result of the combined action of Ca^{2+} influx through Ca^{2+} channels and active energy-dependent Ca^{2+} efflux via Ca^{2+} transporters. Previous studies have already established Ca^{2+} signatures in plants such as *Arabidopsis thaliana* (Knight et al., 1991), *Nicotiana tabacum* (Manzoor et al., 2012), and, more recently in *Oryza sativa* (Zhang et al., 2015). In the next section, the monitoring of these Ca^{2+} signals and the stimulus-specific changes in these signals have been revealed.

1.1 Abiotic stress induced Ca^{2+} measurement in plants

Osmotic pressure at the cell membrane rises in response to environmental stresses such as drought, salinity, temperature change, etc., and this rise is transmitted to signal receptors present on the membrane (Boudsocq & Laurière, 2005). Ca^{2+} influx occurs when the Ca^{2+} channels are triggered by a series of phosphorylation reactions and subsequently causing an increase in the Ca^{2+} concentration (Chinnusamy et al., 2004). The release of Ca^{2+} from intracellular Ca^{2+} storage sites including the endoplasmic reticulum (ER) and vacuoles is a source of rapidly increasing $[\text{Ca}^{2+}]$. The elevated $[\text{Ca}^{2+}]$ and its stimulus-specific patterns (Ca^{2+} signatures) can be measured by using different means such as non-ratio metric Ca^{2+} dyes (fluo, rhod and Calcium Green-1) or genetically encoded Ca^{2+} sensors like aequorin.

The Ca^{2+} binding protein aequorin is isolated from the luminescent jellyfish (*Aequorea victoria*). In the presence of coelenterazine, a luciferin, and oxygen the apoaequorin (an inactive form of aequorin) reassembles to form the holoprotein aequorin. Aequorin contains three EF-hand Ca^{2+} -binding sites which can then bind to free Ca^{2+} when exposed to it (Deng et al., 2005). At this point aequorin changes its conformation and acts as an oxygenase, converting coelenterazine into its excited form coelenteramide, which is then released with carbon dioxide. A blue light ($\lambda = 469 \text{ nm}$) is released as the excited coelenteramide relaxes to its ground state which can then be detected by a luminometer. The emitted light which is expressed as RLU (Relative Luminescence Units) can be calibrated into Ca^{2+} concentrations by a method based on the calibration curve of Allen and co-workers (Allen & Prendergast, 1977). Changes in plant $[\text{Ca}^{2+}]_{\text{cyt}}$ are observed in many different cell types in response to abiotic stimuli such as salt and drought stress (Knight et al., 1998; Ranf et al., 2008), oxidative stress (Evans et al., 2005), and even cold stress (Knight et al., 1996; Knight et al., 1991). In this work, focus was put on two of the most commonly studied abiotic stresses namely salt stress and oxidative stress.

1.1.1 Salinity stress and Ca^{2+} signaling

Salinity is a major global issue that has a negative impact on crop productivity by affecting plant growth and development. All types of soil contain salts, and all irrigation waters, whether from

canals or underground pumping, also contain some form of dissolved salts (Shanker & Venkateswarlu, 2011). This combined with poor drainage causes the most severe damage in productive agricultural land (Zhu, 2007). The most detrimental effects of salinity stress in the roots are the cytotoxicity from excessive uptake of sodium (Na^+) and chloride (Cl^-) ions and damage to the water uptake capacity. High concentrations of salts within the plant itself can be toxic, resulting in nutritional imbalance (Hasegawa et al., 2000). Salt stress causes mainly three types of stress within the plant, osmotic stress, ionic stress, and oxidative stress. During osmotic stress, the salt concentration in the roots starts to increase making it harder for the roots to extract water resulting in the failure of shoot growth. Both roots and shoots change their osmotic pressure to maintain water absorption and cell turgor, enabling physiological processes including stomatal opening, photosynthesis, and cell expansion to take place (Serraj & Sinclair, 2002). Ionic stress is caused due to the increasing accumulation of Na^+ and Cl^- and can result in the premature senescence of adult leaves and, as a result, a reduction in the photosynthetic area available to sustain continued development (Cramer & Nowak, 1992). Due to abnormalities in the electron transport chain, the level of ROS in plant tissues rises under salinity stress causing oxidative stress (AbdElgawad et al., 2016). More about oxidative stress has been described in section 1.4.

High Na^+ levels compete with the absorption of K^+ ions, which is essential for growth and development, resulting in lower productivity and possibly death (James et al., 2011). In Arabidopsis roots, the high-affinity K^+ transporter Type (HKT) is involved in the long-distance transport of Na^+ through the xylem and phloem (Assaha et al., 2017). Monocots have several HKT isoforms, unlike Arabidopsis, which only has the subclass 1, Na^+ selective, AtHKT1 isoform (Berthomieu et al., 2003; Horie et al., 2005). In barley, overexpression of HvHKT2;1 induces Na^+ uptake under salt stress conditions (Mian et al., 2011). Cl^- which is a vital nutrient for plants (Chen et al., 2010), is thought to be transported into the cell through an H^+/Cl^- symport, but the molecular origin of this symport remains unclear. H^+/Cl^- co-transporter Nitrate transporter (NRT) may be involved in Cl^- entry to root cells via the plasma membrane (Teakle & Tyerman, 2010). The Cation-chloride co-transporters (CCCs) are another type of possible Cl^- transporters. AtCCC has been extensively studied in Arabidopsis indicating that it is expressed in root and shoot tissues and is most likely involved in organized K^+ , Na^+ , and Cl^- symport (Colmenero-Flores et al., 2007; Zhang et al., 2010). The usage of mutants should help in understanding the progress regarding Cl^- uptake in plants.

Previous studies already suggest that Ca^{2+} signaling during salt stress represents a rather complex phenomenon (Manishankar et al., 2018). Plants show a rapid increase in $[\text{Ca}^{2+}]_{\text{cyt}}$ within seconds of being treated with NaCl or mannitol (Knight et al., 1997). Furthermore, administration of NaCl to certain areas of Arabidopsis roots was found to produce an initial regionally confined Ca^{2+} signal, which after a few seconds then extended in a wave-like way throughout the root and the entire plant (Choi et al., 2014). CML9 which is a member of the calmodulin-like (CML) gene family, was found to be upregulated during salt stress, and *cml9* loss-of-function mutants showed hypersensitivity in germination assays on a medium containing either NaCl or ABA, whereas adult *cml9* plants showed increased tolerance to irrigation with salt water (Magnan et al., 2008). During the early response to salt stress in rice, SALT-RESPONSIVE ERF1 (SERF1) is thought to act as a key hub to regulate ROS-dependent signaling (Schmidt et al., 2013). In Arabidopsis, Respiratory Burst Oxidase Homolog F (RBOHF), which is an NADPH oxidase that catalyzes ROS production, was found to be required for shoot sodium homeostasis during salt stress (Jiang et al., 2013). Later it was also shown that the RBOHF-dependent salinity-induced ROS accumulation is regulated by protein phosphorylation in a Ca^{2+} -dependent manner (Drerup et al., 2013). More importantly, this study also showed that the NaCl-gated Ca^{2+} channels and H_2O_2 -gated Ca^{2+} channels might be different.

1.1.2 Oxidative stress and Ca^{2+} signaling

In addition to ionic stress, oxidative stress is commonly associated with salinity due to the production of reactive oxygen species (ROS). As a result, studying the link between NaCl, H_2O_2 , and Ca^{2+} in the salt-stress signaling cascade is very appealing. Antioxidative mechanisms normally scavenge ROS quickly, but salt stress can impede this process (Allan & Fluhr, 1997). Oxidative stress is a dynamic chemical and physiological process that occurs in higher plants either directly through ozone emissions or indirectly by biotic and abiotic stresses. It is caused by excessive production and accumulation of ROS levels leading to the generation of superoxide anion ($\text{O}_2^{\cdot-}$), hydrogen peroxide (H_2O_2), and hydroxyl radical (OH^{\cdot}). The electron transport chains (ETC) in the chloroplasts and mitochondria can produce ROS in plants (Møller, 2001; Takahashi & Badger, 2011). During plant growth and in response to stress, membrane-localized NADPH oxidases are also known as ROS producers (Marino et al., 2012). Plants have developed a variety of enzymatic

and non-enzymatic strategies to hunt free ROS in cells to cope with oxidative stress. The enzymatic strategy includes ROS-scavenging molecules such as superoxide dismutase (SOD), ascorbate peroxidase (APX), and catalase (CAT) (Apel & Hirt, 2004). The non-enzymatic strategy includes compounds such as ascorbic acid (AsA), proline, glutathione (GSH), etc. (Ahmad et al., 2010). These processes are well-known today and have been thoroughly examined (Sharma et al., 2012). However, the signaling events caused by oxidative stress led to the deployment of defenses against it that are poorly understood in plants.

The activation of Ca^{2+} -permeable channels in Arabidopsis guard cells was shown in response to ROS treatment (Pei et al., 2000). They also showed that H_2O_2 application stimulated a Ca^{2+} influx through a hyperpolarization-activated Ca^{2+} -permeable channel, followed by partial stomatal closure. Low concentrations of superoxide and H_2O_2 caused rapid increases in $[\text{Ca}^{2+}]_{\text{cyt}}$ in *Commelina communis* guard cells, as measured by changes in Fura-2 fluorescence (McAinsh et al., 1996). In *Nicotiana tabacum* seedlings (tobacco) expressing recombinant aequorin, H_2O_2 induced a rapid but transient increase in $[\text{Ca}^{2+}]_{\text{cyt}}$, which was inhibited by lanthanum chloride (Price et al., 1994). Arabidopsis seedlings, exposed to H_2O_2 caused a biphasic increase in Ca^{2+} where the initial Ca^{2+} peak occurred in the cotyledons, while the late Ca^{2+} rise occurred only in the root and not in the shoot (Rentel & Knight, 2004).

1.2 The source of Ca^{2+} in abiotic stress response

To further investigate the source of Ca^{2+} in NaCl and H_2O_2 induced Ca^{2+} responses certain inhibitors of the Ca^{2+} transients were used that can inhibit Ca^{2+} -dependent activities by engaging with binding sites inside the Ca^{2+} channels or by stimulating Ca^{2+} -ATPases thereby inhibiting the elevation of $[\text{Ca}^{2+}]$. In this work, two inhibitors were used to block the Ca^{2+} transients such as lanthanum chloride (LaCl_3) which is used to block Ca^{2+} channels (Tracy et al., 2008), and thapsigargin to block the intracellular Ca^{2+} stores in ER/Golgi (Treiman et al., 1998). To avoid its harmful influence on cellular energy metabolism, the resting concentration of free $[\text{Ca}^{2+}]_{\text{cyt}}$ is normally maintained at a sub-micromolar range between 50 and 100 nM (Logan & Knight, 2003). A regulated entrance of Ca^{2+} from external and internal reserves into the cytosol is elicited by a wide range of biotic and abiotic stressors, as well as various developmental processes, resulting in

increases in $[Ca^{2+}]_{cyt}$. The Ca^{2+} channels between the Ca^{2+} stores and the cytoplasm open upon signaling and enable Ca^{2+} to travel down its electrochemical gradient. This activity is important for the role of $[Ca^{2+}]_{cyt}$ as a secondary messenger. La^{3+} can inhibit various Ca^{2+} -dependent processes in plant and animal systems by interacting with binding sites within Ca^{2+} channels or stimulating Ca^{2+} -ATPases, hence preventing the elevation of $[Ca^{2+}]_{cyt}$ (Belyavskaya, 1996; Bush, 1995). Because of its high positive charges, $LaCl_3$ is thought to not pass through the plasma membrane (Evans, 2013). As a result, $LaCl_3$ can prevent calcium from entering the cell via the plasma membrane. In Arabidopsis, the first increase in Ca^{2+} in response to H_2O_2 treatment was strongly inhibited by incubation with $LaCl_3$ (Rentel & Knight, 2004). One study in rice suggested that H_2O_2 can induce a $[Ca^{2+}]$ increase via different channels, and some of these channels are insensitive to $LaCl_3$ (Zhang et al., 2015). The same study also reported that $LaCl_3$ nearly inhibited most of the $[Ca^{2+}]$ increase in response to NaCl.

The significance of the ER as a Ca^{2+} storage compartment in animals has long been recognized, with free Ca^{2+} concentrations ranging between 50 and 500 nM (Raffaello et al., 2016). On the other hand, the storage properties of the ER in plants and its role in the Ca^{2+} signaling network, are poorly understood, and exact data on $[Ca^{2+}]_{ER}$ is still lacking (Iwano et al., 2009). Some studies have even suggested that the cytosolic $[Ca^{2+}]$ increase is followed by an increase in the $[Ca^{2+}]_{ER}$ (Bonza et al., 2013). Resting free $[Ca^{2+}]_{Golgi}$ was estimated to be about 700 nM using Golgi-targeted aequorin and transitory variations in $[Ca^{2+}]_{Golgi}$ were detected in response to abiotic stimuli and an auxin analog (Ordenes et al., 2012). In mammalian and yeast cells, thapsigargin acts as an inhibitor of the sarcoendoplasmic reticulum (SR) calcium transport ATPase (SERCA) (Sorin et al., 1997; Treiman et al., 1998). Plant Ca^{2+} -ATPases have been shown to have differential sensitivity to thapsigargin. This might be because thapsigargin is derived from the root of *Thapsia garganica* and therefore could be insensitive to the plant Ca^{2+} -ATPases (Liang & Sze, 1998). The presence of a thapsigargin-sensitive Ca^{2+} uptake in cauliflower (*Brassica oleracea*) and peas (*Pisum sativum*) were identified in the Golgi fractions but not in the ER vesicles (Ordenes et al., 2002). Nevertheless, the TcSCA, which is a Ca^{2+} -pump from *Trypanosoma cruzi*, is also unaffected by thapsigargin (Furuya et al., 2001). The $[Ca^{2+}]$ increase induced by NaCl in rice was substantially inhibited by thapsigargin, suggesting that ER is involved in the $[Ca^{2+}]$ increase induced by NaCl (Zhang et al., 2015). Astonishingly, the same study also showed that thapsigargin had no impact on the $[Ca^{2+}]$ increase caused by H_2O_2 .

1.3 Barley as a model crop for Ca²⁺ signaling

Barley (*Hordeum vulgare*) is the fourth most important cereal crop in the world. It is a self-pollinating monocot, with 14 chromosomes ($2n=14$) (Søgaard & von Wettstein-Knowles, 1987). The Golden promise cultivar of barley is a spring variety created by gamma-ray irradiation (Forster, 2001) and is mainly used for malting. This variant is known to have exceptional salinity tolerance when compared to other cereal crops. Some of the salt-tolerant genotypes can sequester Na⁺ in the vacuoles, allowing them to maintain high K⁺/Na⁺ levels in the cytosol while reducing Na⁺ toxicity damage (Fu et al., 2018). Another explanation for the salinity tolerance is that some genotypes have halophytic characteristics, such as removing Na⁺ from uptake (Chen et al., 2007) and accumulating Na⁺ in tissues (Munns et al., 1988). Several genes that have enhanced salinity tolerance have also been shown (Mwando et al., 2020). Many studies have aimed in providing an insight into different abiotic (Gürel et al., 2016; Kosová et al., 2014) and biotic stress responses in barley (Hura, 2020; Kong et al., 2020). One such study has even identified a gene encoding the calcium-dependent protein kinase HvCPK2a that was significantly upregulated in response to drought (Cieśła et al., 2016). However, not much is known about the downstream processes involved in the stress response in barley.

Plant survival in harsh environments necessitates a significant shift in metabolism, which can be seen extensively via transcriptome analysis. Some of the most interesting results from transcriptome analysis have been mentioned here. While barley and rice are both members of the Poaceae family, their tolerance to salt stress differs. Transcriptome analysis of both barley and rice revealed that genetic alteration of early salt-responsive genes may contribute to the creation of the salt tolerance trait in rice (Ueda et al., 2006). Yan66, which is a metal tolerant genotype, and Ea52 a metal sensitive genotype of barley was subjected to cobalt and copper treatments individually and in a combination. The RNA-Seq analysis revealed several commonly expressed genes in both the genotypes upon both the treatments (wa Lwalaba et al., 2021). A transcriptome-wide approach for Boron tolerance in barley revealed 17% of the transcripts differentially regulated in root and leaf tissues. Surprisingly, certain Ca²⁺ - calmodulin systems were also activated in response to Boron treatment (Tombuloglu et al., 2015). Similarly, high temperature (Mangelsen et al., 2011) and low temperature (Svensson et al., 2006) revealed interesting changes in the gene expressions

of barley. More recently, another study used RNA-Seq to reveal specific genes and their role in building a drought-tolerant barley genotype (Janiak et al., 2018).

1.4 Calcium signaling in plant mitochondria

Previous studies have revealed that plant mitochondria, chloroplasts, and nuclei exhibit calcium-dependent biological processes and evoke their specific Ca^{2+} signals (Xiong et al., 2006). Nevertheless, little is known about the Ca^{2+} signaling network in organelles such as chloroplast and mitochondria. The presence of Ca^{2+} in mitochondria was first detected by a study by Hodges and Hanson in 1965 which suggested that the addition of ATP or high-energy intermediates of oxidative phosphorylation partakes the uptake and accumulation of Ca^{2+} in the mitochondria of *Zea mays* (Hodges & Hanson, 1965). This resulted in further research into the physiological function of Ca^{2+} in the mitochondria of plants. One such study revealed that Ca^{2+} , along with the control of NADH, takes part in the regulation of the mitochondrial functions (Coleman & Palmer, 1971; Miller et al., 1970). It was also shown that the efflux of Ca^{2+} was stimulated by red light (Roux et al., 1981). Unlike the cytosol whose free resting Ca^{2+} concentration is 100 nM ($[\text{Ca}^{2+}]_{\text{cyt}}$), the $[\text{Ca}^{2+}]_{\text{m}}$ was found to be around 200 nM using transgenic plants in which the aequorin apoprotein was targeted to the mitochondria (Logan & Knight, 2003). In the mitochondria, it has also been reported that osmotic stress and extracellular ATP induce mitochondrial Ca^{2+} oscillations, which are different from cytosolic Ca^{2+} signals (Loro et al., 2012). All these studies further confirmed the presence of Ca^{2+} transporters in the mitochondria. While the inner mitochondrial membrane (IMM) needs specialized channels and transporters for Ca^{2+} fluxes, calcium can freely pass through the outer membrane (Csordás et al., 2012). Even as Ca^{2+} export activities have long been identified in the IMM, the protein(s) facilitating its export largely unresolved.

Even though the existence of Ca^{2+} transients in mitochondria indicates the need for Ca^{2+} sensor proteins that can identify these transients and convert them into a functional response, little is known about them. In eukaryotic organisms, CaMs and CMLs exist as a set of Ca^{2+} sensors and are a central part of the Ca^{2+} signaling pathway (Snedden & Fromm, 2001). Genome analysis of *Arabidopsis* revealed at least seven genes that encode CaMs and 50 genes that encode potential

Calmodulin-like proteins (CMLs) (Ranty et al., 2006). In contrast to CaMs, which always contain four EF-hand motifs, CMLs contain 1 - 6 EF-hands which might enable them to respond in different ways to Ca^{2+} signals (McCormack & Braam, 2003; McCormack et al., 2005). In the past years, mitochondrial pyruvate dehydrogenase activity and protein import in plants were found to be affected by calmodulin inhibitors (Kuhn et al., 2009; Miernyk & Randall, 1987). Furthermore, Ca^{2+} /CaM has been described to promote the import of mitochondrial proteins at translocon on the inner mitochondrial membrane (TIM) through TIM22 and TIM23 (Kuhn et al., 2009). By binding to the TOM9 subunit, Ca^{2+} /CaM also affects the assembly of the translocon on the outer mitochondrial membrane (TOM) (Parvin et al., 2017). For most of the identified 50 CMLs, the localization and functions are still unknown. In a former work in our laboratory, CML30 (At2G15680) was shown to be localized in the mitochondria most likely in the intermembrane space (Chigri et al., 2012), Some preliminary results from our working group indicated that two CMLs, CML37 (At5g42380) and CML38 (At1g76650) are dual localized in the mitochondria matrix and cytosol (Bachelor thesis of Kathrin-Marie Pleßner, 2018 and Sandro Sieger, 2019). AtCML37 has already been shown to be a positive regulator of ABA accumulation that is induced by drought stress (Scholz et al., 2015). Not long ago evidence was found that AtCML38 functions as one of the core hypoxia-response proteins since it associates with cytosolic hypoxia-induced stress granules and to messenger RNA nucleoprotein (mRNP) particles that accumulate during flooding stress responses (Lokdarshi et al., 2016). In the Ph.D. thesis of Nargis Parvin, the Rieske iron-sulfur protein (RISP) was identified as a potential CaM binding protein and therefore required further investigation with regard to its CaM binding function.

RISP, which contains a 2Fe-2S cluster is a catalytic subunit of the *b₆f* and *bc₁* complex present in many photosynthetic and mitochondrial respiratory chains respectively (Schneider & Schmidt, 2005). In the photosynthetic electron transport chain located in the chloroplasts, RISP facilitates the transport of electrons between the membrane-enclosed heme group of Cyt *b₆* and the lumen-exposed Cyt *f* (Adam & Ostersetzer, 2001). The mitochondrial electron transport chain which contains the *bc₁* complex consists of three subunits: cytochrome *b*, cytochrome *c₁*, and Rieske iron-sulfur protein (RISP). The main function of this complex is the transfer of an electron from ubiquinol to cytochrome *c₁* to generate a proton electrochemical gradient required for ATP synthesis (Trumpower & Edwards, 1979). To better understand the function of this protein, it is important to study the topology of this protein. One of the earlier studies on RISP was performed

by Harnisch *et al.*, in 1985 where they first analyzed the primary structure of the iron-sulfur subunit in *Neurospora* (Harnisch *et al.*, 1985). Their results showed that the larger hydrophobic domain which carries the iron-sulfur cluster is exposed to the intermembrane space of the mitochondria leaving the smaller, hydrophilic, N- terminal domain exposed to the matrix. This agrees with the results published by Conte and Zara, 2011 showing that the C- terminal domain is in the intermembrane space of the mitochondria and the N-terminal domain is facing the matrix (Conte & Zara, 2011). The structure of the bovine mitochondrial RISP also was shown to exist in the same model, although it undergoes some conformational changes (Iwata *et al.*, 1998; Xia *et al.*, 1997). These results showed that RISP has only one transmembrane domain, however, the possibility of a second transmembrane domain might still be existential (Zhang *et al.*, 1998).

Complex III being the principal source of ROS production, inhibition of the cytochrome C results in increased ROS generation (Chen *et al.*, 2003). The overexpression of *Brassica campestris* RISP1 (*BcRISP1*) in Arabidopsis affected some of the genes in the mitochondrial respiratory chain and yielded lesser seeds (Liu *et al.*, 2014). In the same study, it was also shown that the mitochondrial ROS content was much higher in the *BcRISP1* than in the wild type as a result of the dysfunctional electron transport chain. In mice, RISP depletion resulted in increased ROS signaling in the mitochondrial intermembrane space and cytosol and nullified hypoxia-induced increases in Ca^{2+} (Waypa *et al.*, 2013). In the Ph.D. thesis of Nargis Parvin, RISP was identified as a potential CaM binding protein in mitochondria by CaM – agarose affinity chromatography of mitochondrial proteins. These CaM binding to RISP could play a role in Ca^{2+} and ROS signaling. However, the topology of RISP, specifically the position of the CaM binding site in plants is unclear. Therefore, it is important to further investigate the exact topology of RISP and its function. The mitochondrial RISP in higher plants is imported into the mitochondria after translation and cleavage of the transit peptide (Huang *et al.*, 1991). The same study also showed that two-thirds of the C-terminus of RISP, including the catalytic site, have the same function in yeast and plants. In contrast, the N-terminus is species-specific. In a very recent study, it was found that for the membrane insertion of RISP the plant mitochondrial Twin arginine translocation (TAT) pathway is required (Schäfer *et al.*, 2020). More interesting was the fact that the N terminus of RISP was shown to be facing the matrix side of the inner membrane; however, the orientation of the C terminus remains unknown. Also, in plants, the RISP protein exists in two homologs as RISP1 and RISP2, but it is not known, whether they play different roles or if they are just a gene duplication.

1.5 Aim of this work

Previously, many advances have been made in elucidating the Ca^{2+} signatures in response to various environmental stresses in Arabidopsis by establishing Ca^{2+} sensor lines. However, this had not been done in most of the crops including barley. Therefore, the main aim of this work was to analyze the Ca^{2+} signatures in response to salt and oxidative stress in different tissues of barley using the cytosol-targeted barley-Aeq line. The second aim was to elucidate the source of the Ca^{2+} through which these Ca^{2+} signatures are created. Another goal was to identify the downstream molecular mechanisms activated by the Ca^{2+} signal upon application of oxidative stress. To that end, RNA-Seq analysis of barley tissues was performed under different conditions to elucidate stress-induced transcriptomic changes. In a second project, the Calmodulin-binding ability, the topology, and the function of the mitochondrial RISP protein in Arabidopsis were investigated.

2.1 Materials

All chemicals used in this work were purchased from high-standard manufacturers having the highest purity available.

2.1.1 Chemicals

Table 1: List of special chemicals used in this study.

Name	Company
Lanthanum chloride	Sigma-Aldrich GmbH, Germany
Thapsigargin	Millipore, Germany
1-(4-Hydroxy-3,5-dimethoxyphenyl)ethan-1-one	Sigma-Aldrich GmbH, Germany
Calmodulin agarose	Sigma-Aldrich GmbH, Germany
1-Ethyl-3-[3-Dimethylaminopropyl]Carbodiimide	Pierce, Germany
Sulfo-N-Hydroxysulfosuccinimide (Sulfo-NHS)	
n-Dodecyl β -D-maltoside	Sigma-Aldrich GmbH, Germany
Oligonucleotides	Thermo Scientific, Germany
Coelenterazine	Carl Roth, Germany
Murashige and Skoog medium (MS) medium	Duchefa Biochemie, Netherlands

2.1.2 Buffers, enzymes and kits

Table 2: List of Buffers, enzymes, and kits used in this study.

Name	Company
NotI , ApaI, SapI	Thermo scientific, Germany
PstI	Fermentas, Germany
Buffer G	Thermo scientific, Germany
Buffer Tango	Thermo scientific, Germany
DNA polymerases	New England Biolabs, Germany
DNA restriction enzymes	Fermentas, Germany
Phusion polymerase	New England Biolabs, Germany
Taq polymerase	Genaxxon, Germany
T4 DNA ligase Kit (Buffer and ligase)	Thermo scientific, Germany
GeneRuler™1kb Plus DNA Ladder	Thermo scientific, Germany
Plasmid mini kit	Macherey-Nagel (Düren, Germany).
Gel/PCR Fragment Extraction Kits	Macherey-Nagel (Düren, Germany).
peqGOLD Protein-Marker I	Peqlab, Germany
PageRuler Prestained Protein Ladder Plus	Fermentas, Germany
Quick-RNA mini prep kit	Zygmo Research, Germany

2.1.3 Plasmid DNA vectors

Table 3: List of Vectors used in this study.

Vector	Feature	Company
pTwin1	Protein expression plasmid	Stratagene, USA
pBIN:saGFP 1-10	Plant transformation vector	Kind gift from Dr. Simon Lander Stael, University of Vienna
pBIN:saGFP 11		

2.1.4 Constructs

Table 4: List of constructs used in this study.

Construct	AGI code	Plasmid	Purpose	Author
RISP2: saGFP1-10C	At5g13440 CDS	pBIN-saGFP1-10C	Protein localization	This work
RISP2: saGFP11C	At5g13440 CDS	pBIN-saGFP11C	Protein localization	This work
RISP2 Fragment 1	At5g13440 CDS	pTWIN-RISP2 ₅₂₋₁₀₇	Protein overexpression	This work
RISP2 Fragment 2	At5g13440 CDS	pTWIN-RISP2 ₅₂₋₁₃₂	Protein overexpression	This work
RISP2 Fragment 3	At5g13440 CDS	pTWIN-RISP2 ₅₂₋₂₀₃	Protein overexpression	This work

2.1.5 Bacterial strains

Table 5: List of bacterial strains used in this study.

Organism	Strain	Usage	Company
<i>E. coli</i>	DH10 β	Amplification of Plasmid DNA /cloning	Stratagene, USA
	BL21 Codon Plus (DE3)-RIPL	Protein expression	
<i>A. tumefaciens</i>	LBA1334	Plant transformation	Van Larebeke <i>et al.</i> , 1974

2.1.6 T-DNA insertion lines

Table 6: List of T-DNA insertion mutant lines used in this study.

Name	AGI code	Gene name
SALK_115315.45.80.x	At5g13430	RISP 1
SALK_146627.18.05.x	At5g13430	RISP1
SALK_064243.54.25.x	At5g13440	RISP2
SALK_135742.49.95.n	At5g13440	RISP2
SALK_011488.53.95.x	At5g42380	CML37
SALK_066538.54.75.x	At1g76650	CML38

2.1.7 Primers

Table 7: List of primers used in this study.

Name	Sequence 5' \rightarrow 3'	Amplicon
fl_RISP1_cdna_fw	ATGCTGCGTGTAGCAGGGA GGAG	At5g13430 CDS
fl_RISP1_cdna_rv	ACCGATGAGTAACTTATTC TCTTCCAGG	At5g13430 CDS

fl_RISP2_cdna_fw	ATGCTGCGAGTAGCAGGAA GG	At5g13440 CDS
fl_RISP2_cdna_rv	ACCAATGAGTAATTTATTC TCTTCCAAG	At5g13440 CDS
fl_RISP1_ApaI_fw	CCTGGGCCCCATGCTGCGTG TAGCAGGG	At5g13440 CDS with ApaI overhang
fl_RISP1_NotI_rv	CTTGCGGCCCGCCACCGATG AGTAACTTATTCTCTTC	At5g13440 CDS with NotI overhang
fl_RISP2_ApaI_fw	CTTGGGCCCCATGCTGCGAG TAGCAGGAAG	At5g13440 CDS with ApaI overhang
fl_RISP2_NotI_rv	CTTGCGGCCCGCCACCAATG AGTAATTTATTCTCTTCC	At5g13440 CDS with NotI overhang
SALK_064243_LP	TTGAAGGTCTTCGAAATGT CG	At5g13430 gDNA
SALK_064243_RP	AATGAGATAGGTTTTGGTT CGG	At5g13430 gDNA
SALK_135742_LP	GGGGGTCTATACTTGGTAA AGG	At5g13430 gDNA
SALK_135742_RP	CCTAGGGAGCATAGAACCA GG	At5g13430 gDNA
SALK_115315_LP	TCATTCACGGGATGTCTTA CG	At5g13440 gDNA
SALK_115315_RP	TTCTCAAGTCCTTGCTCAA GG	At5g13440 gDNA
SALK_146627_LP	GCTGTTTAAAGGCATGCTG AG	At5g13440 gDNA
SALK_146627_RP	GGATTCTTGACCCTAACCG AG	At5g13440 gDNA
LBb1.3_DNA	ATTTTGCCGATTTTCGGAAC	T-DNA insert

RISP_SapI_ptwin_fw	GGTGGTTGCTCTTCCA ACT ACCACCGGAGC	At5g13440 CDS (52-107 bp) with SapI-pTWIN overhang
RISP_PstI_ptwin_rv_frag1	GGTGGTCTGCAGTTAAGG GTCACCAGGTGGG	At5g13440 CDS (52-132 bp) with PstI-pTWIN overhang
RISP_PstI_ptwin_rv_frag2	GGTGGTCTGCAGTTAAGCA GGCGGAGAACAG	AAAt5g13440 CDS (52-203 bp) with PstI-pTWIN overhang
RISP_PstI_ptwin_rv_frag3	GGTGGTCTGCAGTTATCT TCT TGT GGG TCC CTC AG	At5g13440 CDS with PstI- pTWIN overhang
SALK_011488_LP	GAGAATATACGCGCGTTAT CG	At5g42380 gDNA
SALK_011488_RP	TCGTGGTCAACTTGACCTT TC	At5g42380 gDNA
SALK_066538_LP	TTTCTATGTGTGCCTTGTT TG	At1g76650 gDNA
SALK_066538_RP	GCGCATCATAAGAGCAAAC TC	At1g76650 gDNA

2.1.8 Antibodies

For the detection of aequorin, α -aequorin was ordered from Abcam, Germany. The self-made α -RISP₂₅₂₋₁₀₇ polyclonal antibody was generated by David's Biotechnologie GmbH (Regensburg, Germany) in rabbits using purified recombinant RISP₂₅₂₋₁₀₇ as antigen.

2.2 Methods

2.2.1 Molecular and cell biological methods

2.2.1.1 Plant material and growth conditions

Apoaequorin was amplified from the vector pEVP11/AEQ (Batiza et al., 1996) and cloned into the vector pUbi-AB (Nagy et al., 2011). The entire expression cassette was further sub-cloned into the binary vector pLH7000 (NCBI: txid226215) and transformed into the barley wild type cultivar Golden promise (barley-Aeq) via agrobacterium-mediated gene transfer. The entire cloning as well as the transformation into barley was performed by the group of Dr. Jafargholi Imani and colleagues from the Plant Biotechnology department at the University of Giessen (Imani et al., 2011). As a control, the previously established Arabidopsis lines (Arabidopsis-Aeq) containing the apoaequorin targeted to the cytosol were used (Knight et al., 1991). Both Arabidopsis-Aeq and barley-Aeq were grown on commercially available vermiculite for five, seven, or eleven days based on the experiment type. The vermiculite was watered only once per week which was enough to maintain the required moisture level for the plants. The seedlings were grown at long day conditions under 16 hours light at 20 °C with a light intensity of 100-120 $\mu\text{mol m}^{-2} \text{s}^{-1}$ and 8 hours darkness at 18 °C, the humidity was set to 65%. For isolation of mitochondria, Arabidopsis seedlings were grown similar to the conditions mentioned above for fourteen days in liquid $\frac{1}{2}$ MS media.

2.2.1.2 Luminescence imaging of aequorin

For the luminescence imaging, intact barley plant expressing the apoaequorin (barley-Aeq) were mounted on a petri dish and aequorin was reconstituted from the apoaequorin by spraying the seedlings with 2.5 μM coelenterazine followed by overnight incubation in the dark. Luminescence imaging was performed according to (Kiep et al., 2015) using a high-resolution photon counting camera system (HRPCS218, Photek, St Leonardson Sea, UK). Photons were detected by an intensified CCD camera (ICCD218, Photek) and a camera controller (HRPCS4, Photek) mounted on a dark box (DB-2, Photek). The Petri dishes were injected with either 250 mM NaCl or 10 mM

H₂O₂ through an integrated tubing system at 90 seconds. Afterward, the remaining aequorin was discharged after 600 seconds with 1 M CaCl₂ in 10% ethanol. Images were taken after every 10 seconds and the [Ca²⁺]_{cyt} dependent light emission was analyzed with the IFS32 software (Photek).

2.2.1.3 Ca²⁺ measurements in barley and Arabidopsis

Whole seedlings, leaf tips, or root tips of five-days-old transgenic barley-Aeq and for comparison whole seedlings, shoot or roots of five days-old transgenic Arabidopsis-Aeq were used to investigate possible changes in [Ca²⁺]_{cyt} in response to salt and oxidative stress. To that end, the whole seedling or the tissue was reconstituted overnight in the dark in 2.5 μM coelenterazine. On the next day, the samples were quickly washed in water to remove any remaining coelenterazine and transferred to the appropriate microplate for measurement. In this work, due to their oversize the seedlings of barley were measured in a 24-well plate (Berthold Technologies). For barley tissues as well as all samples from Arabidopsis were measured in a 96-well microplate. The samples were then allowed to recover in light for one hour and to avoid subjecting the tissues to any touch-response. For the inhibitor treatment experiments, after overnight reconstitution in the dark, the plant tissues were pre-treated with LaCl₃ or thapsigargin for one hour in light and then washed thoroughly with water. The tissues were then transferred to an appropriate microplate and subjected to the measurement in a TriStar² LB 942 Microplate Reader by Berthold Technologies for 90 seconds with an integration time of 1 second to record the baseline before the injection of 100 μl the stress treatment (NaCl or H₂O₂). After the application of the stressor, the luminescence was measured for 600 seconds before the injection of the discharge solution which consisted of 1 M CaCl₂ in 10% ethanol (100 μl), and the luminescence was further recorded for another 300 seconds. The measured luminescence intensity values were translated into calcium concentrations by applying a formula explicitly designed for the apoaequorin variant present in the construct (Rentel & Knight, 2004).

2.2.1.4 Sample preparation for RNA isolation and sequencing

The shoots and roots of barley were subjected to four different sets of treatment as shown in Table 8. The five-days-old barley seedling was harvested and washed several times without damaging the seedling to get rid of any remaining vermiculite from the tissues. The seedling was then incubated in water (control) or 3 hours in 10 mM H₂O₂ (Sample A) or 1 hour in 10 mM LaCl₃ (Sample B) or both 1h in 10 mM LaCl₃ followed by 3h in 10 mM H₂O₂ (Sample C).

Table 8: Table indicating the four different treatments that were applied to the shoots and roots of five-days-old barley.

Sample	1 hour in 10 mM LaCl₃	3 hours in 10 mM H₂O₂
Control	-	-
Sample A	-	+
Sample B	+	-
Sample C	+	+

After the appropriate treatment, the shoots were separated from the roots and ground into fine powder in liquid nitrogen. At this point, the powdered sample can be stored at -80 °C until further use or used for RNA isolation immediately. RNA isolation was performed following the instructions of the manufacturer (Zygmo Research, Quick-RNA mini prep kit). After powdering, the sample was weighed to add the appropriate amount of RNA lysis buffer. Approximately 80-100 mg plant tissue per isolation is required for each replicate. The elution was done twice with 15 µl of DNase/RNase-free water (30 µl of the total eluted sample). After the isolation, the RNA was separated on a 1% agarose gel and then quantified using a Nanodrop. The samples were stored until further use at -80 °C and sent for RNA-Seq analysis to the NGS facility (Medical Faculty of University Bonn, Germany).

2.2.1.5 Polymerase chain reaction

PCR was used to amplify DNA fragments for cloning, genotyping, and other analytical purposes. The elongation time and annealing temperature were adjusted according to the product size and melting temperature of the primers, respectively. The standard PCR components used are given in Table 9. Restriction sites useful for the cloning into the appropriate plasmid were introduced by installing the corresponding sequences in the forward and reverse primers.

Table 9: Components of a PCR reaction.

Components	Taq polymerase reaction mix	Phusion polymerase reaction mix
H ₂ O _{MilliQ}	17.3 μ l	16.8 μ l
Buffer	5 μ l	5 μ l
MgCl ₂ (25 mM)	-	1.25 μ l
dNTPs (200 μ M)	0.5 μ l	0.25 μ l
Primer 1 (1 μ M)	0.5 μ l	0.25 μ l
Primer 2 (1 μ M)	0.5 μ l	0.25 μ l
Polymerase	0.2 μ l	0.2 μ l
DNA (10–20 ng)	1 μ l	1 μ l

The optimized settings used in a PCR are given in Table 10. The annealing temperature was determined empirically for each primer pair. Elongation time was estimated depending on expected PCR product size and polymerase applied.

Table 10: Optimized PCR settings.

Steps	Temperature (°C)	Time (seconds)	Number of cycles
Initial denaturation	94	300	1
Denaturation	94	30	30

Annealing	-	30	
Elongation	72	-	
Final elongation	72	300	1

The amplified PCR products were analyzed by separation on 1 % Agarose gel. The gel was stained using DNA stain G (SERVA Electrophoresis GmbH, Heidelberg, Germany) according to the manufacturer's instructions. The electrophoresis was carried out at 150 V for 10-15 min. Documentation was performed on a Gel documentation system with a CCD-Camera-Gerix 1050 (Biotec-Fischer, Deutschland).

2.2.1.6 Cloning strategy

To clone into plasmids of choice, genomic DNA (gDNA) or complementary DNA (cDNA) were amplified using appropriate primers with restriction sites (Table 7). After amplification, the PCR products were purified using the Gel/PCR Fragment Extraction Kits. The purified PCR products were first checked on a 1% agarose gel and then sent to Microsynth Seqlab (Göttingen, Germany) for sequencing to verify that it is free of mutations. Afterward, the PCR amplicon was subjected to digestion with respective restrictions enzymes according to the manufacturer's instructions. The restriction-digests were then separated on agarose gels, purified, and ligated with the digested plasmid DNA at 22°C for 1 hour with T4 DNA ligase applying a molar vector: insert ratio of 1:4 in a 20 µl reaction assay, and then transformed into competent *E. coli* cells via heat-shock.

2.2.1.7 Isolation of genomic DNA from Arabidopsis

A single leaf from approximately 25 days-old Arabidopsis plants was ground in 400 µl of extraction buffer (200 mM Tris-HCl pH 7.5, 250 mM NaCl, 25 mM EDTA). The ground samples were then centrifuged for 10 minutes at 13,000 rpm to remove cell debris. 285 µl of the supernatant were mixed with 715 µl of 70% Ethanol in a new tube and centrifuged again at 13,000 rpm for 10 minutes to precipitate the DNA. The supernatant was removed, and the pellet was dried at 50°C.

The dried DNA pellets were re-suspended in 50 μ l of 10 mM Tris-HCl pH 8.5 and stored at -20°C until further use.

2.2.1.8 Self-assembly GFP (saGFP) assay

The green fluorescent protein (GFP) contains 11 β -sheets, which could be split into two parts, one containing the first 10 β -sheets (saGFP₁₋₁₀) and the second part containing the 11th β -sheet (saGFP₁₁). In contrast to split-GFP, they can assemble and emit fluorescence if they are simply present in the same cellular compartment. A modified pBIN19 binary vector carrying C-terminally to the MCS the sequence coding either for saGFP₁₋₁₀ or saGFP₁₁ was used to transiently transform tobacco (Bevan, 1984). The genes of interest carrying an ApaI and NotI overhang were cloned in the pBIN19 vector either carrying saGFP₁₁ or saGFP₁₋₁₀ tag. Agrobacteria were transformed with these constructs via electroporation. Transformed cells were grown overnight in LB medium supplemented with 50 mg/ml kanamycin in a 5 ml culture volume. Cells were harvested by centrifugation and re-suspended in infiltration media (10 mM MES KOH pH 5.6, 10 mM MgCl₂, 100 μ M acetosyringone) to get a final OD at 600 nm between 0.5 and 1. After 2 hours of incubation at 30°C , the respective cell suspensions were mixed accordingly and used to co-infiltrate leaves of 3-4 weeks old tobacco plants (*Nicotiana benthamiana*). Infiltrated leaves were allowed to transiently express the proteins of interest for 48–72 hours in the dark. Subcellular localization of the proteins was analyzed by confocal laser scanning microscopy using the FluoView FV1000 confocal laser scanning microscope (OLYMPUS) and the images were processed with the FV10-ASW Viewer software.

2.2.2 Biochemical methods

2.2.2.1 Isolation of mitochondria and mitoplast

Fourteen-days-old Arabidopsis grown on liquid $\frac{1}{2}$ MS media were ground thoroughly in grinding buffer (0.3 M Sucrose, 2 mM EDTA, 10 mM KH₂PO₄, 25 mM Tetrasodium pyrophosphate, 1% PVP-40, 1% (w/v) BSA, 20 mM ascorbate, pH 7.5) into a homogenous suspension and filtered through four layers of gauze. The filtered homogenate was then centrifuged at 2,450 g for 5 min

at 4°C to remove cell debris and larger organelles that were in the pellet. The supernatant was centrifuged at 17,400 g for 20 min at 4°C to pellet down mitochondria. The supernatant was discarded, and the pellet was gently resuspended in washing buffer (0.3 M Sucrose, 10 mM TES pH 7.5, 0.1% (w/v) BSA) and centrifuged again at 2,450 g for 5 min at 4°C to pellet any remaining chloroplasts. To pellet down the mitochondria, the supernatant was transferred to new tubes and centrifuged at 17,400 g for 20 min at 4°C. The pellet was then resuspended in washing buffer and loaded onto linear PVP-40 gradients (0-4.4% PVP in 28% Percoll in washing buffer) and then centrifuged at 40,000 g for 40 min at 4°C without brake. The contaminating fractions were discarded, and the intact mitochondria were collected, washed twice with washing buffer, and pelleted at 31,000 g for 15 min at 4°C. The mitochondria pellet was resuspended in a small volume of washing buffer, aliquoted, and then either used immediately or frozen in liquid nitrogen and stored at -80°C until further use.

2.2.2.2 Expression and purification of recombinant proteins

N-terminally Intein-tagged proteins were expressed in ER2566 *E. coli* cells and purifications were performed using the IMPACT-pTWIN protein purification system (NEB, Germany) according to the manufacturer's instructions.

2.2.2.3 SDS-PAGE and western blot analysis

For analysis on SDS PAGE, the protein samples were denatured by adding the appropriate amount of 2x or 4x Laemmli buffer (Laemmli, 1970) and incubating at 96°C for 3-5 min. the samples were then separated on 10% or 12% polyacrylamide gels. To estimate the size of the protein, either Peqlab Marker Gold I or PageRuler™ protein ladder plus Prestained marker were used. Samples were separated at 20 mA and detection of proteins was achieved by staining the gels overnight with Colloidal-Coomassie (10% (w/v) ammonium sulphate, 2% (w/v) phosphoric acid, 5% (w/v) Coomassie Brilliant Blue G-250). For western blotting, the proteins separated on the SDS gels were transferred onto a PVDF membrane (Thermo Scientific, U.S.A.) and then incubated in blocking buffer (1 x TBS, 0.05 % Tween 20®, 5 % milk powder) for 30 min with shaking at room

temperature to saturate the membrane. After blocking, the membrane was incubated with the antibody (α -RISP2₅₂₋₁₀₇) which was diluted at 1:1000 in a TBS-T buffer (1 x TBS, 0.05 % Tween 20®, 5 % milk powder) while shaking and 4°C overnight. Afterward, the membrane was washed three times for 10 min each with a blocking buffer to remove excess antibodies. The membrane was then incubated in the corresponding secondary antibody (Anti-Rabbit IgG) diluted 1:10,000 in TBS-T for 1 hour at room temperature after which the membranes were washed three times for 10 min each with TBS-T without milk powder. Detection of the secondary antibody was achieved using a horseradish peroxidase-ECL detection system following the manufacturer's instructions (Serva, Germany). Documentation was performed on a ChemiDoc MP Imaging system (Bio-Rad, Germany).

2.2.2.4 Blue Native PAGE

Mitochondria corresponding to 25 μ g proteins first quantified using the Coomassie Plus (Bradford) Protein Assay and then resuspended in 20 mM Tris-HCl pH 7.4, 0.1 mM EDTA, 50 mM NaCl, 10% (w/v) glycerol, and 5% (w/w) digitonin and incubated on ice for 30 min. Insolubilized components were pelleted down by centrifuging at 10,000 g for 15 min at 4°C. The supernatant was transferred to a fresh tube to which BN-sample buffer (100 mM Bis-tris, pH 7.0, 750 mM ϵ -aminocaproic acid, 5% (w/v) Coomassie G250) was added and the protein complexes were resolved on a 4 - 16 % continuous Blue Native acrylamide gel as described previously (Schägger and Jagow, 1991; Jansch et al., 1998). Protein complexes were either visualized by Coomassie colloidal staining or blotted onto the PVDF membrane for immunodetection with α -RISP2₅₂₋₁₀₇.

2.2.2.5 Affinity chromatography on CaM-agarose

After isolation of intact mitochondria, mitochondrial membrane proteins were extracted using 1% n-Dodecyl β -D-maltoside in binding buffer (20 mM Tris-HCl, pH 7.5, and 150 mM NaCl). The sample was incubated for 30 minutes on ice and then centrifuged at 50,000g for 20 minutes, the supernatant containing the solubilized proteins was diluted 10-fold with binding buffer and adjusted to get either 1 mM CaCl₂ (Sample A) or 5mM EDTA+EGTA (Sample B). The samples

were then incubated with 50 μ l CaM-agarose (pre-equilibrated in binding buffer) for 16h at 4°C and under constant gentle rotation. Afterward, unbound proteins were collected through centrifugation flow-through), and the beads were washed three times with 500 μ l washing buffer (20 mM Tris-HCl, pH 7.5, 500 mM NaCl, and 1 mM CaCl₂ (Sample A) or 5mM EDTA + EGTA (Sample B). Proteins that bind specifically to the beads were eluted using elution buffer containing 5mM EDTA + EGTA (Sample A) and 1 mM CaCl₂ (Sample B) in the binding buffer. In the last elution step (E4), the beads were boiled for 10 minutes with an SDS-protein loading buffer. The samples were then analyzed on a 12% SDS gel and immunodetected with an antibody specific to RISP2₅₂₋₁₀₇.

2.2.3 Bioinformatics

The RNA-Seq analysis of the samples was performed by a Ph.D. student Mr. Sabarna Bhattacharyya. The Illumina HiSeq 2500 v4 reads were processed for quality control using fast QC. The reads were then aligned using Tophat2 (Kim et al., 2013) against an *H. vulgare* IBSC v2 reference genome obtained from Ensembl (<http://plants.ensembl.org/info/data/ftp/index.html>), using a Bowtie index (Langmead & Salzberg, 2012) created with the help of the above-mentioned reference genome (in FASTA format). The alignment with Tophat2 was performed on an Ubuntu 18.04 LTS operating system, in a UNIX shell environment. Every step after alignment was performed using Rstudio version 4.0.0. Gene counts from the aligned BAM files were generated using feature Counts (Liao et al., 2014) from the Rsubread package. Differential gene expression analysis was carried out using DESeq2 (Love et al., 2014). The p-values were adjusted using the False Discovery Rate method (Benjamini & Hochberg, 1995), and subsequently, the p-value (adjusted) and the logFC cutoffs were set to 0.01 and 0.5, respectively. A variance stabilizing transformation (VST) was also performed for PCA using the DESeq2 package. The Venn diagrams were prepared by using an online tool called InteractiVenn (<http://www.interactivenn.net>).

The gene and protein sequences of RISP1 (At5g13430) and RISP2 (At5g13440) were extracted from Aramemnon (<http://aramemnon.uni-koeln.de/>). RISP1 and RISP2 were aligned using the online tool for multiple sequence alignment (MSA) (<https://www.ebi.ac.uk/Tools/msa/clustalo/>). The transmembrane domain in RISP1 and RISP2 was predicted using the tool TMPRED

(https://embnet.vital-it.ch/software/TMPRED_form.html). The prediction for CaM binding domain in RISP1 and RISP2 was done employing the Calcium target database tool (<http://calcium.uhnres.utoronto.ca/ctdb/ctdb/sequence.html>). To look for RISP2 in other species, the protein BLAST was performed using RISP2 as a query (<https://blast.ncbi.nlm.nih.gov/Blast.cgi?PAGE=Proteins>).

3. Results

3.1 Ca²⁺ signaling in barley

To analyze changes in the cytosolic Ca²⁺ concentration [Ca²⁺]_{cyt} in *H. vulgare* (barley), wild-type plants were stably transformed to express apoaequorin in the cytosol (Imani et al., 2011). Apoaequorin was originally isolated from the jellyfish family Aequorea (Shimomura et al., 1963) and requires the presence of coelenterazine, a prosthetic group, to get fully functional as a Ca²⁺ sensor (aequorin). Aequorin can report changes in the cellular Ca²⁺ by catalyzing the decarboxylation of coelenterazine to form the coelenteramide which at an intensity peak of 469 nm emits a luminescence light. The emitted light can then be recorded by a luminometer or a Photon counting camera system (Photek). Under physiological Ca²⁺ levels, a double logarithmic correlation exists between the Ca²⁺ ion concentration and the detected luminescence light (Allen & Prendergast, 1977). To compare these measurements with a well-accepted control, the experiments were also performed in Arabidopsis. Two of the commonly used stress inducers were used in this work to study the Ca²⁺ signatures in barley: salt (NaCl) and oxidative (H₂O₂) stress.

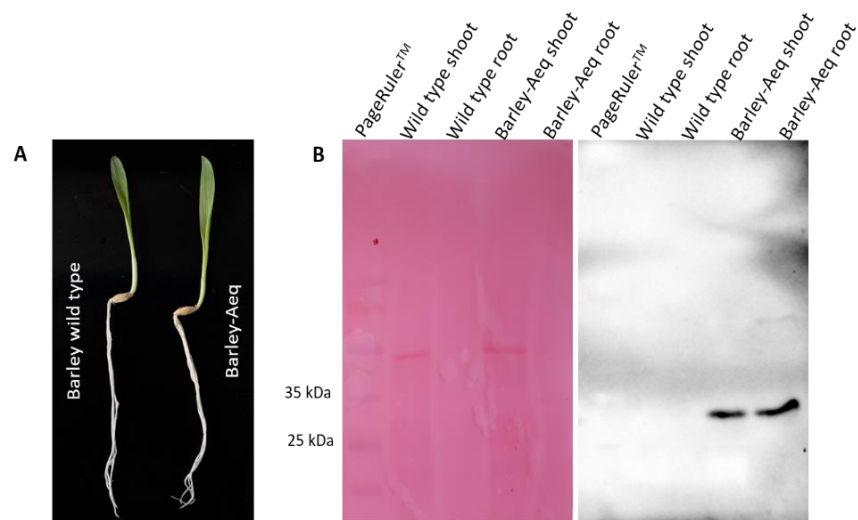


Figure 1. Phenotype and expression of Apoaequorin in the barley wild type and barley-Aeq lines: **(A)** Five-days-old barley-Aeq showed no outward phenotype when compared to wild type barley. **(B)** Protein extracts from the shoots and roots of barley wild type and barley-Aeq were separated on a 12% SDS gel and transferred to a PVDF membrane. The membrane was subjected to Ponceau staining (left panel) followed by immunodetection using an antibody that detects aequorin (right panel).

Wild type barley seeds (*H. vulgare* cultivar Golden promise) expressing a cytosol-targeted recombinant apoaequorin (barley-Aeq) were obtained in a collaborative work from Prof. Dr. Peiter (Department of Plant Nutrition, Martin-Luther-University Halle-Wittenberg, Germany). These seeds were checked for homozygosity and among them, barley-Aeq line #18 showed the highest Ca^{2+} signal as measured by Dr. Meier (Working group of Prof. Dr. Peiter). This line was then used for all further investigations. Five-days-old wild type and barley-Aeq seedlings were checked for their outward phenotype under normal growth conditions and no differences could be observed (Fig. 1A). The presence of the apoaequorin protein in the barley-Aeq shoot and root was confirmed by performing an immunodetection with an antibody that recognizes aequorin. The whole proteins from the shoots and roots of both wild type and barley-Aeq seedlings were extracted and separated on a 12% SDS gel. The proteins were then transferred to a PVDF membrane, and the protein of interest was detected by immunodetection with α -aequorin (Fig. 1B). A specific band could be detected in both the shoot and root samples of the barley-Aeq line but not in the wild type, indicating the successful transformation and expression of aequorin in the transgenic plants (Fig. 1B, right panel). The ponceau staining of the PVDF membrane was used to show that equal amounts of the samples from the wild type and barley-Aeq lines were loaded on the gel (Fig. 1B, left panel).

3.1.1 Ca^{2+} response measured in the whole seedlings of barley-Aeq

To study the Ca^{2+} response in barley, barley-Aeq whole seedlings were used and the $[\text{Ca}^{2+}]_{\text{cyt}}$ measurements were performed using the Photek system as well as the luminometer. As control Arabidopsis-Aeq seedlings were used.

3.1.1.1 Measurements using a Photek system

Luminescence imaging of the intact barley seedlings was performed in collaboration with Prof. Dr. Peiter. Three-days-old barley seedlings which were grown on vermiculite were washed several times in water and reconstituted overnight in coelenterazine. The seedlings were then allowed to

recover in light for an hour and the aequorin-luminescence imaging was performed as mentioned in Methods 2.2.1.2.

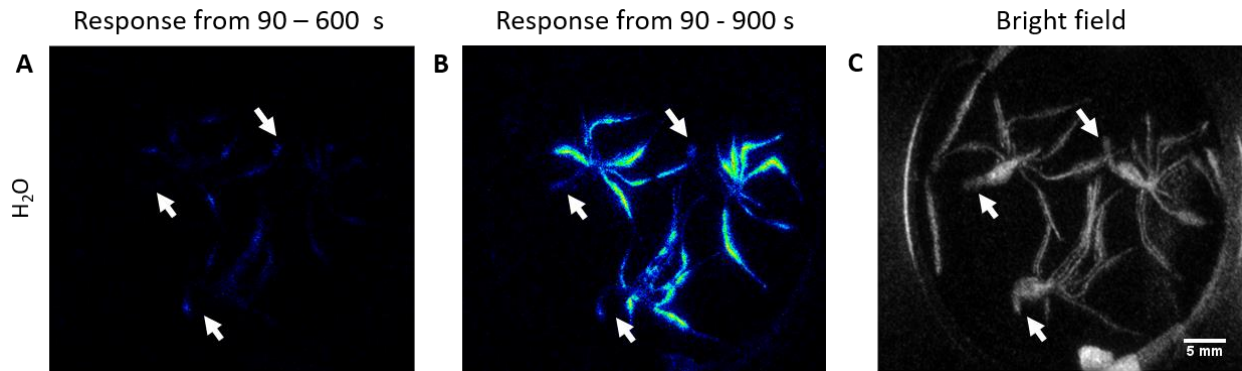


Figure 2. Aequorin-based luminescence in barley-Aeq in response to H₂O treatment measured in the Photek: Cumulative images of (A) $[Ca^{2+}]_{cyt}$ changes in response to H₂O and (B) of the entire experiment including a discharge of the seedlings. (C) Bright-field image of the three-days-old barley seedling used for luminescence imaging. White arrows indicate the leaf of the three seedlings.

Seedlings of barley-Aeq were placed on a petri dish and a bright-field image was taken (Fig. 2C). Upon injection of water (H₂O), as expected, no luminescence was visible in the leaf and root of all the seedlings (Fig. 2A). Upon injection of the discharge solution containing 1 M CaCl₂ in 10 % ethanol, the remaining aequorin was discharged as shown by the strong luminescence signal in the whole seedling (Fig. 2B). These results indicated the successful reconstitution of aequorin from apoaequorin and also its functionality to sense changes in the Ca²⁺ concentration.

In another experiment, the luminescence imaging was done upon injection of 250 mM NaCl or 10 mM H₂O₂ in the barley-Aeq seedlings. Under both stresses a strong signal could be observed in the roots, however, the leaves showed more response to the H₂O₂ than to NaCl (Fig. 3A and D). Upon the application of the discharge solution, the discharge of the remaining aequorin from the seedlings was achieved (Fig. 3B and E). These results indicated that barley-Aeq seedlings are reacting to salt as well as oxidative stress and that the response in the roots is much higher as in the leaf. These results taken together, along with the fact of the absence of a signal upon injection of H₂O (Fig. 2) indicated the specificity of the reaction of aequorin in response to stress.

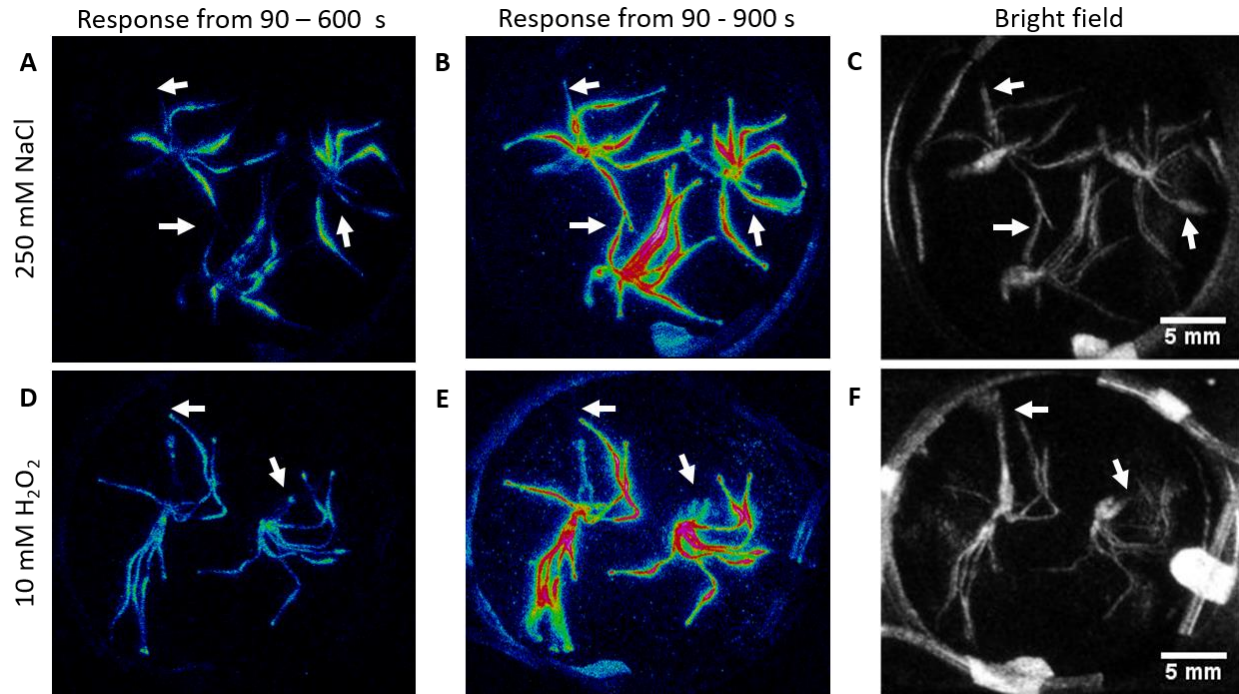


Figure 3. Aequorin-based luminescence in barley-Aeq in response to NaCl and H₂O₂ treatment measured in the Photek: Cumulative images of (A and D) [Ca²⁺]_{cyt} changes in response to 250 mM NaCl or 10 mM H₂O₂ and of (B and E) the entire experiment including a discharge of the seedling (C and F) Bright-field image of the three-days-old barley seedling used for luminescence imaging. White arrows indicate the leaf of the three seedlings.

3.1.1.2 Measurements using a luminometer

Photons emitted from the bioluminescent reaction could also be measured using a luminometer. Since barley seedlings are larger than Arabidopsis, the measurements were done in a 24-well microplate rather than a 96-well microplate as in the case of Arabidopsis. In this method, the seedlings were reconstituted overnight in coelenterazine in the dark. On the next day, the seedlings were transferred to the microplate and allowed to recover in the light for one hour. This ensured that the response from the tissues is specific to the stress applied and not due to the wounding or touch response. The microplate was placed in the luminometer and then the seedlings were subjected to the appropriate stress treatment followed by the discharge (Fig. 4). These experiments were performed in Arabidopsis plants expressing the recombinant apoaequorin (Arabidopsis-Aeq) as well. In barley-Aeq, an increase in the [Ca²⁺]_{cyt} was observed in response to NaCl and H₂O₂ (Fig. 4A and B), confirming the results obtained using the Photek system (Fig. 3). The pattern of the [Ca²⁺]_{cyt} increase are different between NaCl and H₂O₂ in term of the time point at which the

signal appears, the amplitude of the peak and the duration of the signal (Fig. 4). These differences are an indication of the specificity of Ca^{2+} response to the stress which is called the “ Ca^{2+} signature”. The pattern of the Ca^{2+} signal in barley-Aeq seedlings for each stress is quite similar to those in Arabidopsis-Aeq seedlings (Fig. 4), except the amplitude of the peaks which is higher in Arabidopsis especially for salt stress. These results indicated that either barley is less sensitive to both stresses as Arabidopsis and maybe these differences are due to the microplate size (24 vs 96- well) which could influence the Ca^{2+} measurements. Therefore, all the measurements in the further experiments were done in a 96-well microplate and using a smaller section of either the leaf or root instead of the whole seedling of the barley-Aeq line.

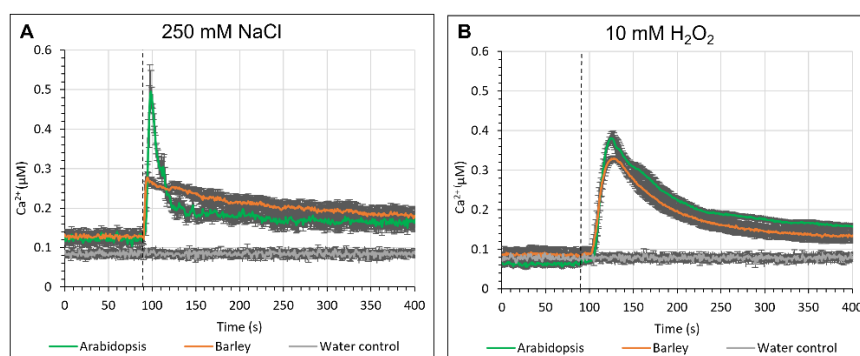


Figure 4. Aequorin-based luminescence in barley-Aeq and Arabidopsis-Aeq in response to NaCl and H_2O_2 treatment measured in the luminometer: **(A)** Changes in $[\text{Ca}^{2+}]_{\text{cyt}}$ (μM) in response to 250 mM NaCl in the barley-Aeq seedlings and Arabidopsis-Aeq seedlings determined in a luminometer. **(B)** Similarly, the changes in $[\text{Ca}^{2+}]_{\text{cyt}}$ (μM) in response to 10 mM H_2O_2 in the barley-Aeq seedlings (orange) and Arabidopsis-Aeq seedlings (green) determined in a luminometer. Water control is shown in grey. Error bar represents SE of triplicate reactions ($n=3$).

3.1.2 NaCl induced Ca^{2+} response

Using NaCl as a stress inducer, the Ca^{2+} response in the cytosol was checked in barley leaf tip and root tip. First, a dosage response upon application of five different NaCl concentrations was investigated. The optimal concentration which produces the highest response was used for further analyses. The Ca^{2+} response after pre-treatment with Ca^{2+} channels and Ca^{2+} -ATPases inhibitors were also analyzed. As mentioned in the previous section all the measurements were done in a 96-well microplate in a luminometer and only the leaf tip or root tip of barley-Aeq were used. For comparison, the whole shoot and roots of Arabidopsis-Aeq were used.

3.1.2.1 Ca²⁺ response to different NaCl concentrations

Salt stress was induced by applying NaCl in different concentrations (50 mM, 100 mM, 150 mM, 200 mM, and 250 mM) to barley-Aeq leaf tips and root tips. As seen in the whole seedling (Fig. 4A), salt stress in both leaf tip and root tip, resulting in a rapid increase in $[Ca^{2+}]_{cyt}$, reaching a peak within 10 seconds (Fig. 5A and B). The amount of Ca²⁺ increased with increasing (NaCl) and the highest peak was observed in both tissues with 250 mM NaCl. The kinetic of the salt stress response was quite similar in the leaf tip and root tip, indicating similar Ca²⁺ signatures in both the tissues. Arabidopsis shoots and roots reacted to an increasing amount of NaCl similar to barley, however, in Arabidopsis several delayed and small spikes could be observed, which are not existing in barley. In general, the response in Arabidopsis shoots and roots was much higher than those in barley tissues (Fig. 5C and D) confirming the results obtained using the whole seedling and thus, indicated that barley is less sensitive to salt stress than Arabidopsis. Since 250 mM NaCl gave the highest response in all the tissues, this concentration was used for further experiments.

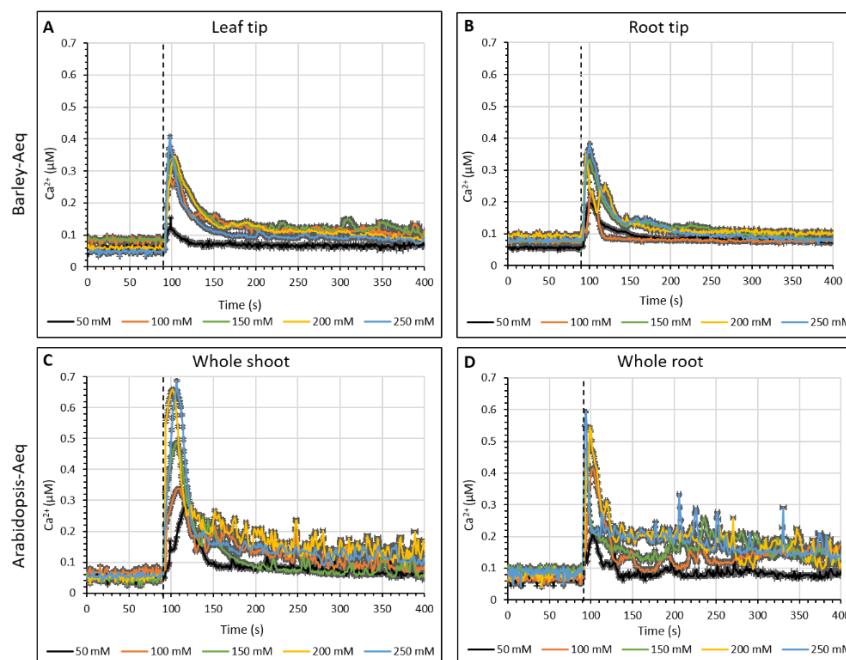


Figure 5. Aequorin-based luminescence in barley-Aeq and Arabidopsis-Aeq measured in response to NaCl treatment in the luminometer: Changes in $[Ca^{2+}]_{cyt}$ (μM) in response to various concentrations of NaCl (50, 100, 150, 200, and 250 mM) in barley leaf tips (A), root tips (B), and Arabidopsis whole shoots (C) and roots (D) determined in a luminometer. The dotted line indicates the injection of the stress, and the error bar represents SE of triplicate reactions ($n=3$).

3.1.2.2 NaCl induced Ca^{2+} response in five, seven, and eleven- days-old barley leaf

To analyze if the rest of the leaf reacts to the salt stress similar to the leaf the tip, the leaf was cut into 5 mm sections from the tip to the base and these sections were used for $[\text{Ca}^{2+}]_{\text{cyt}}$ upon application of 250 mM NaCl. The measurements were performed in leaves of different ages as well to see if the measurements are dependent on the age of the plant. For the five-days-old barley leaf, five sections from S1 (tip) to S5 (base) were cut and all the sections showed roughly the same amount of $[\text{Ca}^{2+}]_{\text{cyt}}$, with a slight increase from the tip to the base (Fig. 6A and D). The seven-days-old leaf samples were cut into ten sections from S1 - S10 and here a clear increase of the signal from the tip to the base of the leaf was observed (Fig. 6B and E). The response stayed the same even in eleven-days-old barley where the highest response was observed in the base (S9 - S14) and the lowest response in the tip of the leaf (S1 - S6) (Fig. 6C and F).

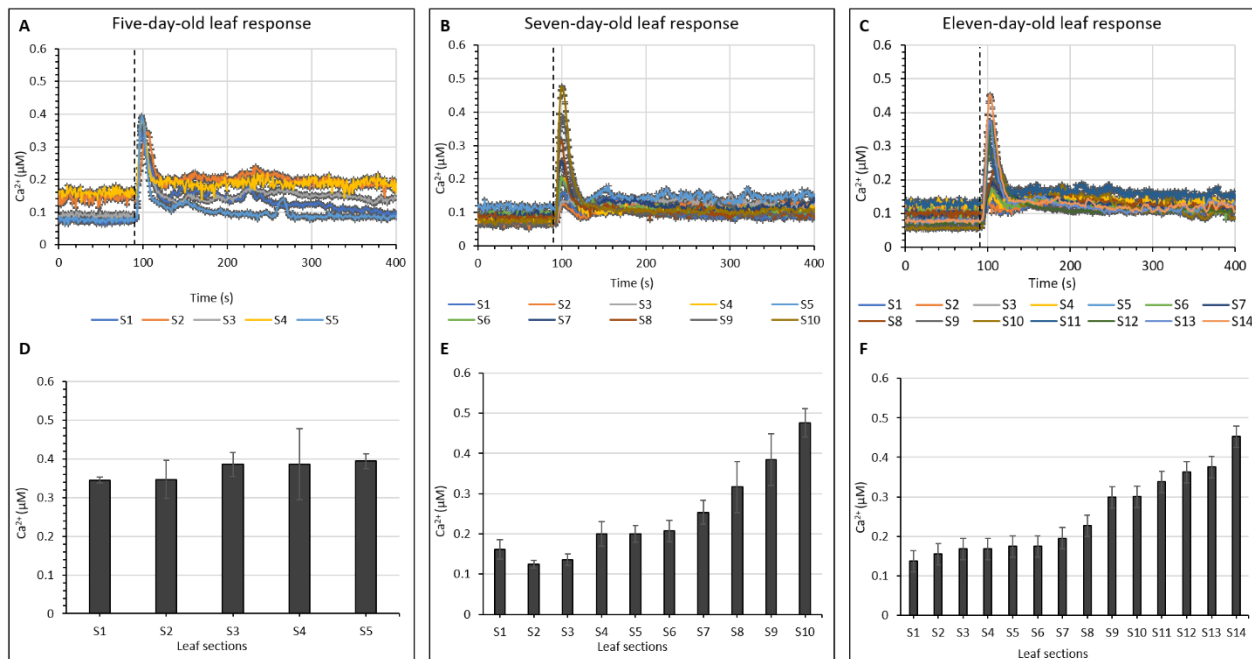


Figure 6. Aequorin-based luminescence in different ages and sections of the barley-Aeq leaf in response to NaCl treatment measured in the luminometer: Changes in $[\text{Ca}^{2+}]_{\text{cyt}}$ (μM) in response to 250 mM NaCl in five, seven and eleven-days-old barley leaf. S1 - S5 indicates the five sections in a five-days-old barley leaf, S1 - S10 indicates the ten sections in a ten-days-old leaf, and S1 - S14 indicates the fourteen sections in an eleven-days-old leaf. **A-C** shows the kinetics and **D - F** shows the $[\text{Ca}^{2+}]_{\text{cyt}}$ in a bar graph representation. In A, B, and C the dotted line indicates injection of the stress. Error bar represents SE of triplicate reactions ($n=3$).

It is also noteworthy here that the Ca^{2+} response in the leaf tip (S1) was $0.34 \mu\text{M}$ in the five-days-old leaf which was then reduced to $0.18 \mu\text{M}$ and $0.14 \mu\text{M}$ in the seven and eleven-days-old leaf,

respectively (Fig. 6D - F). By contrast, in all ages, the Ca^{2+} response in the leaf base seems to be only slightly different ranging between 0.4 and 0.47 μM . This indicated that the $[\text{Ca}^{2+}]_{\text{cyt}}$ in the leaf tip keeps decreasing as the age of the leaf increased, while in the base the $[\text{Ca}^{2+}]_{\text{cyt}}$ stays constant. Interestingly, apart from the amplitude of the peaks, the other pattern of the Ca^{2+} response seems to be similar in all sections (Fig. 6A - C) indicating a quite similar Ca^{2+} signature in response to salt stress in barley in the whole leaf and irrespective of the age of the plants.

3.1.2.3 Ca^{2+} response after pre-treatment with Ca^{2+} channels and Ca^{2+} -ATPases inhibitors

To identify the source of the Ca^{2+} involved in the response to NaCl stress, inhibitors of the Ca^{2+} channels and Ca^{2+} -ATPases such as Lanthanum chloride (LaCl_3) and Thapsigargin (Tpg) were used. LaCl_3 is a blocker of the Ca^{2+} channels in the plasma membrane and thus inhibiting the release of Ca^{2+} from the extracellular matrix into the cytosol, while Tpg is a blocker of the Ca^{2+} -ATPases in the endomembrane system (Tracy et al., 2008; Treiman et al., 1998). Blocking the release of Ca^{2+} from the stores should contribute to no luminescence signal upon application of the stress. In this study, different concentrations of LaCl_3 (0.01, 0.1, 0.5 and 1 mM) and Tpg (0.1, 0.5, 1 and 10 μM) were used to perform the inhibition experiments.

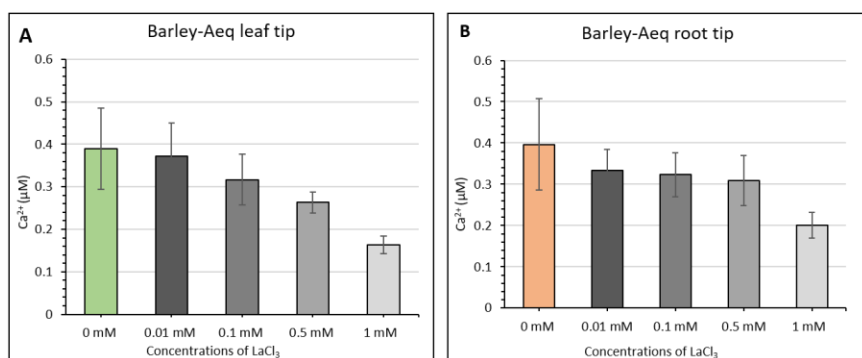


Figure 7. Effect of the inhibitor LaCl_3 on the NaCl induced $[\text{Ca}^{2+}]_{\text{cyt}}$ measured in the luminometer: Changes in $[\text{Ca}^{2+}]_{\text{cyt}}$ (μM) in response to 250 mM NaCl after pre-treatment with four different concentrations of LaCl_3 (0, 0.01, 0.1, 0.5 and 1 mM) in the (A) leaf tip and (B) root tip of barley-Aeq. Error bar represents SE of triplicate reactions (n=3).

In the case of LaCl_3 , the inhibition in the leaf tip was getting stronger with increasing concentration of the inhibitor with 1mM LaCl_3 causing the strongest inhibition, while at 0.01, 0.1, and 0.5 mM of LaCl_3 were less effective (Fig. 7A). By contrast, in the root tip, the lower concentration of 0.01, 0.1, and 0.5 mM LaCl_3 had approximately the same effect wherein the inhibition was not strong

(Fig. 7B). Using 1 mM LaCl_3 , 49% of inhibition was achievable. This indicates that the leaf tip is more sensitive to LaCl_3 than the root tip in the NaCl -mediated Ca^{2+} response.

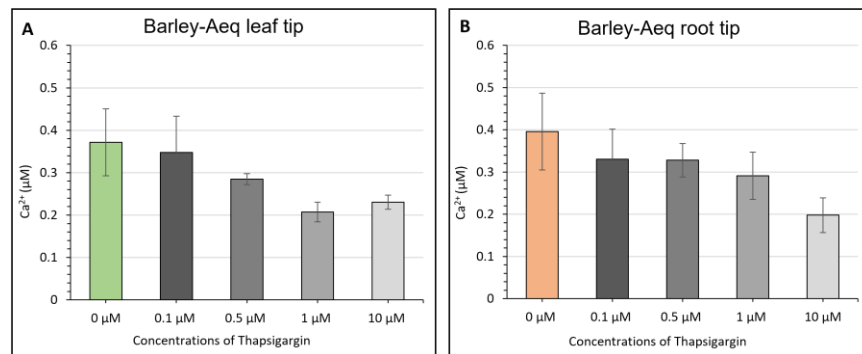


Figure 8. Effect of the inhibitor Thapsigargin on the NaCl induced $[\text{Ca}^{2+}]_{\text{cyt}}$ measured in the luminometer: Changes in $[\text{Ca}^{2+}]_{\text{cyt}}$ (μM) in response to 250 mM NaCl after pre-treatment with four different concentrations of Thapsigargin (0, 0.1, 0.5, 1 and 10 μM) in the leaf tip (A) and root tip (B) of barley-Aeq. Error bar represents SE of triplicate reactions (n=3).

Upon injection of salt stress in the leaf tip of barley, 0.1 μM Tpg pre-treatment had almost no inhibition whereas 1 and 10 μM Tpg were more effective, but with less than 50% reduction of the response (Fig. 8A). Similarly, in the root tip 0.1, 0.5, and 1 μM Tpg pre-treatment showed very weak inhibition, and 10 μM Tpg caused a stronger inhibition with a 55% reduction of the response (Fig. 8B). In both the leaf tip and root tip Tpg had a similar inhibitory effect on the Ca^{2+} responses with the leaf slightly more sensitive than the root. The fact that a 100% inhibition of the Ca^{2+} response was not achievable with any of the used inhibitor's concentrations suggests that the source of Ca^{2+} in the response to salt stress could be both the extracellular matrix and the ER. To verify this suggestion, a combination of both LaCl_3 and Tpg was used at a concentration of 1 mM and 10 μM , respectively (Fig. 9).

As shown above, the pre-treatment with 1 mM LaCl_3 and 10 μM Tpg in the leaf tip had 46% and 30% inhibition of the Ca^{2+} responses, respectively (Fig. 9A). A combination of both inhibitors had 58% inhibition which is slightly more effective than the effect of using LaCl_3 or Tpg alone. While in the root tip, pre-treatment with 1 mM LaCl_3 and 10 μM Tpg had 49% inhibition of the Ca^{2+} responses (Fig. 9B). The inhibition of the Ca^{2+} responses could further be reduced to 57% upon pre-treatment with the combination of 1 mM LaCl_3 and 10 μM Tpg (Fig. 9B). Since the combination of the inhibitors could not fully inhibit the Ca^{2+} response, it could be assumed that

other Ca^{2+} sources apart from the extracellular matrix and the endomembrane system are involved in salt stress-mediated Ca^{2+} response in barley.

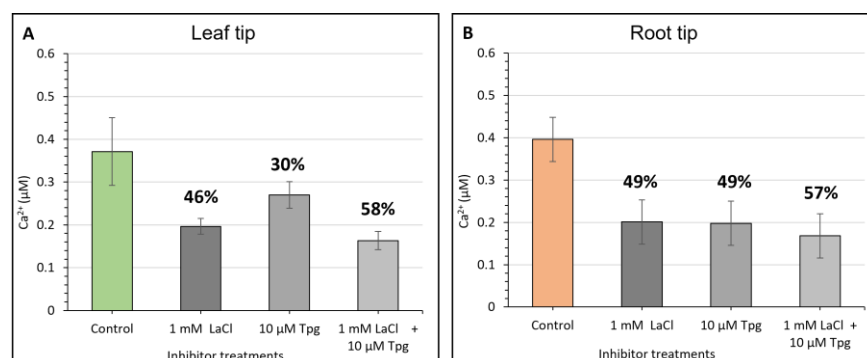


Figure 9. Effect of the inhibitor combination of LaCl_3 and Thapsigargin on the NaCl induced $[\text{Ca}^{2+}]_{\text{cyt}}$ signature measured in the luminometer: Changes in $[\text{Ca}^{2+}]_{\text{cyt}}$ (μM) in response to 250 mM NaCl after pre-treatment with 1 mM LaCl_3 , 10 μM Tpg and a combination of 1 mM LaCl_3 + 10 μM Tpg in the leaf tip (A) and root tip (B) of barley-Aeq. Percentage (%) indicates the percentage inhibition of the Ca^{2+} response. Error bar represents SE of triplicate reactions ($n=3$).

3.1.3 H_2O_2 induced Ca^{2+} responses

Similar to the salt stress response, oxidative stress-mediated Ca^{2+} response was investigated in the leaf tip and root tip of barley-Aeq using a luminometer. First, a dosage response upon application of different H_2O_2 concentrations was performed. The optimal concentration which produces the highest response was used for further analyses. The Ca^{2+} responses after pre-treatment with two inhibitors of the Ca^{2+} transients were also elucidated.

3.1.3.1 Ca^{2+} response to different H_2O_2 concentrations

Different concentrations of H_2O_2 , such as 2.5 mM, 5 mM, 10 mM, 15 mM, and 20 mM, were injected into leaf tip and root tip of barley-Aeq five-days-old seedling. Unlike the NaCl response, the H_2O_2 induced increase in $[\text{Ca}^{2+}]_{\text{cyt}}$ in both tissues was slightly delayed, appearing 20-30 seconds after injecting H_2O_2 (Fig. 10A and B). This signal appeared at 110 seconds and lasted until 200 seconds. The dose-dependent Ca^{2+} transient in response to H_2O_2 was seen for lower concentrations with the maximum $[\text{Ca}^{2+}]_{\text{cyt}}$ reached at 10 mM. Interestingly, at higher concentrations of H_2O_2 , a decrease of the $[\text{Ca}^{2+}]_{\text{cyt}}$ was observed in the tissues. While 2.5 mM

showed no effect in leaf, in the root it contributes to an increase in $[Ca^{2+}]_{cyt}$ similar to that caused by 5 mM H_2O_2 (Fig. 10A and B).

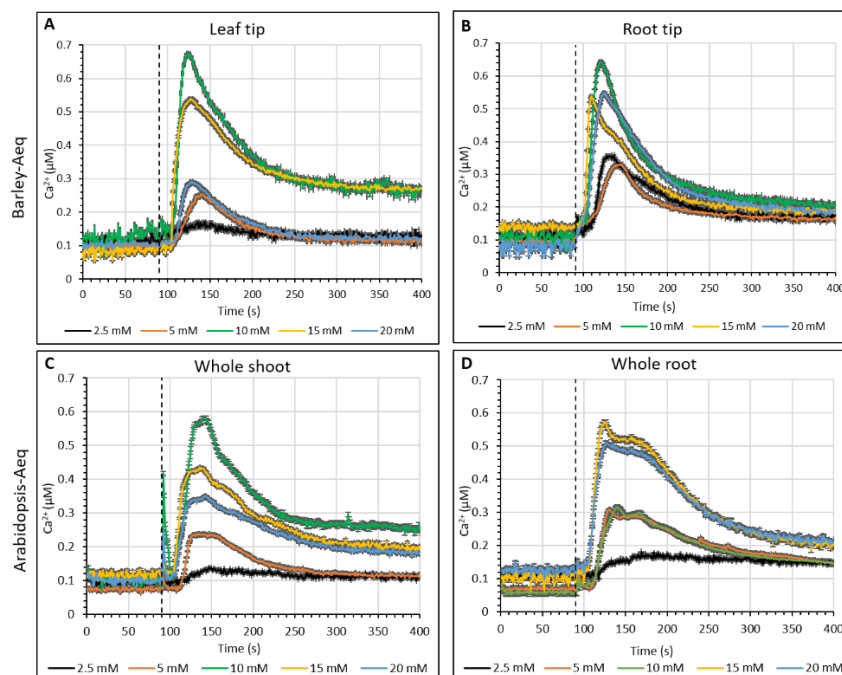


Figure 10. Aequorin-based luminescence in barley-Aeq and Arabidopsis-Aeq tissues measured in response to H_2O_2 treatment in the luminometer: Changes in $[Ca^{2+}]_{cyt}$ (μM) in response to various concentrations of H_2O_2 (2.5, 5, 10, 15 and 20 mM) in barley leaf tips (A), root tips (B), and in Arabidopsis shoots (C) and roots (D) determined in a Luminometer. The dotted line indicates the injection of the stress. Error bar represents SE of triplicate reactions ($n=3$).

By contrast, 20mM H_2O_2 caused only a slight decrease in $[Ca^{2+}]_{cyt}$ in the roots as compared to the leaf. Apart from these differences, the pattern of the Ca^{2+} kinetics is quite similar, indicating that both tissues, leaf, and root, have the same Ca^{2+} signature in response to H_2O_2 stress. By contrast, the kinetics of the Ca^{2+} response in Arabidopsis showed clear differences to those obtained with barley in both leaf and root (Fig. 10C and D), suggesting different H_2O_2 induced Ca^{2+} signatures in both organisms.

3.1.3.2. H_2O_2 induced Ca^{2+} response in five, seven, and eleven- days-old barley leaf

As performed for salt stress response, the Ca^{2+} response to H_2O_2 stress was investigated in different sections of the leaf and at different ages of the plant. Here, five, seven, and eleven-days-old barley leaf which was cut into five, ten, and eleven sections, respectively were used. In the five-days-old

leaf, the Ca^{2+} response was higher in the leaf tip (S1) and decreased continually in the direction of the base (Fig. 11D). Interestingly, the seven-days-old leaf showed a kind U-shaped response wherein the response was highest at the tip (S1 - S3) and basal (S9 - S10) region of the leaf but lower in the mid-region (S4 - S8) (Fig. 11). In the eleven-days-old leaf, the response showed a U-shaped form, like for the seven-days-old leaf, from the tip S1 to the section S5, afterward the signal decreased more or less continually in the direction of the basal region of the leaf (S6 - S14) (Fig. 11F). No explanation could be found until now for this behavior, even though some patterns seem to be similar to those for the salt stress, such as that of the leaf tip (S1) response which kept decreasing (0.54, 0.38, 0.34 μM) as the age of the leaf increased (five, seven, and eleven- days-old). However, analyzing the kinetics of the Ca^{2+} response to oxidative stress showed that except for the amplitude of the peaks all other patterns are quite similar and thus indicated that the Ca^{2+} signature is nearly the same independently of the section or the age of the leaf (Fig. 11A - C).

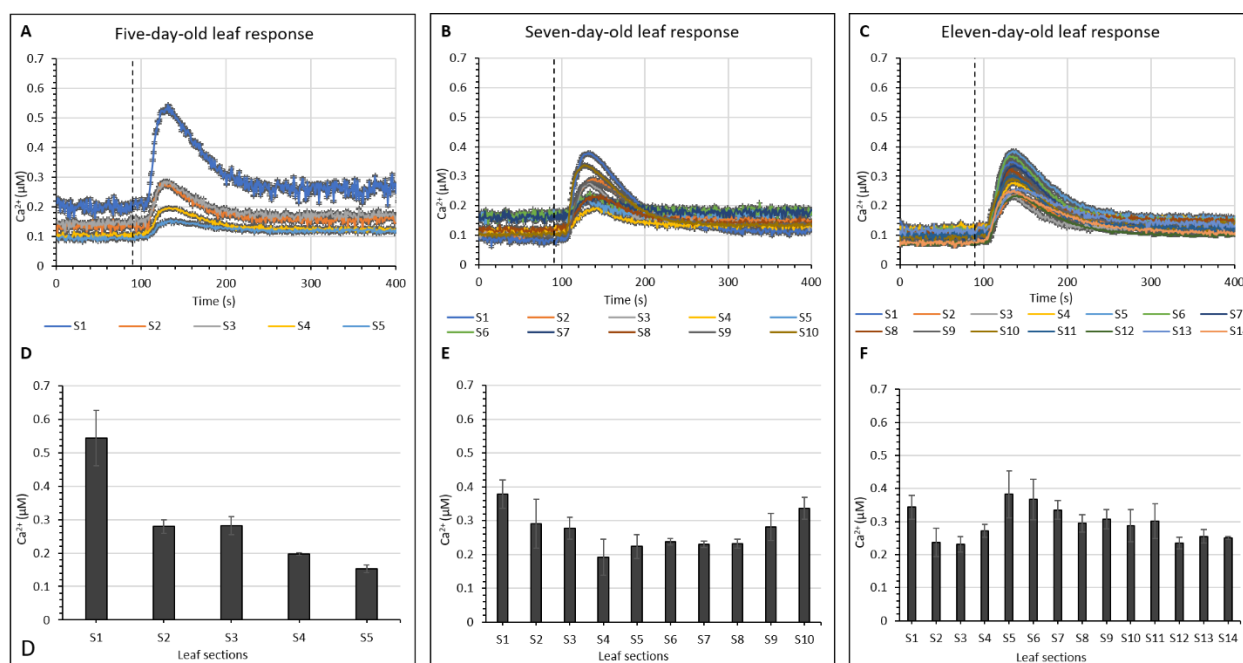


Figure 11. Aequorin-based luminescence in different ages and sections of the barley-Aeq leaf in response to H_2O_2 treatment measured in the luminometer: Changes in $[\text{Ca}^{2+}]_{\text{cyt}}$ (μM) in response to 10 mM H_2O_2 in five, seven and eleven-days-old barley leaf. S1 - S5 indicates the five sections in a five-days-old barley leaf, S1 - S10 indicates the ten sections in a ten-days-old leaf, and S1 - S14 indicates the fourteen sections in an eleven-days-old leaf. **A - C** shows the kinetics and **D - F** shows the Ca^{2+} concentrations in a bar graph representation. In A, B, and C the dotted line indicates injection of the stress. Error bar represents SE of triplicate reactions ($n=3$).

3.1.3.3 Ca²⁺ response after pre-treatment with Ca²⁺ channels and Ca²⁺ -ATPases inhibitors

To identify the source(s) of the Ca²⁺ during the response to oxidative stress, the inhibitors LaCl₃ and Tpg were used. Different concentrations of the inhibitors were used for pre-treatment of the leaf tip and root tip of barley before injecting 10 mM H₂O₂. Upon pre-treatment with LaCl₃, even a low concentration of 0.01mM contributed to a strong inhibition with more than 70% reduction of the response in the leaf tip of barley (Fig. 12A). Higher concentrations such as 0.1, 0.5, and 1 mM LaCl₃ increased the inhibition slightly more than 0.01mM. In the root tip, by contrast, 0.01 mM contributed only to a reduction of approximately 20%, while the strongest inhibition of approximately 70% reduction was reached with higher concentrations of 0.5 mM and 1 mM LaCl₃ (Fig. 12 B). These results indicated that the leaf tip is more sensitive to LaCl₃ than the root tip in barley.

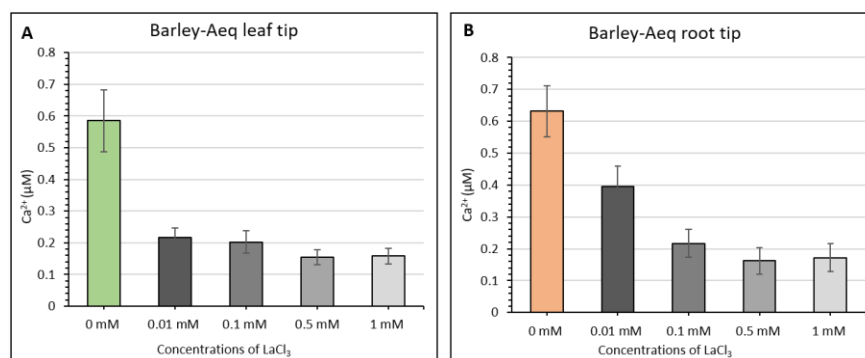


Figure 12. Effect of the inhibitor LaCl₃ on the H₂O₂ induced [Ca²⁺]_{cyt} signature measured in the luminometer: Changes in [Ca²⁺]_{cyt} (μM) in response to 10 mM H₂O₂ after pre-treatment with four different concentrations of LaCl₃ (0, 0.01, 0.1, 0.5 and 1 mM) in the leaf tip (A) and root tip (B) of barley-Aeq. Error bar represents SE of triplicate reactions (n=3).

In another experiment, the inhibition was performed by pre-treating with different concentrations of Tpg. As for LaCl₃, the inhibition was strong even with a low concentration of 0.01μM of Tpg in the leaf tip and reaching a maximum inhibition of 78% reduction of the [Ca²⁺]_{cyt} with 10 μM Tpg (Fig. 13A). By contrast, in the root tip, lower concentrations had an exceedingly small effect on the [Ca²⁺]_{cyt} (Fig. 13B). However, 10 μM Tpg showed a stronger inhibition with a 70% reduction of the [Ca²⁺]_{cyt}. From these results, it could be seen that the leaf tip of barley was more sensitive to the Tpg treatment than the root tip. Taken together, it could be concluded that, while the leaf is sensitive to both inhibitors, the roots seem to be less sensitive to Tpg compared to LaCl₃ in barley.

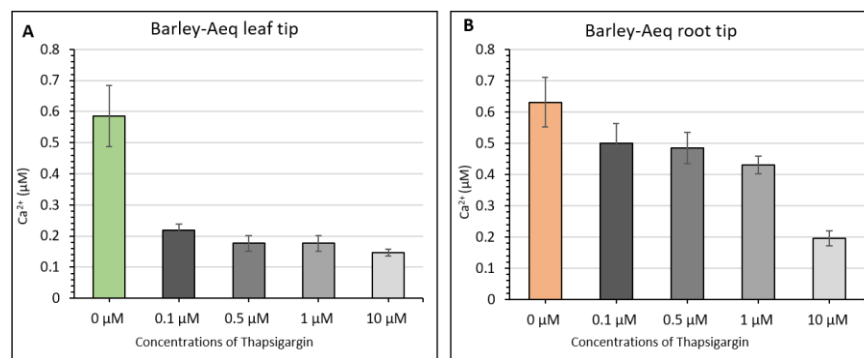


Figure 13. Effect of the inhibitor Thapsigargin on the H₂O₂ induced [Ca²⁺]_{cyt} signature measured in the luminometer: Changes in [Ca²⁺]_{cyt} (μM) in response to 10 mM H₂O₂ after pre-treatment with four different concentrations of Thapsigargin (0, 0.1, 0.5, 1 and 10 μM) in the leaf tip (A) and root tip (B) of barley-Aeq. Error bar represents SE of triplicate reactions (n=3).

To see the combined effect of both inhibitors and if this would fully inhibit the Ca²⁺ response mediated by H₂O₂ stress, a combination of both LaCl₃ and Tpg were used at a concentration of 1 mM and 10 μM, respectively. The inhibition of the Ca²⁺ response in the leaf tip after pretreatment with 1 mM LaCl₃ or 10 μM Tpg was 74% and 78%, respectively (Fig. 14A). This could further be increased to 84% by combining both the inhibitors. In the root tip, pretreatment with 1 mM LaCl₃ and 10 μM Tpg contributed to the inhibition of 73% and 70% of the Ca²⁺ response, respectively, which could further be increased to 79% when a combination of both inhibitors was used (Fig. 14B). Both inhibitors used alone or in combination could not fully inhibit the Ca²⁺ response, indicating that in addition to the extracellular matrix and the endomembrane system, it might be there are other Ca²⁺ sources involved in Ca²⁺ response to oxidative stress.

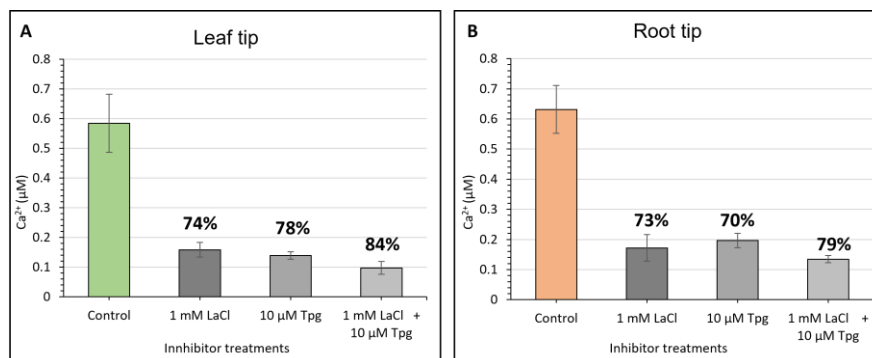


Figure 14. Effect of the inhibitor combination of LaCl₃ and Thapsigargin on the H₂O₂ induced [Ca²⁺]_{cyt} signature measured in the luminometer: Changes in [Ca²⁺]_{cyt} (μM) in response to 10 mM H₂O₂ after pretreatment with 1 mM LaCl₃, 10 μM Tpg and a combination of 1 mM LaCl₃ + 10 μM Tpg in the leaf tip (A) and root tip (B) of barley-Aeq. Percentage (%) indicates the percentage inhibition of the Ca²⁺ response. Error bar represents SE of triplicate reactions (n=3).

3.1.4 Barley transcriptome analysis upon oxidative stress

Transcriptomic studies offer an insight into the mechanisms of plant stress responses at molecular levels; hence, oxidative stress-induced global gene expression profiling was done in the shoots and roots of five-days-old wild type barley. To check if the LaCl_3 induced inhibition of the Ca^{2+} response affected the gene expression profile as well, the shoots and roots were pre-treated with 1 mM LaCl_3 before the application of oxidative stress. In this work, four different experimental conditions were used in which the barley shoots and roots were subjected to different treatments such as non-treated sample (Control), pre-treatment with LaCl_3 (1 hour), treatment with H_2O_2 (3 hours), and treatment with both LaCl_3 and H_2O_2 (pre-treatment with LaCl_3 for 1h followed by treatment with H_2O_2). Total RNA was extracted from these samples and then sent for RNA-Seq analysis. Since the results from the RNA-Seq analysis are still in progress, a summary of the differentially expressed genes (DEGs) in the shoots and roots has been presented here. A Venn diagram is shown here to compare different experimental conditions in terms of the number of DEGs.

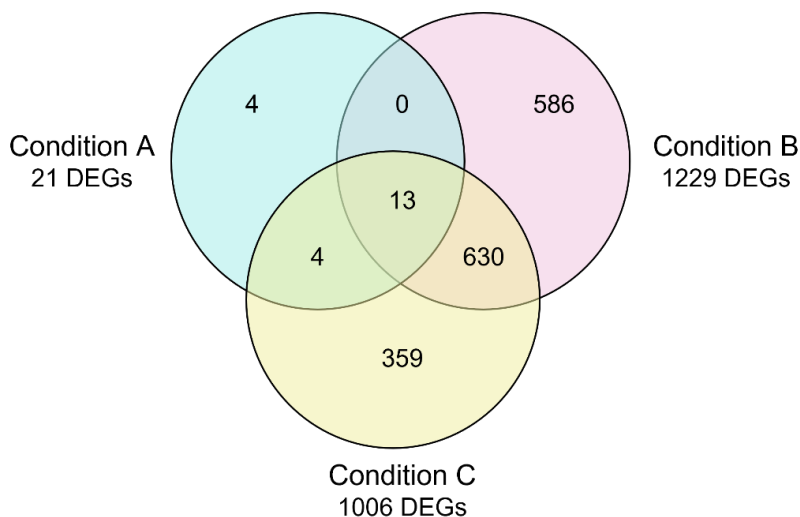


Figure 15. Venn diagram describing overlaps among differentially expressed genes (DEGs) in the shoots of barley upon different treatments: Condition A, B, and C indicate the DEGs expressed after pre-treatment with LaCl_3 , treatment with H_2O_2 , and a combination of both the pre-treatment with LaCl_3 followed by the treatment with H_2O_2 , respectively.

The DEGs from three conditions applied to the shoots of barley were used to create a Venn diagram as shown in Fig. 15. In the shoots, a total of 21, 1229, and 1006 DEGs were expressed in shoots pre-treated with LaCl_3 , treatment with H_2O_2 , and both pre-treatment with LaCl_3 followed by H_2O_2

treatment, respectively (Fig. 15). From the Venn diagram, it can also be seen that 0, 630, and 4 DEGs are commonly expressed between Condition A and B, Condition B and C, and Condition C and A, respectively. It can also be concluded from this diagram that there are 13 DEGs commonly expressed under pre-treatment with LaCl₃, treatment with H₂O₂, and with both LaCl₃ pre-treatment followed by H₂O₂ treatment. The 359 DEGs specifically expressed in Condition C (pre-treatment with LaCl₃ followed by treatment with H₂O₂) are of interest since these are specifically involved in Ca²⁺-signaling in response to oxidative stress. A gene ontology analysis revealed that these genes belong to categories such as the auxin, hormone, and chemical signaling-response genes, secondary metabolic process such as glutathione and lignin biosynthetic, and other metabolic processes. Out of the 359 DEGs, 130 were upregulated and 229 were downregulated.

Table 11: Summary of differentially expressed genes in barley shoots.

Condition	Sample	Upregulated	Downregulated
A	Control vs. treatment with LaCl ₃	1	20
B	Control vs. treatment with H ₂ O ₂	672	557
C	Control vs. treatment with both LaCl ₃ and H ₂ O ₂	430	576

From the RNA-Seq analysis, it was also possible to quantify the number of DEGs that are up and down-regulated under each condition in the shoot. As seen in the table above (Table 11), only 1 DEG was upregulated upon pre-treatment with LaCl₃ and 20 DEGs were downregulated. The treatment with H₂O₂ showed 672 and 557 DEGs up and down-regulated, respectively. The treatment with both LaCl₃ and H₂O₂ showed 430 and 576 DEGs up and downregulated in this condition.

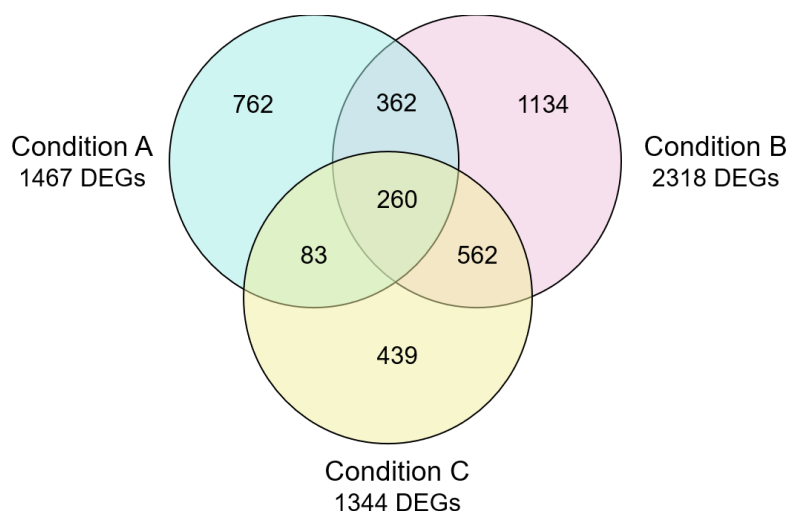


Figure 16. Venn diagram describing overlaps among differentially expressed genes (DEGs) in the roots of barley upon different treatments: Condition A, B, and C indicates the DEGs expressed after pre-treatment with LaCl_3 , treatment with H_2O_2 , and a combination of both the pre-treatment with LaCl_3 followed by the treatment with H_2O_2 , respectively.

Similar to the shoots, in the roots, a total of 1467, 2318, and 1344 DEGs were expressed after pre-treatment with LaCl_3 , treatment with H_2O_2 , and a combination of both the pre-treatment with LaCl_3 followed by the treatment with H_2O_2 , respectively (Fig. 16). From the Venn diagram, it can also be seen that there are 362, 562, and 83 DEGs that are commonly expressed between Condition A and B, Condition B and C, and Condition C and A, respectively. It can also be concluded from this diagram that there are 260 DEGs commonly expressed under treatment with LaCl_3 , H_2O_2 , and both LaCl_3 and H_2O_2 . As described earlier, among them the 439 DEGs are of interest since they might be involved in the Ca^{2+} -signaling in response to oxidative stress. Gene ontology analysis of these DEGs showed the involvement of these genes in response to wounding, the biological process involved in interspecies interaction between organisms, defense response, and nucleobase-containing compound metabolic process. Out of the 439 DEGs, 218 were upregulated and 221 were downregulated.

Table 12: Summary of differentially expressed genes in barley roots.

Condition	Sample	Upregulated	Downregulated
A	Control vs. treatment with LaCl_3	831	636
B	Control vs. treatment with H_2O_2	957	1361
C	Control vs. treatment with both LaCl_3 and H_2O_2	912	432

As seen in the table above (Table 12), 831 DEGs are upregulated in the pre-treatment with LaCl_3 and 636 DEGs are downregulated. The treatment with H_2O_2 showed 957 and 1361 DEGs up and downregulated in this condition. The pre-treatment with LaCl_3 followed by treatment with H_2O_2 showed 912 and 432 DEGs up and downregulated in this condition, respectively.

3.2 Analysis of RISP in Arabidopsis

For many years now, it is well known that mitochondria have their own Ca^{2+} -signaling (Slater & Cleland, 1953), although little is known about the pathways controlling it. The number of identified proteins that bind to the Ca^{2+} sensor, Calmodulin (CaM), is increasing not only in the cytosol but also in organelles such as chloroplast and mitochondria (Fuchs et al., 2011). Former investigations in our laboratory had identified RISP (Rieske iron-sulfur protein) as a CaM-binding protein in mitochondria of Arabidopsis (Nargis Parvin, Ph.D. thesis, 2016). Therefore, in this work, the exact function concerning CaM-binding and topology of RISP was analyzed.

3.2.1 Sequence analysis of RISP1 and RISP2

Using the bioinformatics tools available online, an in-depth analysis of RISP was performed as mentioned in Methods 2.2.3. In Arabidopsis RISP exists as two isoforms RISP1 (At5g13430) and RISP2 (At5g13440). A closer look at the genomic sequence of both proteins revealed that there is an overlap in the genome annotation between RISP1 and RISP2 in a way that a part of the 5' UTR of RISP1 is overlapping with the whole 3' UTR, whole exon 2, and a part of the intron of RISP2 (Fig. 17A). RISP1 protein is 272 AA in length and weighs about 26.9 kDa and RISP2 is 274 AA in length and weighs 29.9 kDa. The protein sequence of the two was subjected to a Multiple sequence alignment (MSA) and this revealed that there is a 94% sequence similarity between the two sequences (Fig. 17B). Both proteins contain an N-terminal transit peptide of 30 AA used for the targeting into the mitochondria. RISP proteins are predicted to have a consensus transmembrane domain (TMD1, A₁₁₁ to I₁₃₆ in RISP1 and A₁₁₃ to I₁₃₈ in RISP2) and a non-consensus TMD (TMD2, W₂₀₈ to W₂₂₇ in RISP1 and W₂₁₀ to W₂₂₉ in RISP2) (https://embnet.vital-it.ch/software/TMPRED_form.html). Both proteins also contain a potential CaM-binding domain (S₁₀₈ to Y₁₂₄ in RISP1 and S₁₁₀ to Y₁₂₆ in RISP2) as shown in Fig. 17B

(<http://calcium.uhnres.utoronto.ca/ctdb/ctdb/sequence.html>). The predicted CaM-binding domain is situated in the N-terminus of the proteins with a big part of it being on the TMD1.

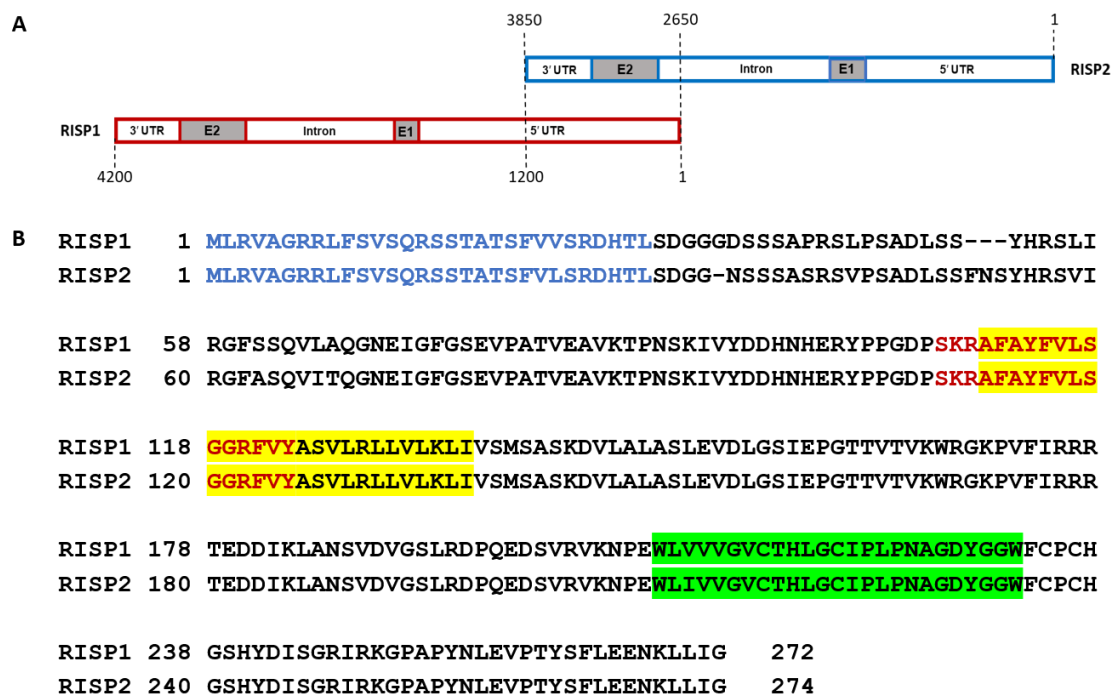


Figure 17. Gene assembly and protein sequence alignment of RISP1 and RISP2: (A) The genes of RISP1 and RISP2 are localized in the genome in such a way that the 5' UTR of RISP1 is overlapping with the 3' UTR, Exon 2, and Intron of RISP2. E1 and E2 indicate exon 1 and exon 2 respectively and 5' and 3' UTR indicates the 5' and 3' untranslated region. (B) The protein sequence of both RISP1 and RISP2 were extracted from Aramemnon (<http://aramemnon.uni-koeln.de/>) and subjected to MSA showing a 94% similarity between the two proteins. In blue is the transit peptide (M₁ to L₁₃₀), and in red is the potential CaM binding domain (S₁₀₈ to Y₁₂₄ in RISP1 and S₁₁₀ to Y₁₂₆ in RISP2), highlighted in yellow is the first consensus Transmembrane domain, and highlighted in green is the second non-consensus transmembrane domain.

At this point on, further analysis on RISP was carried out only with RISP2. BLAST analysis of RISP2 in other species including some of the Brassicaceae species, yeast, and human proteome was done (Fig. 18) (<https://blast.ncbi.nlm.nih.gov/Blast.cgi>). The transit peptide of *A. thaliana* RISP2 from M₁ to L₃₀ is well conserved in all the Brassicaceae species, but not in yeast and human indicating a mitochondrial targeting of RISP in plants. Throughout the rest of the protein, high sequence conservation was observed between *A. thaliana* and some of the Brassicaceae species such as *A. lyrata*, *C. sativa*, *C. rubella*, *B. rapa*, and *E. salsugineum*, however, less similarity has been found in other plant species such as *R. sativus*, *B. napus*, and *B. oleracea* and organisms like *H. sapiens* and *S. cerevisiae*. In *A. thaliana*, *A. lyrata*, *C. sativa*, *C. rubella*, *B. rapa*, and *E.*

salsugineum the sequence conservation also includes the predicted CaM-binding domain, suggesting a similar regulation of RISP by CaM in these species.

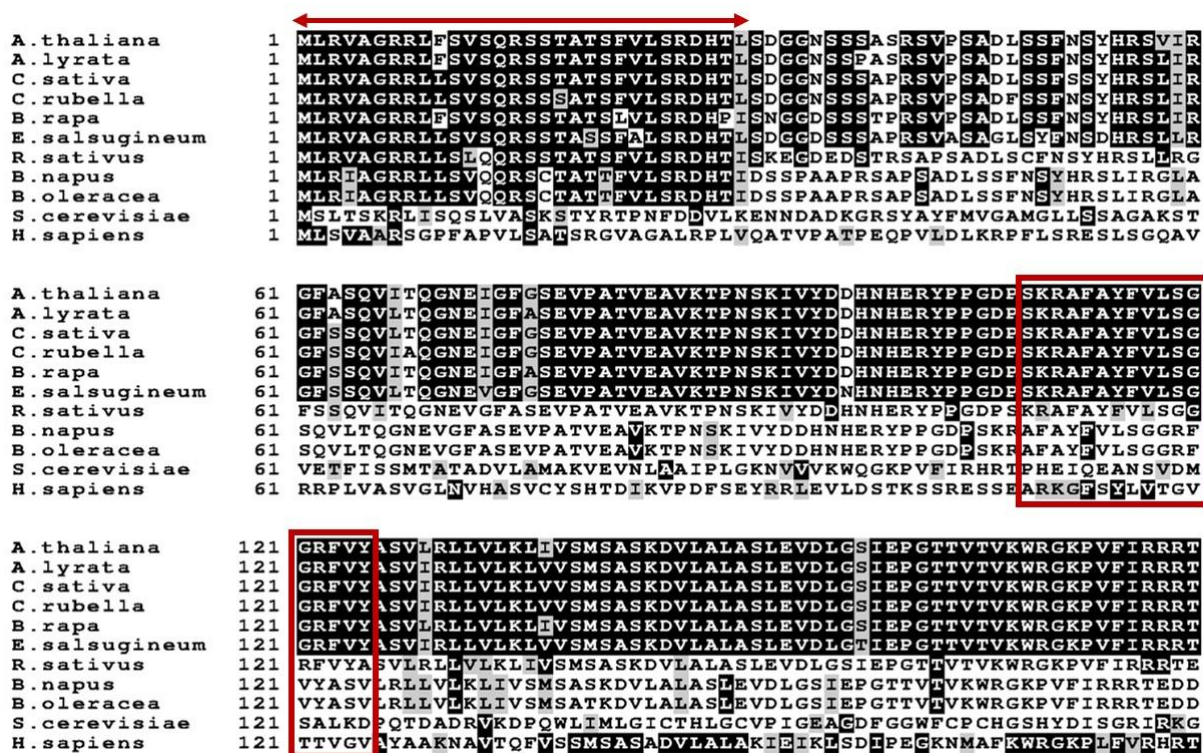


Figure 18. Alignment of the amino acid sequence of RISP from different organisms: The transit peptide (red arrow) is well conserved in all the Brassicaceae species, but the rest of the sequence stretch is conserved only in some of the Brassicaceae species including *A. lyrata*, *C. sativa*, *C. rubella*, *B. rapa* and *E. salsugineum*. The red box shows the predicted CaM binding domain which is also conserved in the mentioned Brassicaceae species. In some of the Brassicaceae species such as *R. sativus*, *B. napus*, and *B. oleracea* the CaM-binding domain is not conserved. This is also seen in *S. cerevisiae* and *H. sapiens*. Black shading – identical residue present in all sequences at the respective position. Grey shading – identical chemical property present in all sequences at the respective position. For species list and complete sequences see Appendix I.

The predicted CaM-binding sequence was then analyzed *in silico* using a web-based program (<http://calcium.uhnres.utoronto.ca/ctdb/ctdb/sequence.html>). The amino acids between 109 and 125 showed a high propensity for CaM binding (Fig. 19A). The criteria used for numbering are normalized by the program where score 0 and 9 represents the lowest and highest probable score, respectively. The sequence with the highest probable score was then used to form a helical wheel projection (<http://lbqp.unb.br/NetWheels/>). From this, it is also clear that a non-polar amphiphilic helix having a net charge of +3 can be formed in the region between Lys-110 (K) and Valine-124 (V) of RISP2 (Fig. 19B), which is a classic feature involved in CaM binding (O'Neil & DeGrado, 1990).

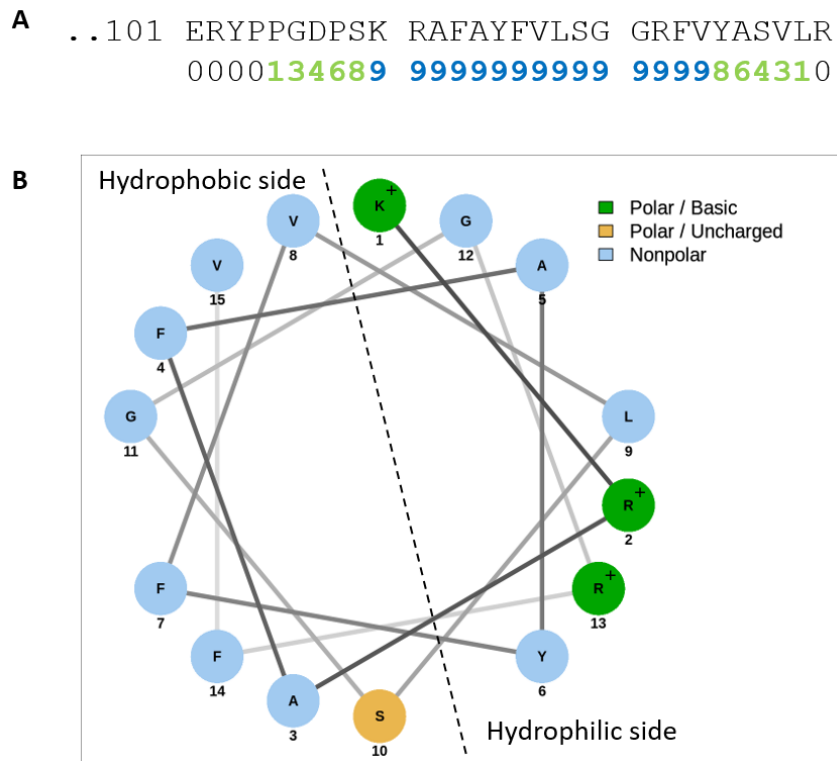


Figure 19. Analysis of the RISP2 CaM-binding domain: (A) Search analysis using the tool provided on the CaM target database (<http://calcium.uhnres.utoronto.ca/ctdb/ctdb/sequence.html>) predicted a potential CaM-binding site between AAs 110 and 124 of RISP2 (B) Helical wheel projection (<http://lbqp.unb.br/NetWheels/>) showed the formation of amphiphilic helix between AAs 110 and 125 of RISP2 sequence. Polar and nonpolar amino acids are shown using different colors as mentioned in the figure legend. The black dotted line separates the hydrophobic side from the hydrophilic side.

3.2.2 Production of specific antibody against RISP

For both the RISP isoforms several trials were made to express and purify the recombinant protein using the whole gene or truncated variants of it, different vectors, and different bacteria lines for the protein expression, which were all unsuccessful. However, a smaller fragment of the gene, RISP₂₅₂₋₁₀₇ (YHRSVIRGFASQVITQGNEIGFGSEVPATVEAVKTPNSKIVYDDHNERYPGDP) fused to an Intein-tag was successfully cloned into the pTWIN1 vector, which was then expressed, purified, and used as an antigen to produce specific antibodies.

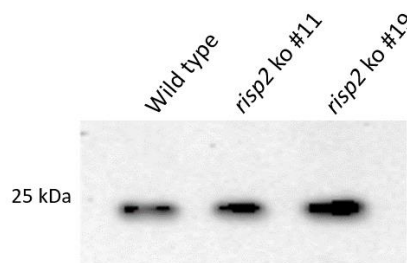


Figure 20. Immunodetection of wild type and *risp2 ko* mitochondrial extracts: Mitochondria extracted from Arabidopsis wild type and two *risp2* knockouts (ko #11 and #19) seedlings were separated on a 12% SDS gel, transferred to a PVDF membrane, and immunodetected with a self-made antibody that detects RISP2₅₂₋₁₀₇.

Two T-DNA insertion seed lines for RISP1 (SALK_146627 and SALK_115315) and RISP2 (SALK_064243 and SALK_135742) having a T-DNA insertion in the Exon 2 were obtained from NASC. These plants were screened for T-DNA insertions via PCR-genotyping. Homozygous mutants of RISP2 were obtained from both the SALK lines in the F3 generation but unfortunately, homozygous mutants of RISP1 were showing certain germination defects. Purified mitochondria from the wild type and two of the obtained homozygous *risp2* knockout lines (SALK_115315 - *risp2 ko* #11 and *risp2 ko* #19) were analyzed by immunodetection with the produced α -RISP2₅₂₋₁₀₇ antibody (Fig. 20). In the wild type, a band at 25 kDa could be detected, which fits the size of RISP2, indicating the successful reactivity of the produced antibody (Fig. 20). However, this antibody was not reacting specifically with RISP2, since a band at 25 kDa, similar to that detected in the wild type, could also be detected in the *risp2 ko* mutants. This band could correspond to RISP1 which is still expressed in the *risp2 ko* and has high similarity to the protein sequence of RISP2 could also be recognized by α RISP2₅₂₋₁₀₇.

3.2.3 RISP2 is a CaM-binding protein

To confirm the binding of RISP2 to CaM, affinity chromatography on CaM agarose was performed with mitochondrial extracts from Arabidopsis plants. After isolation of intact mitochondria, membrane proteins were obtained by solubilization using a non-ionic detergent. The extract was then used for affinity chromatography on CaM-agarose. The chromatography was performed in the presence or absence of CaCl₂ (Fig. 21). In the absence of CaCl₂, a mixture of EGTA + EDTA was added instead of CaCl₂. After collecting the flow-through (FT), the unbound proteins were

removed by washing extensively the beads with wash buffer (W). The proteins that were specifically bound to the CaM-agarose beads were then eluted competitively with elution buffer containing EGTA + EDTA or CaCl₂ depending on whether the chromatography was performed in the presence or absence of CaCl₂, respectively (Fig. 21, E1-E4).

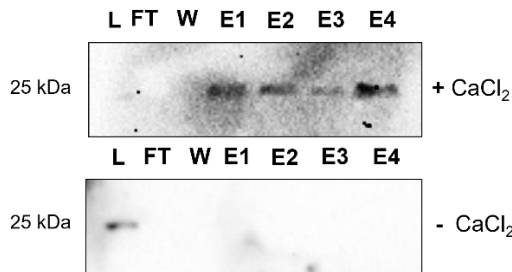


Figure 21. CaM-agarose affinity chromatography of Arabidopsis mitochondrial proteins: Affinity chromatography with n-Dodecyl β -D-maltoside-solubilized mitochondrial extract on CaM-agarose either in the presence of 1 mM CaCl₂ (+ CaCl₂, upper panel) or 5 mM EGTA + EDTA (- CaCl₂, lower panel). The samples were analyzed on SDS-PAGE followed by immunodetection with α -RISP2₅₂₋₁₀₇. Load (L), flow-through (FT), wash (W), elute (E1-4).

Aliquots from all samples were then separated on an SDS-PAGE, transferred to PVDF membrane, and then detected via immunodetection using the antibody α -RISP2₅₂₋₁₀₇. On the membrane, RISP2 could be detected in all four elutions in the assay performed in the presence of CaCl₂ but not in the absence of CaCl₂ (Fig. 21). The fact that RISP2 binds to CaM-agarose beads in the presence of CaCl₂ and can be eluted with EGTA + EDTA means that the interaction between CaM and RISP2 is Ca²⁺-dependent and that RISP2 is a genuine CaM target.

3.2.4 Topology of RISP

The transmembrane domain predictions of RISP were done using a web software (https://embnet.vital-it.ch/software/TMPRED_form.html) and the predicted TMDs are shown in Fig. 17B. As mentioned above two TMDs in RISP2 could be detected, TMD1, from A₁₁₃ to I₁₃₈, and a non-consensus TMD2 from W₂₁₀ to W₂₂₉. Since TMD2 is predicted as a non-consensus TMD, it was assumed that RISP has only one TMD, the TMD1 (Fig. 22A). Based on this, four different topology models could be supposed for RISP2 in the inner membrane of mitochondria (Fig. 22B). In the model I: C-terminus faces the intermembrane space (IMS), and N-terminus faces the matrix; in model II: both N- and C-terminus faces the matrix; in model III: N-terminus faces

the IMS, and C-terminus faces the matrix; and in model IV: both N- and C- terminus faces the IMS (Fig. 22B). To analyze which of these topology models are true, two different methods were used.

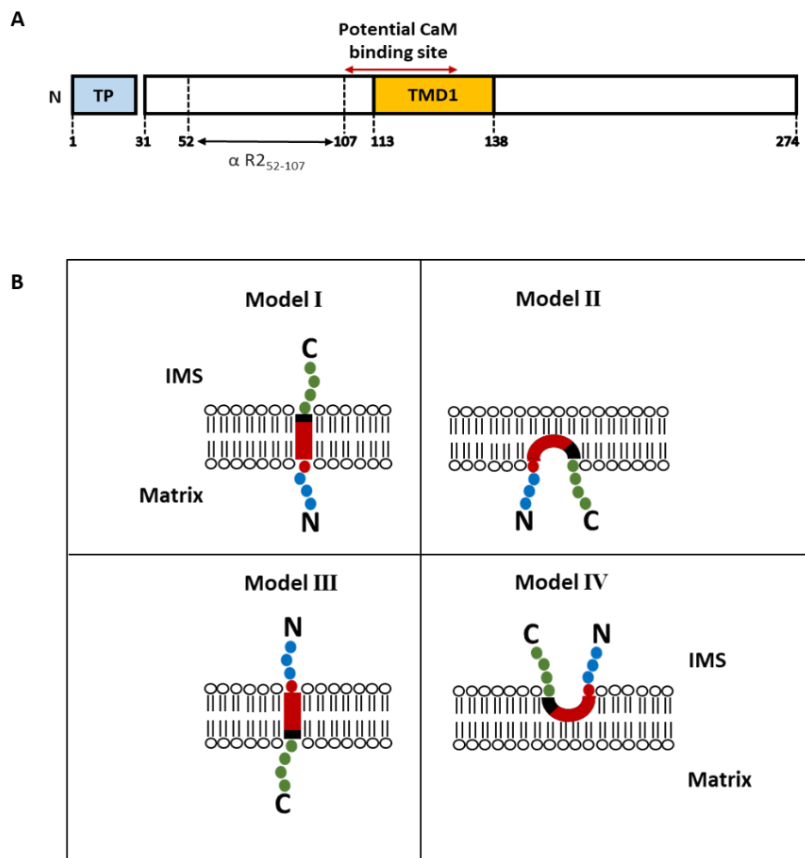


Figure 22. Topology model of RISP2: (A) Schematic presentation of RISP showing the transit peptide (TP), potential CaM binding site, and the consensus transmembrane domain (TMD1). The antibody was designed against the N-terminus (α -RISP2₅₂₋₁₀₇) as shown with the black arrow. (B) Four different topology models could be assumed for RISP protein in the inner membrane of the mitochondria. IMS: mitochondria intermembrane space, N: N- terminus; and C: C- terminus.

3.2.4.1 Localization of the C-terminus of RISP2

The self-assembly GFP (saGFP) system is a reliable tool used to confirm the subcellular localization of the proteins. In this system, the larger 1-10th β -sheets of GFP (saGFP₁₋₁₀) and the smaller 11th β -sheet (saGFP₁₁) are fused separately at the C-terminus of the protein of interest. The basic principle behind this experiment is that the two GFP-can fuse to each other only when they are in the same sub-compartment, without depending on the interaction of proteins that are fused to them. Therefore, the GFP can emit fluorescence only when both proteins fused to the

GFP-tags are targeted into the same cellular sub-compartment (Wiesemann et al., 2013). In this experiment, the RISP2 was fused to both saGFP₁₋₁₀ as well as saGFP₁₁. As a marker for the mitochondrial matrix, the protein Oxoglutaratdehydrogenase (OGD) was used and fused also to both saGFP₁₋₁₀ and saGFP₁₁. Tobacco leaves were co-transformed with various combinations of the constructs such as OGD-saGFP₁₋₁₀ + OGD-saGFP₁₁ (control) and OGD-saGFP₁₋₁₀ + RISP2-saGFP₁₁ using *Agrobacteria* bacteria mediated transient transformation.

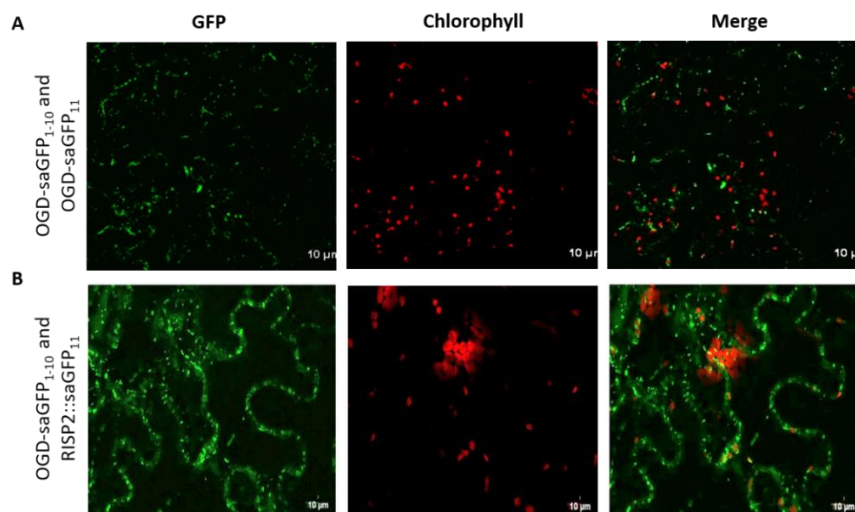


Figure 23. Analysis of the localization of C-terminus of RISP2: Leaves of *Nicotiana benthamiana* transiently co-expressing the saGFP constructs (A) OGD-saGFP₁₋₁₀ + OGD-saGFP₁₁ and in (B) OGD-saGFP₁₋₁₀ + RISP2-saGFP₁₁.

The transformation with the constructs OGD-saGFP₁₋₁₀ + RISP2-saGFP₁₁ showed a clear GFP-fluorescence signal with a dot-like structure in the whole cell of tobacco leaves (Fig.23B, GFP). These signals are not overlapping with the autofluorescence of the chlorophyll in the chloroplasts (Fig.23B, Chlorophyll and Merge) and seem to be similar to those show with the constructs OGD-saGFP₁₋₁₀ + OGD-saGFP₁₁ (Fig. 23A). OGD is used here as a marker protein for the mitochondrial matrix, therefore, the obtained results indicate that the C-terminus of RISP is localized in the matrix which in turn mean that model II or III for the topology of RISP could be correct and exclude the model I and IV (Fig. 22B).

3.2.4.2 Localization of the N-terminus of RISP2

To examine the localization of the RISP N-terminus, outer membrane ruptured mitochondria (mitoplast) and whole mitochondria as control were subjected to treatment with the protease

thermolysin. With this treatment, all the proteins or parts of its which are exposed outside of the inner membrane of mitochondria will be degraded by the thermolysin. The treated samples were then separated on a 12% SDS gel, transferred to a PVDF membrane, and then immunodetected with the α -RISP2₅₂₋₁₀₇ antibody. If model II is true, upon treatment with thermolysin the N-terminus should get digested, and a signal should no longer be visible after immunodetection. On the other hand, if model III is true, then the treatment with thermolysin will not digest the N-terminus since it is well protected within the membrane. Therefore, a signal should be visible after immunodetection. The blots of the thermolysin-untreated mitochondria and mitoplast samples revealed an expected band of 25 kDa size corresponding to the full-length RISP2 (Figure 24). However, the thermolysin-treated mitoplasts and mitochondria revealed an unexpected strong band at 20 kDa and a weak band at 25 kDa. The 25 kDa band corresponds to the rest of the undigested full-length RISP2. The 20 kDa band indicates that only a small part of the RISP protein was digested, while the rest of the protein is well protected inside the membrane. The digested 5 kDa of the protein might correspond to the N-terminus sequence between 31-81 AA which is not protected within the inner membrane or the matrix, while the rest of the N-terminus (82 - 113 AA) is protected and could still be detected by the α -RISP2₅₂₋₁₀₇ antibody. These results indicated that the N-terminus might be facing the intermembrane space, however, in a very recent article, the N-terminus of RISP in Arabidopsis was shown to be facing the mitochondrial matrix (Schäfer et al., 2020). Unfortunately, no conclusive results were obtained due to the contrasting evidence.

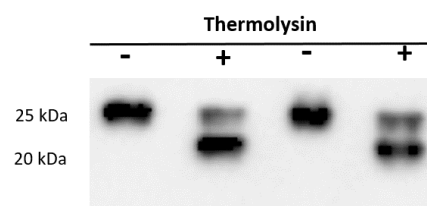


Figure 24. Immunodetection-based localization of the N-terminus of RISP2: Thermolysin treated and untreated mitoplast and mitochondria samples were resolved on a 12% SDS gel, transferred to a PVDF membrane, and then immunodetected with an antibody specific to RISP2₅₂₋₁₀₇. A double band was observed in the western blot for the mitoplast and mitochondria samples in the presence of thermolysin and in the absence of thermolysin, only a single band was observed in both samples.

3.2.5 Mitochondrial complex analysis in wild type and *risp2* knockout

RISP is a catalytic subunit of the complex III in the mitochondrial electron transport chain. To investigate if *risp2* ko could affect the complex formation in the mitochondria, solubilized mitochondrial protein complexes from wild type and *risp2* ko #19 mutant (SALK_115315) were analyzed by BN-PAGE. BN-PAGE is a technique for separating multiprotein complexes in their native conformation with a higher resolution, making it useful for determining protein complex sizes and relative abundance. Observable differences were seen clearly in Complex I and Complex III which are much less abundant in the mutant compared to the Wild type (Fig. 25). Differences could be also seen at the level of Complex F1, Complex IV, and two bands below Complex II which are more abundant in the mutant as in the wild type. This indicates that RISP2 could affect the formation of these complexes, however, it was not possible to confirm these results in other *risp2* ko lines (*risp2* ko #11, SALK_115315).

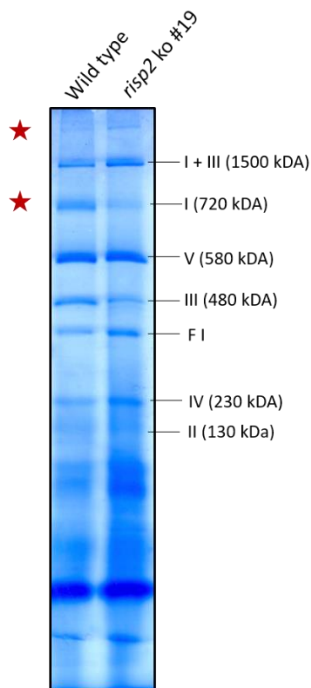


Figure 25. BN-PAGE analysis of mitochondria isolated from wild type and *risp2* ko #19: The running pattern of the protein samples gives us an indication that there are some clear differences in the Complex I and I + III in both samples. The most apparent differences are indicated by a red star.

4. Discussion

4.1 Ca²⁺ signaling in barley

Ca²⁺ serves as a secondary messenger in plant cells and is involved in a wide range of cellular processes. In the past years, researchers have gained more interest in investigating the role of the Ca²⁺ signaling network in plants (Pirayesh et al., 2021). Using recombinant aequorin for selectively monitoring Ca²⁺ concentration in the intracellular compartments is the most widely used technique of choice for studying the *in vivo* Ca²⁺ signatures. One of the significant benefits of using aequorin is the ability to target it to a specific intracellular compartment and thus measure [Ca²⁺] in that organelle selectively. Other advantages of using aequorin for Ca²⁺ measurements include the lack of side effects usually associated with fluorescent probes, such as buffering capability or toxicity (Brini et al., 1999). In Arabidopsis, many advances have been made in understanding the Ca²⁺ signatures in response to various biotic and abiotic stresses (Jiang et al., 2013; Kiegle et al., 2000). In this work, a transgenic line of barley (barley-Aeq), harboring the recombinant protein apoaequorin targeted to the cytosol was used to study the Ca²⁺ signatures for the very first time in this crop. Ca²⁺ signatures are Ca²⁺ transients that have a particular frequency, shape, and duration in response to various abiotic and biotic stresses, and they play an important role in the generation of stimulus-specific responses. In this work, changes in the [Ca²⁺]_{cyt} in the barley leaf tip, root tip, and whole seedling in response to different abiotic elicitors, such as salt and oxidative stress. Additionally, the Ca²⁺ response observed in barley-Aeq was compared to an established system in the model plant Arabidopsis (Knight, 1996; Knight et al., 1991).

4.1.1 Functionality of the barley-Aeq line

First, the functionality of the barley-Aeq line in reporting changes in [Ca²⁺]_{cyt} in response to salt and oxidative stresses was tested using the Photek and the luminometer. The luminescence imaging from the seedlings revealed a strong response in the roots to both salt and oxidative stresses (Fig. 3A and D). By contrast, the luminescence in the leaf was extremely weak especially in response to salt. One justification for this result might be that apoaequorin is not expressed or less expressed in the shoots compared to the roots or that the reconstitution of the aequorin from

the apoaequorin failed in the shoots. However, discharging the tissues with 1 M CaCl₂ solution showed that aequorin is expressed and reconstituted successfully in both leaf and roots (Fig. 3C and F). Despite the weak signals in the shoots, the expression of the aequorin could be confirmed by performing a western blot analysis using an antibody specific for aequorin (Fig. 1B). Due to the lower sensitivity of the Photek, further experiments were carried out only in the luminometer. To test the specificity of the response to the stress, the seedlings were injected with water (H₂O) instead of stressors and indeed, no signal could be recorded (Fig. 2). Using the luminometer, [Ca²⁺]_{cyt} measurements in the seedlings of barley-Aeq and Arabidopsis-Aeq were performed in a 24-well microplate and a 96-well microplate, respectively, due to their size difference. In barley, the pattern of the [Ca²⁺]_{cyt} increase is different between NaCl and H₂O₂ in terms of shape, amplitude, timing, and duration of the signal, indicating different Ca²⁺ signatures induced by these stimuli. Interestingly, the kinetics of the Ca²⁺ response to NaCl and H₂O₂ in Arabidopsis seedlings showed patterns quite similar to those obtained in barley. However, the amplitude of the peak varied especially upon salt stress application for which the response was much higher in Arabidopsis than in barley (Fig. 4). These results suggested that barley seedlings might be less sensitive to salt stress than Arabidopsis. The functionality and the specificity of the newly generated barley-Aeq line to report changes in the [Ca²⁺]_{cyt} in response to stress were confirmed from this experiment. To investigate the Ca²⁺ response in barley in a precise and detailed manner, further experiments were performed with the leaf tips and root tips of barley-Aeq.

In a previous study, aequorin-expressing tobacco cell cultures showed a biphasic [Ca²⁺]_{cyt} signature in response to H₂O₂ application (Lecourieux et al., 2005), where the appearance of the peaks was identical to that of the two [Ca²⁺]_{cyt} peaks seen in entire Arabidopsis seedlings (Rentel & Knight, 2004). In barley-Aeq seedlings a second peak was not observable until 5 minutes after application of H₂O₂, hence, it has to be investigated if a second peak occurs after 5 minutes. Comparing the results obtained in this experiment with the results published previously, it could be seen in the Arabidopsis-Aeq [Ca²⁺]_{cyt} measurements, that the measured [Ca²⁺]_{cyt} varied widely. In Arabidopsis, one study showed that 200 mM NaCl caused an increase to 0.8 μM Ca²⁺ in thirteen-days-old seedlings (Schmöckel et al., 2015) whereas in another study 200 mM NaCl showed an increase to 1.25 μM Ca²⁺ in twelve-days-old seedlings (Jiang et al., 2019). In this work, the maximum concentration used to test the five-days-old seedling was 250 mM NaCl, which detected only 0.5 μM Ca²⁺. Similarly, 10 mM H₂O₂ showed 2 μM Ca²⁺ (Jiang et al., 2013), whereas in

another study, only 0.45 μM Ca^{2+} could be detected (Rentel & Knight, 2004). In agreement with the experiment performed by Rentel and Knight, 2004 only 0.5 μM Ca^{2+} could be detected in this study as well. These results indicate that depending on the system or method of measurement used, the $[\text{Ca}^{2+}]_{\text{cyt}}$ can vary significantly. Another factor that could cause the difference in measured $[\text{Ca}^{2+}]_{\text{cyt}}$ could be the growth medium of the seedlings. In this work, the seedlings were grown on vermiculite whereas, in the above-mentioned experiments, the seedling was grown on $\frac{1}{2}$ MS media which contains macronutrients, micronutrients, and vitamins that could influence the measurement of Ca^{2+} .

4.1.2 NaCl induced Ca^{2+} response

To induce salt stress, different concentrations of NaCl were applied to leaf and root tips of five-days-old barley-Aeq seedlings. In both tissues, a dose-dependent increase in $[\text{Ca}^{2+}]_{\text{cyt}}$ was seen with the concentration of NaCl ranging from 50 mM to 250 mM NaCl (Fig. 5A and B). Salt stress in both tissues, resulted in a rapid increase in $[\text{Ca}^{2+}]_{\text{cyt}}$ within 10 seconds and declined quickly to reach basal levels (Fig. 5A and B) which is in agreement with the Ca^{2+} signatures observed in previous studies in rice (Zhang et al., 2015) and Arabidopsis (Knight et al., 1997). It could be possible that the salt sensors are present on the surface of the tissues and hence are strongly associated with Ca^{2+} channels, although there is no evidence for this in plants. These salt sensors can directly respond to different salt concentrations. The kinetics of the salt stress response was quite similar in the leaf tip and root tip, indicating similar Ca^{2+} signatures in both tissues. In Arabidopsis, the shoots and roots reacted to an increasing amount of NaCl in a similar manner to the barley tissues when comparing the first main Ca^{2+} spike, indicating a similar Ca^{2+} signature at this time point of the response (Fig. 5). However, in Arabidopsis, several delayed and small spikes could be observed, which are not present in barley (Fig. 5C and D). These small spikes might be a result of some delayed Ca^{2+} responses to salt stress in Arabidopsis. In general, the response in Arabidopsis shoots and roots was much higher than in barley tissues, confirming the results obtained in the whole seedling. These results suggested that barley is less sensitive to salt stress than Arabidopsis, which could be explained by the fact that barley is a salt-tolerant crop (Wu et al., 2014; Zhu et al., 2020). In Arabidopsis, it was found that the primary downstream targets in

salt induced Ca^{2+} signals are the calcium sensor SCaBP8 and the protein kinase2 (SOS2), which control and shape the Ca^{2+} signal by changing the activity of the calcium transporter or cofactor AtANN4 (Ma et al., 2019). Therefore, it is quite possible that this is true in barley as well and will have to be further investigated.

In another experiment, the Ca^{2+} signatures in different areas of the barley leaf and at different plant ages were elucidated. Comparing the kinetics of the Ca^{2+} response observed in the different leaf sections showed that except the $[\text{Ca}^{2+}]_{\text{cyt}}$, the patterns of the Ca^{2+} response were quite similar, indicating a similar Ca^{2+} signature in all leaf areas independent of the age of the leaf. Here, it could also be seen that independent of the age of the plant, the $[\text{Ca}^{2+}]_{\text{cyt}}$ in response to the applied salt stress was increasing from the tip to the base of the leaf. (Fig. 6). It was also worth noting that the $[\text{Ca}^{2+}]_{\text{cyt}}$ in the leaf tip kept decreasing with age, while in the base it stayed more or less the same. Barley being a monocot, cell division occurs at the base of the leaf, cells expansion in the mid-region and maturation of the cells are found at the tip of the leaf (Nelissen et al., 2016). This means the younger tissue in barley (base of the leaf) are more responsive to salt stress compared to the older tissues (tip of the leaf). In a study performed in *Coriandrum sativum* L. cv. Lemon, leaves of plants grown in hydroponics had elevated calcium in the older parts of the leaf (leaf center) compared with the younger parts of the leaf (leaf margin) (Kerton et al., 2009).

To investigate the source of Ca^{2+} in response to NaCl stress, inhibitors of the Ca^{2+} channels and Ca^{2+} -ATPases such as LaCl_3 and Tpg, respectively, were used. Due to its high positive charges, LaCl_3 cannot pass through the plasma membrane, thus it can prevent Ca^{2+} from entering the cells from the extracellular matrix which is considered as a Ca^{2+} store (Evans, 2013). On the other hand, Tpg is considered as a Ca^{2+} -ATPases blocker in the endomembrane compartments (Ordenes et al., 2002; Zhang et al., 2015). LaCl_3 and Tpg used alone or in combination could inhibit the Ca^{2+} response in barley leaf and roots, but not completely (Fig. 9), indicating that the source of Ca^{2+} during the response to salt stress could be other internal Ca^{2+} stores which still remain unknown. LaCl_3 and Tpg are affecting the Ca^{2+} response to the nearly same extent, indicating that the Ca^{2+} channels and the Ca^{2+} -ATPases contribute equally to the increase of $[\text{Ca}^{2+}]_{\text{cyt}}$ upon exposure to salt stress.

4.1.3 H₂O₂ induced Ca²⁺ response

Similar to salt stress response, the Ca²⁺ response in barley leaf tip and root tip was elucidated using different concentrations of H₂O₂. Unlike salt stress induce Ca²⁺ response, oxidative stress resulted in a delayed increase in [Ca²⁺]_{cyt} which lasted for about 100 seconds and took a long time to reach basal levels (Fig. 10) which is in agreement with the Ca²⁺ signatures observed in previous studies in rice (Zhang et al., 2015) and Arabidopsis (Rentel & Knight, 2004). Treatment of the tissues with H₂O₂ may cause oxidation in the first instance, and this might influence the calcium fluxes once it has been taken up by the cell through aquaporins, resulting in a delay in the Ca²⁺ response. The prolonged duration of the Ca²⁺ signal could indicate a complex and implicit the way of H₂O₂-induced [Ca²⁺]_{cyt} response. The Ca²⁺ signature in both tissues was quite similar, although the root tip showed a slightly higher [Ca²⁺]_{cyt} (Fig. 10A and B). The maximum response was seen in the leaf tip and root tip of barley-Aeq after the injection of 10 mM H₂O₂. However, a higher concentration of H₂O₂ evoked a decrease in the [Ca²⁺]_{cyt} response. An explanation for this may be that the high concentrations of H₂O₂ which are not physiological can result in cell death in barley, hence, causing a weaker [Ca²⁺]_{cyt} response. Another possibility is that the tissue simply does not respond in terms of [Ca²⁺]_{cyt} to higher levels of H₂O₂. The kinetics of the Ca²⁺ response in Arabidopsis showed clear differences, especially in the shape and duration of the spikes, to those obtained in barley in both leaf and root (Fig. 10C and D), suggesting different H₂O₂ induced Ca²⁺ signatures in both organisms. These results are not fitting to the results obtained with the whole seedlings which showed a similar Ca²⁺ signature in response to H₂O₂ in both barley and Arabidopsis. In shoot and root tissues of Arabidopsis, H₂O₂ induced Ca²⁺ peaks differed significantly (Rentel & Knight, 2004) as seen in the results from this study as well (Fig. 10C and D), and the reason for these changes remains unknown. In Arabidopsis, the activation of hyperpolarization activated Ca²⁺ permeable channels may be responsible for the [Ca²⁺]_{cyt} increase observed in response to H₂O₂ treatment (Rentel & Knight, 2004). These channels play a key role in abscisic acid signaling and mediate Ca²⁺ influx across the plasma membrane in response to H₂O₂ treatment in Arabidopsis guard cells (Pei et al., 2000). If similar channels also play a key role in the H₂O₂ induced Ca²⁺ signals in barley will have to be further investigated.

In the leaf area response experiment, the H₂O₂ induced Ca²⁺ response was investigated at different ages of barley leaves. In younger leaf (five-days-old), a decreasing Ca²⁺ response was seen from

the tip to base of the leaf (Fig. 11A and D). In the seven-days-old leaf, a “U-shaped” Ca^{2+} response was observed where the $[\text{Ca}^{2+}]_{\text{cyt}}$ decreased from the tip to the mid-area of the leaf and then increased in the direction of the base (Fig. 11B and E). In the older leaf (eleven-days-old), a stranger pattern in the Ca^{2+} response was obtained, where the response first behaved like in the seven-days-old leaf, but then the signal started decreasing in direction of the basal region of the leaf. (Fig. 11C and F). Why the different areas of the leaf are responding differently to oxidative stress is not yet clear. However, it is noteworthy that in all the leaf sections, the kinetics of the Ca^{2+} responses were similar indicating that the Ca^{2+} signature induced by H_2O_2 is the same in the whole leaf independent of the age and developmental stage. Natural accumulation of H_2O_2 is vital for seed germination (Bailly et al., 2008), plant growth (Černý et al., 2018), and senescence (Prochazkova et al., 2001) which occurs from the tips to the base of the leaves (Feller & Fischer, 1994). Therefore, one proposed explanation for the leaf blade's decreasing reaction to H_2O_2 could be the onset of early senescence, at the leaf tip being the oldest component of the leaf.

To investigate the source of Ca^{2+} in response to H_2O_2 stress, the Ca^{2+} channels and Ca^{2+} -ATPase inhibitors, LaCl_3 and Tpg, respectively, were used. While even small concentrations of LaCl_3 affected both the leaf tip as well as the root tip strongly, Tpg seemed to affect the leaf tip more than the root tip (Fig. 12 and 13). In the leaf tip, LaCl_3 and Tpg are affecting the Ca^{2+} response to the nearly same extent, indicating an equal contribution of the Ca^{2+} channels and Ca^{2+} -ATPase in the increase of $[\text{Ca}^{2+}]_{\text{cyt}}$ upon exposure to oxidative stress. LaCl_3 and Tpg used alone or in combination evoked a strong inhibition of the Ca^{2+} response in barley leaf and roots, but a total inhibition of Ca^{2+} was not observed indicating that there are other sources responsible for the increase in $[\text{Ca}^{2+}]_{\text{cyt}}$ apart from the Ca^{2+} channels and Ca^{2+} -ATPase of the endomembrane system, which has to be further elucidated (Fig. 14).

4.1.4 RNA-Seq analysis

RNA-sequencing (RNA-Seq) is a method that uses Next-Generation sequencing (NGS) to analyze the quantity and the RNA sequence in a sample. It examines the transcriptome, which is the gene expression patterns encoded in the RNA of a sample. Since the beginning of Ca^{2+} measurements in plants and mammals, Ca^{2+} signatures have been established in various species in response to

different abiotic and biotic stresses, nevertheless, the underlying reason for these specific signatures has never been studied further. To understand the downstream gene regulations in response to changes in the $[Ca^{2+}]_{\text{cyt}}$, barley shoot, and root samples were pretreated with $LaCl_3$ for or H_2O_2 or both and sent for RNA-Seq analysis. The RNA-Seq analysis clearly showed a significant number of up-and down-regulated genes in the stressed shoot and root samples. Although 1 mM $LaCl_3$ was enough to inhibit the Ca^{2+} response by 73% and 74% in the leaf tip and root tip of barley, respectively, for the RNA-Seq analysis 10 mM $LaCl_3$ was used to induce complete inhibition of the Ca^{2+} response. Among the three conditions used (Fig. 15 and 16 Condition A, B, and C), Condition C is more interesting wherein the shoots and roots have 359 and 439 DEGs specifically regulated due to the combined effect of $LaCl_3$ and H_2O_2 , respectively. Even though these numbers do not signify much at this stage, they are a clear indication that the tissues responded differently to the treatments and that this response is tissue specific. These results would have to be further analyzed to get conclusive results. To evaluate the contribution of increasing $[Ca^{2+}]_{\text{cyt}}$ responses in the NaCl and H_2O_2 induced gene expression, the expression levels of genes that were previously reported to be induced by abiotic stress in barley should be investigated. For example, these may include: HVA1 which is a group 3 LEA proteins that showed high accumulation during the response to abiotic stresses (Bhatnagar-Mathur et al., 2008) and the overexpression of barley HvWRKY38 (Xiong et al., 2010), HvDREB1 (Xu et al., 2009), HvSNAC1 (Al Abdallat et al., 2014), and HvCBF4 (Oh et al., 2007) has proven to be very effective in conferring abiotic stress tolerance.

In conclusion, the barley-Aeq line was able to respond to different concentrations of salt and oxidative stress. From the first look at the Ca^{2+} signatures in response to salt and oxidative stress, one can see the clear difference in signature concerning the magnitude and duration of the $[Ca^{2+}]_{\text{cyt}}$ response in both Arabidopsis and barley. The response was weaker in the whole seedlings, which were measured in the 24-well microplate, compared to the leaf tip and root tip which were measured in a 96-well microplate. The leaf tip and root tip samples showed an appropriate amount of response when compared to the shoot and root of Arabidopsis. However, to analyze the response from the whole leaf or whole root of barley, and to detect better signals from the seedling, a more appropriate method of photon detection will be essential. One possibility could be using a more sensitive luminometer that can detect the photons better from a 24-well microplate and using s

higher concentration of ethanol and CaCl_2 in the discharge solution to flush out the remaining aequorin which is essential for the precise Ca^{2+} measurements. Though the leaf area response could be studied by sectioning the leaves into different sections, it is possible that the cutting and handling of the sections could induce additional stress in the tissues. Nevertheless, this experiment helped in understanding that different areas of the leaf respond differently, and this difference is dependent on the age of the leaf. This experiment could not be done in the roots due to the varying root lengths and number of roots in each seedling. To investigate the Ca^{2+} response to other stresses such as drought, cold and heat stress, and other biotic stresses more experiments will have to be done by mimicking these stresses in the luminometer. All the measurements presented in this work are specifically for the cytosolic $[\text{Ca}^{2+}]$, therefore, to analyze the organellar $[\text{Ca}^{2+}]_{\text{cyt}}$ it would be necessary to target the apoaequorin to different organelles such as the chloroplast, mitochondria, vacuole, etc. and then study the stimulus-specific responses. In previous studies, this has already been established in *Arabidopsis* where the Aequorin was targeted to different organelles such as chloroplast stroma, thylakoid lumen, and thylakoid membrane (Sello et al., 2018) and mitochondria (Logan & Knight, 2003). Results from the RNA-Seq analysis showed some promising differences in the number of DEGs regulated between the shoots and roots upon pre-treatment with LaCl_3 and H_2O_2 . These results would be further analyzed to identify the gene clusters, gene ontologies, heat maps, and the selected candidates would be subjected to RT-qPCR analysis.

4.2 Analysis of RISP in *Arabidopsis*

Ca^{2+} being an important secondary messenger affects almost every aspect of the cellular metabolism in plants. By now, it is well known that a clear crosstalk exists between Ca^{2+} signaling and different signal transduction pathways induced by other messengers and hormones. Different Ca^{2+} sensors, like CaM and CMLs, can detect and decode stimulus-specific Ca^{2+} signals and forward the decoded information to downstream targets. These include a wide range of CaM-binding proteins in the cytosol as well as in organelles. RISP (Rieske iron-sulphur protein) is a subunit of the cytochrome *bc₁* complex in the mitochondria and was identified as a CaM-binding protein using CaM-agarose affinity chromatography followed by LC-MS/MS in previous work in

our laboratory (Nargis Parvin, Ph.D., 2016). In higher plants, the Rieske protein is a subunit of the chloroplast cytochrome *b₆f* complex and the mitochondrial cytochrome *bc₁* complex and is encoded in the nucleus (Huang et al., 1994; Knight et al., 2002). After the protein synthesis in the cytosol, the chloroplast and mitochondrial proteins are then targeted to their respective destinations via N-terminal transit peptides that mediate the transfer of polypeptides into the chloroplast or mitochondria. The chloroplast (At4g03280) and mitochondrial RISP (At5g13440) are only 40% identical (Appendix IV) and therefore might not have the same function as each other.

In Arabidopsis, RISP exists as two isoforms RISP1 (At5g13430) and RISP2 (At5g13440). A closer look at the gene annotation revealed that RISP1 and RISP2 have partially overlapping gene loci i.e., the 5' UTR of RISP1 is overlapping with the 3' UTR, Exon 2, and Intron of RISP2 (Fig. 17A). It is still unclear if RISP1 and RISP2 have the same function or if one of them exists as gene duplication. Further work in this project was carried out only with RISP2. Bioinformatics analysis of RISP2 revealed that it has two TMDs (TMD1 and TMD2) out of which TMD2 is considered as a non-consensus TMD. The Rieske iron-sulphur protein in *Saccharomyces cerevisiae* (yeast) mitochondria as well as the mammalian Iron Sulphur Protein (ISP) is known to have only one TMD (Conte & Zara, 2011; Iwata et al., 1998). A protein BLAST was performed to look for orthologs of RISP in other species including some Brassicaceae species, mammals, and yeast (Fig. 18). From the analysis, it could be seen that the transit peptide stretch (M₁ to L₃₀) is highly conserved among the Brassicaceae orthologues but not in mammals and yeast indicating a mitochondrial localization of the proteins in Brassicaceae. The rest of the sequence stretch including the CaM-binding domain is conserved in Arabidopsis, *A. lyrata*, *C. sativa*, *C. rubella*, *B. rapa*, and *E. salsugineum*. By contrast, in other plants like *R. sativus*, *B. napus*, and *B. oleracea* and in human and yeast the CaM-binding domain is not conserved, indicating that RISP in these organisms might not be regulated by CaM.

The cloning of RISP1 into different vectors using different tags for cloning was so far unsuccessful. Therefore, all further work with this isoform was abolished. The cloning of RISP2 also failed several times. However, it was possible to clone a smaller part of the protein (RISP2₅₂₋₁₀₇) into the pTWIN expression system, and hence the recombinant protein could be purified, although the expression of intein tagged RISP2₅₂₋₁₀₇ did not work reliably. Further cloning of this protein into other vectors has remained unsuccessful. To study the Ca²⁺/CaM interaction with RISP,

solubilized mitochondrial proteins were subjected to CaM affinity chromatography in the presence and absence of Ca^{2+} . In the presence of Ca^{2+} , RISP2 could be detected in the elutions. However, RISP2 did not appear in the elutions when Ca^{2+} was replaced with EDTA + EGTA (Fig. 21). A mixture of EDTA and EGTA is more selective for calcium ions and therefore can chelate all the remaining Ca^{2+} . These results confirmed that RISP2 is a CaM-binding protein and that the binding is Ca^{2+} -dependent.

RISP is known to be a part of the complex III of the mitochondrial respiratory chain. However, the exact topology remains unclear. Four predicted topology models have been suggested (Fig. 22B). To confirm which of the model is true, the C-terminus of RISP2 was cloned into the pBIN:saGFP vector for analysis by the self-assembly GFP system. Results from the saGFP analysis showed a clear localization of the C-terminus in the mitochondrial matrix when RISP was co-transformed with a mitochondrial marker protein (OGD) (Fig. 23). The localization in the intermembrane space was not possible since a fluorescence signal could not be observed when co-transformed with a marker for the IMS (data not shown). This indicated that the C-terminus of RISP2 faces the matrix, therefore models II or III are more likely to be true. To confirm which of the two models are true, the localization of the N-terminus was performed by immunodetection. Here the mitochondria and mitoplast (outer membrane ruptured mitochondria) treated with and without thermolysin were separated on an SDS gel and then immunodetected using the α -RISP₂₅₂₋₁₀₇. Treatment with thermolysin will digest any part of the protein which is exposed outside of the inner membrane of mitochondria. The results from the immunodetection were not entirely conclusive because when the mitoplast and mitochondrial samples were treated with thermolysin double bands were visible on the blots at 20 kDa and 25 kDa (Fig. 24). While the 25 kDa band represents the full-length RISP gene, the smaller band could indicate partial digestion of RISP. This implies only a part of RISP2 (~5 kDa) was digested by thermolysin and the rest of the protein might be still well protected within the respiratory complex III in the inner membrane. This means that a small part of the N-terminus is located in the intermembrane space (IMS). In a recent study, it was shown that the N-terminus of RISP faces the matrix but no clear evidence was shown about the C-terminus localization in Arabidopsis (Schäfer et al., 2020). In bovine heart mitochondria, the N and C-terminus of RISP was also shown to be facing the matrix (Xia et al., 1997). A year later, another group suggested that the bovine heart mitochondrial RISP undergoes a conformational change to form a “c1” state and a “b” state leaving the protein in two different

models (Iwata et al., 1998). In the absence and presence of stigmatellin, an inhibitory ligand, crystal structures of the chicken *bc₁* complex revealed that the Rieske protein's peripheral domain travels back and forth between sites proximal to cytochrome *b* and cytochrome *c₁* (Trumpower, 2013). All these results put together it might be concluded that plant mitochondrial RISP might exist as topology model II where the N and C- terminus faces the mitochondrial matrix and might also undergo conformational changes (Fig. 22B). Therefore, a crystal structure analysis of RISP might be required to confirm the exact topology of RISP.

If the N-terminus, which is harboring the CaM-binding domain, is facing the matrix that means that CaM regulation/interaction with RISP takes place on the matrix side. In our laboratory preliminary evidence of two CMLs, CML37 and CML38; to be localized in the matrix of mitochondria was identified. However, for confirming the mitochondrial matrix localization of both the CMLs in Arabidopsis, further experiments will be required. Once their mitochondrial matrix localization has been confirmed, they could be considered as potential interaction partners of RISP. Homozygous *risp1* and *risp2* T-DNA insertion lines were obtained from the F3 generation. Since one isoform is always active in both of the knockouts, a *risp1risp2* double knockout mutant would have to be established for further experiments. While the *risp2* knockouts did not show any phenotypic difference when compared to the wild type, the *risp1* knockout mutants had been consistently showing some germination defects on soil and on ½ MS plates. However, it is not quite clear whether these defects are indeed a phenotypic consequence of the disruption of the RISP1 locus. A more difficult problem is presented by the fact that RISP1 and RISP2 have partially overlapping gene loci, which implies that the single mutant cannot be successfully crossed to generate a double mutant. Hence, an RNAi or CRISPR/Cas9 approach might be needed to generate a double knockout mutant. From the BN-PAGE analysis, certain differences in the protein complexes could be seen between the wild type and *risp2* ko #19, but these differences could not be seen in other *risp2* knockouts. Though it is not clear why the different *risp2* knockouts behave differently, it could be possible that the presence of RISP1 in these knockouts might be a reason for the altered behavior of the mutants.

In this work, it was possible to identify the localization of the C-terminus of RISP2 facing the matrix via the self-assembly GFP assay and the N-terminus facing matrix via immunodetection using a self-made antibody. However, there is a possibility that the N and C- terminus are

interchangeable. Therefore, a crystal structure analysis of RISP might be required to confirm the exact topology of RISP. To confirm that RISP1/2 is a CaM binding protein that can bind to CaM exquisitely in the presence of Ca^{2+} a CaM affinity chromatography was performed. However, this could not be confirmed via cross-linking when whole mitochondrial extracts were used (data not shown). Due to the large pool of other proteins in this extract, it might be possible that RISP could not bind to CaM. Therefore, a recombinant protein or truncated version of RISP would be necessary to confirm the CaM binding feature of RISP. As discussed in the previous section, to further analyze the exact function of RISP in Arabidopsis it would be necessary to establish double knockout mutants and characterize them by comparison to the wild type. Additionally, to know which CaM/CML could be an interaction partner of RISP, interaction studies such as FRET analysis and/or biochemical interaction studies will have to be performed with mitochondrial CaMs and/or CMLs. To date only one CML, AtCML30 is known to be localized in the mitochondria (Chigri et al., 2012).

5. Summary

Ca^{2+} signatures are Ca^{2+} transients that have a particular frequency, shape, and duration in response to various abiotic and biotic stresses, and they play an important role in the generation of stimulus-specific responses. For the first time, in this work, Ca^{2+} signatures were established in *Hordeum vulgare* (barley) by using a transgenic line expressing the apoaequorin protein targeted to the cytosol. Using this barley-Aeq line it was possible to study changes in the $[\text{Ca}^{2+}]_{\text{cyt}}$ in the barley leaf, root, and whole seedling in response to different abiotic elicitors, such as salt and oxidative stress. Moreover, it allowed to compare the response of a crop to an established system in the model plant *Arabidopsis*. In general, both organisms show similar responses, even though in response to salt stress, barley showed a lower $[\text{Ca}^{2+}]_{\text{cyt}}$ spike compared to *Arabidopsis*. Using sections of five, seven, and eleven-days-old leaves of barley, it was further shown that different areas of the leaf respond differently to these stresses in terms of Ca^{2+} concentration, depending on the age of the seedling and the stress applied. In this study, it was also possible to further analyze the source of increasing $[\text{Ca}^{2+}]_{\text{cyt}}$ in response to the salt and oxidative stress using inhibitors of different Ca^{2+} channels. Furthermore, attempts were made in understanding the downstream processes following oxidative stress by performing an RNA-Seq analysis. Pretreatment of the samples with LaCl_3 before the oxidative stress allowed the differentiation between stress responses that require a Ca^{2+} signal and those that are Ca^{2+} independent.

Ca^{2+} sensor proteins are required to decode the Ca^{2+} signals induced by different stimuli to facilitate the appropriate response. Comprehending organellar Ca^{2+} signaling thus also requires the identification and characterization of new players as well as a better understanding of the previously discovered components of this signaling pathway. In previous work, RISP was identified as a mitochondrial $\text{CaM}/\text{Ca}^{2+}$ binding protein. In this work, efforts were made to further understand the topology and function of RISP especially concerning a potential CaM regulation. The *Arabidopsis* RISP has a conserved CaM binding domain predicted to be in the N-terminus. The $\text{CaM}/\text{Ca}^{2+}$ binding property of RISP2 was confirmed by performing a CaM affinity chromatography. From this work it could be assumed that the N- and C- terminus of RISP was found to be localized in the matrix, indicating that $\text{CaM}/\text{Ca}^{2+}$ regulation occurs from inside the organelle. However, it might be possible that RISP exists in a more complex, dynamic assembly within the mitochondrial inner membrane.

Zusammenfassung

Als Ca^{2+} -Signaturen bezeichnet man zeitliche Änderungen der Konzentration freier Ca^{2+} -Ionen, die eine bestimmte Frequenz, Form und Dauer besitzen. Diese besitzen einen Bezug zu verschiedenen biotischen und abiotischen Stressfaktoren, und können so eine Stimulus-abhängige Reizantwort erzeugen. In dieser Arbeit wurden zum ersten Mal Ca^{2+} -Signaturen in einer transgenen Linie von *Hordeum vulgare* (Gerste) etabliert. Durch Expression von Apoaequorin wurde eine Untersuchung der cytosolischen Ca^{2+} -Konzentration $[\text{Ca}^{2+}]_{\text{cyt}}$ in den Blättern, Wurzeln und kompletten jungen Pflanzen in Reaktion auf Salz und oxidativen Stress möglich. Auch konnten die Calcium-Signale der Nutzpflanze Gerste mit der etablierten Modellpflanze Arabidopsis verglichen werden. Generell waren die Reizantworten sehr ähnlich, allerdings zeigte Gerste bei Salzstress ein deutlich niedrigeres $[\text{Ca}^{2+}]_{\text{cyt}}$ Signal im Vergleich zu Arabidopsis. Weiterhin wurde überprüft, ob die Calciumsignale entlang der gesamten Blattspreite der Gerste identisch sind. Experimente mit Blattsegmenten von fünf-, sieben- und elf-Tage alte Gerstenblätter zeigten, dass die einzelnen Bereiche des Gerstenblattes auf die gesetzten Reize in Abhängigkeit vom Alter der Pflanze unterschiedlich reagieren. Analysen mit Inhibitoren bekannter Ca^{2+} -Kanaltypen gaben Hinweise auf mögliche Quelle der Ca^{2+} Signale. Zur Untersuchung nachgeschalteter Prozesse wurde zudem eine RNA-Seq-Analyse durchgeführt. Vorbehandlung der Proben mit LaCl_3 , einem Inhibitor von Ca^{2+} -Kanälen ermöglichte dabei, Ca^{2+} -abhängige und -unabhängige Stressantworten zu unterscheiden.

Calcium-Signale benötigen calcium-bindende Proteine, welche die Signale in eine zelluläre Reizantwort umwandeln. Das mitochondriale RISP Protein wurde in vorangegangenen Arbeiten als ein $\text{CaM}/\text{Ca}^{2+}$ -bindendes Protein identifiziert. In der hier vorliegenden Arbeit wurden verschiedene Analysen durchgeführt, um Erkenntnisse zur Topologie und die Funktion von RISP zu gewinnen. Für Arabidopsis RISP ist eine konservierte Bindungs-Domäne für CaM im N-Terminalen Bereich prognostiziert. Für die Isoform RISP2 konnte eine $\text{CaM}/\text{Ca}^{2+}$ -Bindung durch CaM -Affinitäts-Chromatographie bestätigt werden. Aus dieser Arbeit konnte angenommen werden, dass, dass N- und C-Terminus von RISP in der Matrix der Mitochondrien lokalisiert sind, was eine Regulierung durch organellinterne Calciumsignale nahe legt. Es kann jedoch nicht ausgeschlossen werden, dass RISP eine komplexere, dynamische Konfirmation aufweist.

Appendices

Appendix I: Protein sequences of RISP subjected to MSA

>*Arabidopsis thaliana*

MLRVAGRRLFSVSQRSSTATSFVLSRDHTLSDGGNSSSASRSVPSADLSSFNSYHRSVIR
GFASQVITQGNEIGFGSEVPATVEAVKTPNSKIVYDDHNHERYPPGDPSKRAFAYFVLSG
GRFVYASVLRLLVLKLVVMSASKDVLALASLEVDLGSIEPGTTVTVKWRGKPVFIRRR
EDDIKLANSVDVGSLRDPQEDSVRVKNPEWLIVVGVCTHLGCIPLNAGDYGGWFCPC
HGSHYDISGRIRKGPAPYNLEVPTYSFLEENKLLIG

>*Arabidopsis lyrata subsp. lyrata*

MLRVAGRRLFSVSQRSSTATSFVLSRDHTLSDGGNSSPASRSVPSADLSSFNSYHRSLIRG
FASQVLTQGNEIGFASEVPATVEAVKTPNSKIVYDDHNHERYPPGDPSKRAFAYFVLSG
GRFVYASVIRLLVLKLVVMSASKDVLALASLEVDLGSIEPGTTVTVKWRGKPVFIRRR
TEDDIKLANSVDVGSLRDPQEDSVRVKNPEWLIVVGVCTHLGCIPLNAGDYGGWFCPC
HGSHYDISGRIRKGPAPYNLEVPTYSFLEENKLLIG

>*Camelina sativa*

MLRVAGRRLLSVSQRSSTATSFVLSRDHTLSDGGNSSSAPRSVPSADLSSFSSYHRSLIRG
FSSQVLTQGNEIGFGSEVPATVEAVKTPNSKIVYDDHNHERYPPGDPSKRAFAYFVLSGG
RFVYASVIRLLVLKLVVMSASKDVLALASLEVDLGSIEPGTTVTVKWRGKPVFIRRRTE
DDIKLANSVDVGSLRDPQEDSVRVKNPEWLIVVGVCTHLGCIPLNAGDYGGWFCPC
GSHYDISGRIRKGPAPYNLEVPTYSFLEENKLLIG

>*Capsella rubella*

MLRVAGRRLLSVSQRSSATS FVLSRDHTLSDGGNSSSAPRSVPSADLSSFNSYHRSLIRG
FSSQVIAQNEIGFGSEVPATVEAVKTPNSKIVYDDHNHERYPPGDPSKRAFAYFVLSGG
RFVYASVIRLLVLKLVVMSASKDVLALASLEVDLGSIEPGTTVTVKWRGKPVFIRRRTE
DDIKLANSVDVGSLRDPQEDSVRVKNPEWLIVVGVCTHLGCIPLNAGDYGGWFCPC
GSHYDISGRIRKGPAPYNLEVPTYSFLEENKLLIG

>*Brassica rapa*

MLRVAGRRLFSVSQRSSTATSLVLSRDHPISNGGDSSSTPRSVPSADLSSFNZYHRSLIRG
 FSSQVITQGNEIGFASEVPATVEAVKTPNSKIVYDDHNHERYPPGDPSKRAFAYFVLSGG
 RFVYASVLRLLVKLIVSMSASKDVLALASLEVDLGSIEPGTTVTVKWRGKPVFIRRRTE
 DDIKLANSVDLGLSLRDPQEDAVRVKNPEWLVVVGVCVTHLGCIPNAGDYGGWFCPC
 GSHYDISGRIRKGPAPYNLEVPTYSFLEENKLLIG

>*Eutrema salsugineum*

MLRVAGRRLLSVSQRSSTASSFALSRDHTLSGGDSSSAPRSVASAGLSYFNSDHRSLLR
 GFSSQVLTQGNEVGFSEVPATVEAVKTPNSKIVYDNHNHERYPPGDPSKRAFAYFVLS
 GGRFVYASVIRLLVLKLVVMSASKDVLALASLEVDLGTIEPGTTVTVKWRGKPVFIR
 RTEDDIKLANSVDVGLSLRDPQEDSVRVKNPEWLVVVGVCVTHLGCIPNAGDYGGWFC
 PCHGSHYDISGRIRKGPAPYNLEVPTYSFLEENKLLIG

>*Raphanus sativus*

MLRVAGRRLSLQQRSSSTATSFVLSRDHTISKEGDEDSTRSAPSADLSCFNZYHRSLLRG
 FSSQVITQGNEVGFASEVPATVEAVKTPNSKIVYDDHNHERYPPGDPSKRAFAYFVLSG
 GRFVYASVLRLLVKLIVSMSASKDVLALASLEVDLGSIEPGTTVTVKWRGKPVFIRRR
 EDDIKLANSVDLGLSLRDPQEDSVRVKNPEWLVVVGVCVTHLGCIPNAGDYGGWFCPC
 HGSYDISGRIRKGPAPYNLEVPTYSFLEENKLLIG

>*Brassica napus*

MLRIAGRRLSVQQRSCATTFFVLSRDHTIDSSPAAPRSAPSADLSSFNZYHRSLIRGLAS
 QVLTQGNEVGFASEVPATVEAVKTPNSKIVYDDHNHERYPPGDPSKRAFAYFVLSGGRF
 VYASVLRLLVKLIVSMSASKDVLALASLEVDLGSIEPGTTVTVKWRGKPVFIRRRTE
 DDIKLANSVDLGLSLRDPQEDAVRVKNPEWLVVVGVCVTHLGCIPNAGDYGGWFCPC
 HGSYDISGRIRKGPAPYNLEVPTYSFLEENKLLIG

>*Brassica oleracea var. oleracea*

MLRIAGRRLSVQQRSCATTFFVLSRDHTIDSSPAAPRSAPSADLSSFNZYHRSLIRGLAS
 QVLTQGNEVGFASEVPATVEAVKTPNSKIVYDDHNHERYPPGDPSKRAFAYFVLSGGRF
 VYASVLRLLVKLIVSMSATKDVLAALASLEVDLGSIEPGTTVTVKWRGKPVFIRRRTE

DIKLANSVDLGTLRDPQEDAVRVKNPEWL VVVG VCTHLGCIPLNAGDYGGWFCPCHG
SHYDISGRIRKGPAPYNLEVPTYSFLEENKLLIG

> *Saccharomyces cerevisiae*

MSLTSKRLISQSLVASKSTYRTPNFDDVLKENNDADKGRSYAYFMVGMGLLSSAGAK
STVETFISSMTATADVLAMAKVEVNLA AIPLGKNVVVKWQGKPVFIRH RTPHEIQEANS
VDMSALKDPQTDADR VKDPQWLIMLGIC THLGCVPIGEAGDFGGWFCPCHGSHYDISG
RIRKGPAPLNLEIPAYEFDGDKVIVG

> *Homo sapiens*

MLSVAARSGPFAPVLSATSRGVAGALRPLVQATVPATPEQPVL DLKRPFLSRESLSGQA
VRRPLVASVGLNVHASVCYSHTDIKVPDFSEYRRLEVLDSTKSSRESSEARKGFSYLV TG
VTTVGVA YAAKNAV TQFVSSMSASADVLALAKIEIKLSDIPEGKNMAFKWRGKPLFVR
HRTQKEIEQEAAVELSQLRDPQHDLDRVKKPEWVILIGVCTHLGCVPIANAGDFGGYYC
PCHGSHYDASGRIRLGPAPLNLEVPTYEFTSDDMVIVG

Appendix II: Transmembrane domain prediction of RISP1



TMpred output for RISP1

[EMBnet-Server] Date: Wed May 5 20:53:26 2021

TMpred prediction output for : TMPRED.27425.7666.seq

Sequence: MLR...LIG length: 272
 Prediction parameters: TM-helix length between 17 and 33

1.) Possible transmembrane helices

=====

The sequence positions in brackets denominate the core region.
 Only scores above 500 are considered significant.

Inside to outside helices : 2 found

from	to	score	center
121 (121)	141 (141)	737	131
208 (208)	227 (227)	1109	218

Outside to inside helices : 2 found

from	to	score	center
111 (111)	136 (131)	1047	122
208 (208)	233 (225)	853	217


2.) Table of correspondences

=====

Here is shown, which of the inside->outside helices correspond to which of the outside->inside helices.
 Helices shown in brackets are considered insignificant.
 A "+" symbol indicates a preference of this orientation.
 A "++" symbol indicates a strong preference of this orientation.

inside->outside	outside->inside
121- 141 (21) 737	111- 136 (26) 1047 ++
208- 227 (20) 1109 ++	208- 233 (26) 853

Appendix III: Transmembrane domain prediction of RISP2



TMpred output for UNKNOWN

[EMBnet-Server] Date: Wed May 5 20:54:28 2021

TMpred prediction output for : TMPRED.26239.7377.seq

Sequence: MLR...LIG length: 274
 Prediction parameters: TM-helix length between 17 and 33

1.) Possible transmembrane helices
 =====
 The sequence positions in brackets denominate the core region.
 Only scores above 500 are considered significant.

Inside to outside helices : 2 found

from	to	score	center
123 (123)	143 (143)	737	133
210 (210)	229 (229)	1122	220

Outside to inside helices : 2 found

from	to	score	center
113 (113)	138 (133)	1047	124
210 (210)	235 (227)	943	219

2.) Table of correspondences
 =====
 Here is shown, which of the inside->outside helices correspond
 to which of the outside->inside helices.
 Helices shown in brackets are considered insignificant.
 A "+" symbol indicates a preference of this orientation.
 A "++" symbol indicates a strong preference of this orientation.

inside->outside	outside->inside
123- 143 (21) 737	113- 138 (26) 1047 ++
210- 229 (20) 1122 +	210- 235 (26) 943

3.) Suggested models for transmembrane topology
 =====
 These suggestions are purely speculative and should be used with
 EXTREME CAUTION since they are based on the assumption that
 all transmembrane helices have been found.
 In most cases, the Correspondence Table shown above or the
 prediction plot that is also created should be used for the
 topology assignment of unknown proteins.

Appendix IV: Sequence alignment between chloroplast and mitochondrial RISP

Descriptions Graphic Summary **Alignments** Dot Plot

Alignment view Pairwise [Restore defaults](#) Download

1 sequences selected

[Download](#) [Graphics](#) [Next](#) [Previous](#) [Descriptions](#)

At5g13440.1
 Sequence ID: **Query_15563** Length: 274 Number of Matches: 1

Range 1: 205 to 273 [Graphics](#) [Next Match](#) [Previous Match](#)

Score	Expect	Method	Identities	Positives	Gaps
55.8 bits(133)	6e-14	Compositional matrix adjust.	29/72(40%)	40/72(55%)	4/72(5%)

```

Query 142 VENDKTLATYGINAVCTHLGCV-VPWKAENKFLCPCHGSQYNAQGRVVRGPAPLSLALA 200
          V+N + L G VCTHLGC+ +P + CPCHGS Y+ GR+ +GPAP +L +
Sbjct 205 VKNPEWLIWVG--VCTHLGCIPLNAGDYGWFCPCCHGSHYDISGRIRKGPAPYNLEVP 261

Query 201 HADIDEAGKVLV 212
          E K+L
Sbjct 262 TYSFLEENKLLI 273
    
```

References

- AbdElgawad, H., Zinta, G., Hegab, M. M., Pandey, R., Asard, H., & Abuelsoud, W. (2016, 2016-March-08). High Salinity Induces Different Oxidative Stress and Antioxidant Responses in Maize Seedlings Organs [Original Research]. *Frontiers in Plant Science*, 7(276). <https://doi.org/10.3389/fpls.2016.00276>
- Adam, Z., & Ostersetzer, O. (2001). Degradation of unassembled and damaged thylakoid proteins. *Biochemical Society Transactions*, 29(4), 427-430. <https://doi.org/https://doi.org/10.1042/bst0290427>
- Ahmad, P., Jaleel, C. A., Salem, M. A., Nabi, G., & Sharma, S. (2010). Roles of enzymatic and nonenzymatic antioxidants in plants during abiotic stress. *Critical Reviews in Biotechnology*, 30(3), 161-175. <https://doi.org/https://doi.org/10.3109/07388550903524243>
- Al Abdallat, A., Ayad, J., Elenein, J. A., Al Ajlouni, Z., & Harwood, W. (2014). Overexpression of the transcription factor HvSNAC1 improves drought tolerance in barley (*Hordeum vulgare* L.). *Molecular Breeding*, 33(2), 401-414. <https://doi.org/https://doi.org/10.1007/s11032-013-9958-1>
- Allan, A. C., & Fluhr, R. (1997). Two distinct sources of elicited reactive oxygen species in tobacco epidermal cells. *The Plant Cell*, 9(9), 1559-1572. <https://doi.org/https://doi.org/10.1105/tpc.9.9.1559>
- Allen, D. G., & Prendergast, F. (1977). Aequorin luminescence: relation of light emission to calcium concentration--a calcium-independent component. *Science*, 195(4282), 996-998. <https://doi.org/https://doi.org/10.1126/science.841325>
- Apel, K., & Hirt, H. (2004). Reactive oxygen species: metabolism, oxidative stress, and signal transduction. *Annual Review of Plant Biology*, 55, 373-399. <https://doi.org/https://doi.org/10.1146/annurev.arplant.55.031903.141701>
- Assaha, D. V. M., Ueda, A., Saneoka, H., Al-Yahyai, R., & Yaish, M. W. (2017, 2017-July-18). The Role of Na⁺ and K⁺ Transporters in Salt Stress Adaptation in Glycophytes [Review]. *Frontiers in Physiology*, 8(509). <https://doi.org/10.3389/fphys.2017.00509>
- Bailly, C., El-Maarouf-Bouteau, H., & Corbineau, F. (2008). From intracellular signaling networks to cell death: the dual role of reactive oxygen species in seed physiology. *Comptes Rendus Biologies*, 331(10), 806-814. <https://doi.org/https://doi.org/10.1016/j.crv.2008.07.022>
- Batistič, O., & Kudla, J. (2012). Analysis of calcium signaling pathways in plants. *Biochimica et Biophysica Acta (BBA)-General Subjects*, 1820(8), 1283-1293. <https://doi.org/https://doi.org/10.1016/j.bbagen.2011.10.012>
- Batiza, A. F., Schulz, T., & Masson, P. H. (1996). Yeast respond to hypotonic shock with a calcium pulse. *Journal of Biological Chemistry*, 271(38), 23357-23362. <https://doi.org/https://doi.org/10.1074/jbc.271.38.23357>

- Belyavskaya, N. A. (1996). Calcium and graviperception in plants: inhibitor analysis. *International Review of Cytology*, 168, 123-185. [https://doi.org/https://doi.org/10.1016/S0074-7696\(08\)60884-0](https://doi.org/https://doi.org/10.1016/S0074-7696(08)60884-0)
- Benjamini, Y., & Hochberg, Y. (1995). Controlling the false discovery rate: a practical and powerful approach to multiple testing. *Journal of the Royal Statistical Society: Series B (Methodological)*, 57(1), 289-300. <https://doi.org/https://doi.org/10.1111/j.2517-6161.1995.tb02031.x>
- Berthomieu, P., Conéjéro, G., Nublat, A., Brackenbury, W. J., Lambert, C., Savio, C., Uozumi, N., Oiki, S., Yamada, K., & Cellier, F. (2003). Functional analysis of AtHKT1 in Arabidopsis shows that Na⁺ recirculation by the phloem is crucial for salt tolerance. *The EMBO Journal*, 22(9), 2004-2014. <https://doi.org/https://doi.org/10.1093/emboj/cdg207>
- Bevan, M. (1984). Binary Agrobacterium vectors for plant transformation. *Nucleic Acids Research*, 12(22), 8711-8721. <https://doi.org/https://doi.org/10.1093/nar/12.22.8711>
- Bhatnagar-Mathur, P., Vadez, V., & Sharma, K. K. (2008). Transgenic approaches for abiotic stress tolerance in plants: retrospect and prospects. *Plant Cell Reports*, 27(3), 411-424. <https://doi.org/https://doi.org/10.1007/s00299-007-0474-9>
- Bonza, M. C., Loro, G., Behera, S., Wong, A., Kudla, J., & Costa, A. (2013). Analyses of Ca²⁺ accumulation and dynamics in the endoplasmic reticulum of Arabidopsis root cells using a genetically encoded Cameleon sensor. *Plant Physiology*, 163(3), 1230-1241. [https://doi.org/ https://doi.org/10.1104/pp.113.226050](https://doi.org/https://doi.org/10.1104/pp.113.226050)
- Boudsocq, M., & Laurière, C. (2005). Osmotic signaling in plants. Multiple pathways mediated by emerging kinase families. *Plant Physiology*, 138(3), 1185-1194. <https://doi.org/https://dx.doi.org/10.1104%2Fpp.105.061275>
- Brini, M., Pinton, P., Pozzan, T., & Rizzuto, R. (1999). Targeted recombinant aequorins: Tools for monitoring [Ca²⁺] in the various compartments of a living cell. *Microscopy Research and Technique*, 46(6), 380-389. [https://doi.org/https://doi.org/10.1002/\(SICI\)1097-0029\(19990915\)46:6<380::AID-JEMT6>3.0.CO;2-Y](https://doi.org/https://doi.org/10.1002/(SICI)1097-0029(19990915)46:6<380::AID-JEMT6>3.0.CO;2-Y)
- Bush, D. S. (1995). Calcium regulation in plant cells and its role in signaling. *Annual Review of Plant Biology*, 46(1), 95-122. <https://doi.org/https://doi.org/10.1146/annurev.pp.46.060195.000523>
- Černý, M., Habánová, H., Berka, M., Luklova, M., & Brzobohatý, B. (2018). Hydrogen peroxide: its role in plant biology and crosstalk with signalling networks. *International Journal of Molecular Sciences*, 19(9), 2812. <https://doi.org/https://doi.org/10.3390/ijms19092812>
- Chen, Q., Vazquez, E. J., Moghaddas, S., Hoppel, C. L., & Lesnefsky, E. J. (2003). Production of reactive oxygen species by mitochondria: central role of complex III. *Journal of Biological Chemistry*, 278(38), 36027-36031. <https://doi.org/https://doi.org/10.1074/jbc.m304854200>

- Chen, W., He, Z. L., Yang, X. E., Mishra, S., & Stoffella, P. J. (2010). Chlorine nutrition of higher plants: progress and perspectives. *Journal of Plant Nutrition*, 33(7), 943-952. <https://doi.org/https://doi.org/10.1080/01904160903242417>
- Chen, Z., Cuin, T. A., Zhou, M., Twomey, A., Naidu, B. P., & Shabala, S. (2007). Compatible solute accumulation and stress-mitigating effects in barley genotypes contrasting in their salt tolerance. *Journal of Experimental Botany*, 58(15-16), 4245-4255. <https://doi.org/https://doi.org/10.1093/jxb/erm284>
- Chigri, F., Flosdorff, S., Pilz, S., Kölle, E., Dolze, E., Gietl, C., & Vothknecht, U. C. (2012). The Arabidopsis calmodulin-like proteins AtCML30 and AtCML3 are targeted to mitochondria and peroxisomes, respectively. *Plant Molecular Biology*, 78(3), 211-222. <https://doi.org/https://doi.org/10.1007/s11103-011-9856-z>
- Chinnusamy, V., Schumaker, K., & Zhu, J. K. (2004). Molecular genetic perspectives on cross-talk and specificity in abiotic stress signalling in plants. *Journal of Experimental Botany*, 55(395), 225-236. <https://doi.org/https://doi.org/10.1093/jxb/erh005>
- Choi, W.-G., Toyota, M., Kim, S.-H., Hilleary, R., & Gilroy, S. (2014). Salt stress-induced Ca²⁺ waves are associated with rapid, long-distance root-to-shoot signaling in plants. *Proceedings of the National Academy of Sciences*, 111(17), 6497-6502. <https://doi.org/https://doi.org/10.1073/pnas.1319955111>
- Cieśla, A., Mituła, F., Misztal, L., Fedorowicz-Strońska, O., Janicka, S., Tajdel-Zielińska, M., Marczak, M., Janicki, M., Ludwików, A., & Sadowski, J. (2016, 2016-October-25). A Role for Barley Calcium-Dependent Protein Kinase CPK2a in the Response to Drought [Original Research]. *Frontiers in Plant Science*, 7(1550). <https://doi.org/https://doi.org/10.3389/fpls.2016.01550>
- Coleman, J., & Palmer, J. (1971). Role of Ca²⁺ in the oxidation of exogenous NADH by plant mitochondria. *FEBS Letters*, 17(2), 203-208. [https://doi.org/https://doi.org/10.1016/0014-5793\(71\)80148-5](https://doi.org/https://doi.org/10.1016/0014-5793(71)80148-5)
- Colmenero-Flores, J. M., Martínez, G., Gamba, G., Vázquez, N., Iglesias, D. J., Brumós, J., & Talón, M. (2007). Identification and functional characterization of cation-chloride cotransporters in plants. *The Plant Journal*, 50(2), 278-292. <https://doi.org/https://doi.org/10.1111/j.1365-313X.2007.03048.x>
- Conte, L., & Zara, V. (2011). The Rieske Iron-Sulfur Protein: Import and Assembly into the Cytochrome bc 1 Complex of Yeast Mitochondria. *Bioinorganic Chemistry and Applications*, 2011. <https://doi.org/https://doi.org/10.1155/2011/363941>
- Cramer, G. R., & Nowak, R. S. (1992). Supplemental manganese improves the relative growth, net assimilation and photosynthetic rates of salt-stressed barley. *Physiologia Plantarum*, 84(4), 600-605. <https://doi.org/https://doi.org/10.1111/j.1399-3054.1992.tb04710.x>
- Csordás, G., Várnai, P., Golenár, T., Sheu, S.-S., & Hajnóczky, G. (2012). Calcium transport across the inner mitochondrial membrane: molecular mechanisms and pharmacology. *Molecular and Cellular Endocrinology*, 353(1-2), 109-113. <https://doi.org/https://dx.doi.org/10.1016%2Fj.mce.2011.11.011>

- DeFalco, T. A., Bender, K. W., & Snedden, W. A. (2010). Breaking the code: Ca²⁺ sensors in plant signalling. *Biochemical Journal*, 425(1), 27-40. <https://doi.org/https://doi.org/10.1042/BJ20091147>
- Deng, L., Vysotski, E. S., Markova, S. V., Liu, Z. J., Lee, J., Rose, J., & Wang, B. C. (2005). All three Ca²⁺-binding loops of photoproteins bind calcium ions: The crystal structures of calcium-loaded apo-aequorin and apo-obelin. *Protein Science*, 14(3), 663-675. <https://doi.org/https://dx.doi.org/10.1110%2Fps.041142905>
- Dodd, A. N., Kudla, J., & Sanders, D. (2010). The language of calcium signaling. *Annual Review of Plant Biology*, 61, 593-620. <https://doi.org/https://doi.org/10.1146/annurev-arplant-070109-104628>
- Drerup, M. M., Schlücking, K., Hashimoto, K., Manishankar, P., Steinhorst, L., Kuchitsu, K., & Kudla, J. (2013). The calcineurin B-like calcium sensors CBL1 and CBL9 together with their interacting protein kinase CIPK26 regulate the Arabidopsis NADPH oxidase RBOHF. *Molecular Plant*, 6(2), 559-569. <https://doi.org/https://doi.org/10.1093/mp/sst009>
- Evans, C. H. (2013). *Biochemistry of the Lanthanides* (Vol. 8). Springer Science & Business Media. <https://doi.org/https://doi.org/10.1007/978-1-4684-8748-0>
- Evans, J. L., Maddux, B. A., & Goldfine, I. D. (2005). The molecular basis for oxidative stress-induced insulin resistance. *Antioxidants & Redox Signaling*, 7(7-8), 1040-1052. <https://doi.org/https://doi.org/10.1089/ars.2005.7.1040>
- Feller, U., & Fischer, A. (1994). Nitrogen metabolism in senescing leaves. *Critical Reviews in Plant Sciences*, 13(3), 241-273. <https://doi.org/https://doi.org/10.1080/07352689409701916>
- Forster, B. P. (2001). Mutation genetics of salt tolerance in barley: an assessment of Golden Promise and other semi-dwarf mutants. *Euphytica*, 120(3), 317-328. <https://doi.org/https://doi.org/10.1023/A%3A1017592618298>
- Fricke, M., Gilroy, S., Read, N., & Trewavas, A. (1991). Visualisation and measurement of the calcium message in guard cells. *Symposia of the Society for Experimental Biology*,
- Fu, L., Shen, Q., Kuang, L., Yu, J., Wu, D., & Zhang, G. (2018). Metabolite profiling and gene expression of Na/K transporter analyses reveal mechanisms of the difference in salt tolerance between barley and rice. *Plant Physiology and Biochemistry*, 130, 248-257. <https://doi.org/https://doi.org/10.1016/j.plaphy.2018.07.013>
- Fuchs, M., Vothknecht, U., & Chigri, F. (2011). Calmodulin and calmodulin-like proteins in *Arabidopsis thaliana*. *J Endocytobiosis Cell Res.*, 21, 114-121.
- Furuya, T., Okura, M., Ruiz, F. A., Scott, D. A., & Docampo, R. (2001). TcSCA complements yeast mutants defective in Ca²⁺ pumps and encodes a Ca²⁺-ATPase that localizes to the endoplasmic reticulum of *Trypanosoma cruzi*. *Journal of Biological Chemistry*, 276(35), 32437-32445. <https://doi.org/https://doi.org/10.1074/jbc.M104000200>

- Gürel, F., Öztürk, Z. N., Uçarlı, C., & Rosellini, D. (2016, 2016-August-03). Barley Genes as Tools to Confer Abiotic Stress Tolerance in Crops [Mini Review]. *Frontiers in Plant Science*, 7(1137). <https://doi.org/https://doi.org/10.3389/fpls.2016.01137>
- Harnisch, U., WEISS, H., & Sebald, W. (1985). The primary structure of the iron-sulfur subunit of ubiquinol—cytochrome c reductase from *Neurospora*, determined by cDNA and gene sequencing. *European Journal of Biochemistry*, 149(1), 95-99. <https://doi.org/https://doi.org/10.1111/j.1432-1033.1985.tb08898.x>
- Hasegawa, P. M., Bressan, R. A., Zhu, J.-K., & Bohnert, H. J. (2000). Plant cellular and molecular responses to high salinity. *Annual Review of Plant Biology*, 51(1), 463-499. <https://doi.org/https://doi.org/10.1146/annurev.arplant.51.1.463>
- Hashimoto, K., & Kudla, J. (2011). Calcium decoding mechanisms in plants. *Biochimie*, 93(12), 2054-2059. <https://doi.org/https://doi.org/10.1016/j.biochi.2011.05.019>
- Hodges, T., & Hanson, J. (1965). Calcium accumulation by maize mitochondria. *Plant Physiology*, 40(1), 101. <https://doi.org/https://doi.org/10.1104/pp.40.1.101>
- Horie, T., Motoda, J., Kubo, M., Yang, H., Yoda, K., Horie, R., Chan, W. Y., Leung, H. Y., Hattori, K., & Konomi, M. (2005). Enhanced salt tolerance mediated by AtHKT1 transporter-induced Na⁺ unloading from xylem vessels to xylem parenchyma cells. *The Plant Journal*, 44(6), 928-938. <https://doi.org/https://doi.org/10.1111/j.1365-313x.2005.02595.x>
- Huang, J., Struck, F., Matzinger, D. F., & Levings, C. S. (1991). Functional analysis in yeast of cDNA coding for the mitochondrial Rieske iron-sulfur protein of higher plants. *Proceedings of the National Academy of Sciences*, 88(23), 10716-10720. <https://doi.org/https://dx.doi.org/10.1073%2Fpnas.88.23.10716>
- Huang, J., Struck, F., Matzinger, D. F., & Levings, C. S. (1994). Flower-enhanced expression of a nuclear-encoded mitochondrial respiratory protein is associated with changes in mitochondrion number. *The Plant Cell*, 6(3), 439-448. <https://doi.org/https://doi.org/10.1105/tpc.6.3.439>
- Hura, T. (2020). Wheat and Barley: Acclimatization to Abiotic and Biotic Stress. *International Journal of Molecular Sciences*, 21(19), 7423. <https://doi.org/https://www.mdpi.com/1422-0067/21/19/7423>
- Imani, J., Li, L., Schaefer, P., & Kogel, K. H. (2011). STARTS—A stable root transformation system for rapid functional analyses of proteins of the monocot model plant barley. *The Plant Journal*, 67(4), 726-735. <https://doi.org/https://doi.org/10.1111/j.1365-313x.2011.04620.x>
- Iwano, M., Entani, T., Shiba, H., Kakita, M., Nagai, T., Mizuno, H., Miyawaki, A., Shoji, T., Kubo, K., & Isogai, A. (2009). Fine-tuning of the cytoplasmic Ca²⁺ concentration is essential for pollen tube growth. *Plant Physiology*, 150(3), 1322-1334. <https://doi.org/https://dx.doi.org/10.1104%2Fpp.109.139329>
- Iwata, S., Lee, J. W., Okada, K., Lee, J. K., Iwata, M., Rasmussen, B., Link, T. A., Ramaswamy, S., & Jap, B. K. (1998). Complete structure of the 11-subunit bovine mitochondrial

- cytochrome bcl complex. *Science*, 281(5373), 64-71.
<https://doi.org/https://doi.org/10.1126/science.281.5373.64>
- James, R. A., Blake, C., Byrt, C. S., & Munns, R. (2011). Major genes for Na⁺ exclusion, Nax1 and Nax2 (wheat HKT1; 4 and HKT1; 5), decrease Na⁺ accumulation in bread wheat leaves under saline and waterlogged conditions. *Journal of Experimental Botany*, 62(8), 2939-2947. <https://doi.org/https://doi.org/10.1093/jxb/err003>
- Janiak, A., Kwasniewski, M., Sowa, M., Gajek, K., Żmuda, K., Kościelniak, J., & Szarejko, I. (2018, 2018-January-09). No Time to Waste: Transcriptome Study Reveals that Drought Tolerance in Barley May Be Attributed to Stressed-Like Expression Patterns that Exist before the Occurrence of Stress [Original Research]. *Frontiers in Plant Science*, 8(2212). [https://doi.org/ https://doi.org/10.3389/fpls.2017.02212](https://doi.org/https://doi.org/10.3389/fpls.2017.02212)
- Jiang, Z., Zhou, X., Tao, M., Yuan, F., Liu, L., Wu, F., Wu, X., Xiang, Y., Niu, Y., & Liu, F. (2019). Plant cell-surface GIPC sphingolipids sense salt to trigger Ca²⁺ influx. *Nature*, 572(7769), 341-346. <https://doi.org/https://doi.org/10.1038/s41586-019-1449-z>
- Jiang, Z., Zhu, S., Ye, R., Xue, Y., Chen, A., An, L., & Pei, Z.-M. (2013). Relationship between NaCl-and H₂O₂-induced cytosolic Ca²⁺ increases in response to stress in Arabidopsis. *PLoS One*, 8(10), e76130. <https://doi.org/https://doi.org/10.1371/journal.pone.0076130>
- Kerton, M., Newbury, H. J., Hand, D., & Pritchard, J. (2009). Accumulation of calcium in the centre of leaves of coriander (*Coriandrum sativum* L.) is due to an uncoupling of water and ion transport. *Journal of Experimental Botany*, 60(1), 227-235. <https://doi.org/https://doi.org/10.1093/jxb/ern279>
- Kiegle, E., Moore, C. A., Haseloff, J., Tester, M. A., & Knight, M. R. (2000). Cell-type-specific calcium responses to drought, salt and cold in the Arabidopsis root. *The Plant Journal*, 23(2), 267-278. <https://doi.org/https://doi.org/10.1046/j.1365-313x.2000.00786.x>
- Kiep, V., Vadassery, J., Lattke, J., Maaß, J. P., Boland, W., Peiter, E., & Mithöfer, A. (2015). Systemic cytosolic Ca²⁺ elevation is activated upon wounding and herbivory in Arabidopsis. *New Phytologist*, 207(4), 996-1004. <https://doi.org/https://doi.org/10.1046/j.1365-313x.2000.00786.x>
- Kim, D., Pertea, G., Trapnell, C., Pimentel, H., Kelley, R., & Salzberg, S. L. (2013). TopHat2: accurate alignment of transcriptomes in the presence of insertions, deletions and gene fusions. *Genome Biology*, 14(4), 1-13. [https://doi.org/ https://doi.org/10.1186/gb-2013-14-4-r36](https://doi.org/https://doi.org/10.1186/gb-2013-14-4-r36)
- Knight, H. (1996). Trewavas. AJ and Knight, MR (1996) Cold calcium signaling in Arabidopsis involves two cellular pools and a change in calcium signature after acclimation. *Plant Cell*, 8, 489-503. <https://doi.org/https://doi.org/10.1105/tpc.8.3.489>
- Knight, H., Brandt, S., & Knight, M. R. (1998). A history of stress alters drought calcium signalling pathways in Arabidopsis. *The Plant Journal*, 16(6), 681-687. <https://doi.org/https://doi.org/10.1046/j.1365-313x.1998.00332.x>

- Knight, H., Trewavas, A. J., & Knight, M. R. (1996). Cold calcium signaling in Arabidopsis involves two cellular pools and a change in calcium signature after acclimation. *The Plant Cell*, 8(3), 489-503. <https://doi.org/https://doi.org/10.1105/tpc.8.3.489>
- Knight, H., Trewavas, A. J., & Knight, M. R. (1997). Calcium signalling in Arabidopsis thaliana responding to drought and salinity. *The Plant Journal*, 12(5), 1067-1078. <https://doi.org/https://doi.org/10.1046/j.1365-313x.1997.12051067.x>
- Knight, J. S., Duckett, C. M., Sullivan, J. A., Walker, A. R., & Gray, J. C. (2002). Tissue-specific, light-regulated and plastid-regulated expression of the single-copy nuclear gene encoding the chloroplast Rieske FeS protein of Arabidopsis thaliana. *Plant and Cell Physiology*, 43(5), 522-531. <https://doi.org/https://doi.org/10.1093/pcp/pcf062>
- Knight, M. R., Campbell, A. K., Smith, S. M., & Trewavas, A. J. (1991). Transgenic plant aequorin reports the effects of touch and cold-shock and elicitors on cytoplasmic calcium. *Nature*, 352(6335), 524-526. <https://doi.org/https://doi.org/10.1038/352524a0>
- Kong, L., Liu, Y., Wang, X., & Chang, C. (2020). Insight into the role of epigenetic processes in abiotic and biotic stress response in wheat and barley. *International Journal of Molecular Sciences*, 21(4), 1480. <https://doi.org/https://doi.org/10.3390/ijms21041480>
- Kosová, K., Vítámvás, P., & Prášil, I. T. (2014, 2014-July-09). Wheat and barley dehydrins under cold, drought, and salinity – what can LEA-II proteins tell us about plant stress response? [Mini Review]. *Frontiers in Plant Science*, 5(343). <https://doi.org/https://doi.org/10.3389/fpls.2014.00343>
- Kudla, J., Batistič, O., & Hashimoto, K. (2010). Calcium signals: the lead currency of plant information processing. *The Plant Cell*, 22(3), 541-563. <https://doi.org/https://dx.doi.org/10.1105%2Ftpc.109.072686>
- Kuhn, S., Bussemer, J., Chigri, F., & Vothknecht, U. C. (2009). Calcium depletion and calmodulin inhibition affect the import of nuclear-encoded proteins into plant mitochondria. *The Plant Journal*, 58(4), 694-705. <https://doi.org/https://doi.org/10.1111/j.1365-313X.2009.03810.x>
- Laemmli, U. K. (1970). Cleavage of structural proteins during the assembly of the head of bacteriophage T4. *Nature*, 227(5259), 680-685. <https://doi.org/https://doi.org/10.1038/227680a0>
- Langmead, B., & Salzberg, S. L. (2012). Fast gapped-read alignment with Bowtie 2. *Nature Methods*, 9(4), 357. <https://doi.org/https://doi.org/10.1038/nmeth.1923>
- Lecourieux, D., Lamotte, O., Bourque, S., Wendehenne, D., Mazars, C., Ranjeva, R., & Pugin, A. (2005). Proteinaceous and oligosaccharidic elicitors induce different calcium signatures in the nucleus of tobacco cells. *Cell Calcium*, 38(6), 527-538. <https://doi.org/https://doi.org/10.1016/j.ceca.2005.06.036>
- Liang, F., & Sze, H. (1998). A high-affinity Ca²⁺ pump, ECA1, from the endoplasmic reticulum is inhibited by cyclopiazonic acid but not by thapsigargin. *Plant Physiology*, 118(3), 817-825. <https://doi.org/https://dx.doi.org/10.1104%2Fpp.118.3.817>

- Liao, Y., Smyth, G. K., & Shi, W. (2014). featureCounts: an efficient general purpose program for assigning sequence reads to genomic features. *Bioinformatics*, *30*(7), 923-930. <https://doi.org/https://doi.org/10.1093/bioinformatics/btt656>
- Liu, T., Qian, Y., Duan, W., Ren, J., Hou, X., & Li, Y. (2014). BcRISP1, isolated from non-heading Chinese cabbage, decreases the seed set of transgenic Arabidopsis. *Horticulture Research*, *1*(1), 1-8. <https://doi.org/https://dx.doi.org/10.1038%2Fhortres.2014.62>
- Logan, D. C., & Knight, M. R. (2003). Mitochondrial and cytosolic calcium dynamics are differentially regulated in plants. *Plant Physiology*, *133*(1), 21-24. <https://doi.org/https://doi.org/10.1104/pp.103.026047>
- Lokdarshi, A., Conner, W. C., McClintock, C., Li, T., & Roberts, D. M. (2016). Arabidopsis CML38, a calcium sensor that localizes to ribonucleoprotein complexes under hypoxia stress. *Plant Physiology*, *170*(2), 1046-1059. <https://doi.org/https://doi.org/10.1104/pp.15.01407>
- Loro, G., Drago, I., Pozzan, T., Schiavo, F. L., Zottini, M., & Costa, A. (2012). Targeting of Cameleons to various subcellular compartments reveals a strict cytoplasmic/mitochondrial Ca²⁺ handling relationship in plant cells. *The Plant Journal*, *71*(1), 1-13. <https://doi.org/https://doi.org/10.1111/j.1365-313x.2012.04968.x>
- Love, M. I., Huber, W., & Anders, S. (2014). Moderated estimation of fold change and dispersion for RNA-seq data with DESeq2. *Genome Biology*, *15*(12), 1-21. <https://doi.org/https://doi.org/10.1186/s13059-014-0550-8>
- Ma, L., Ye, J., Yang, Y., Lin, H., Yue, L., Luo, J., Long, Y., Fu, H., Liu, X., Zhang, Y., Wang, Y., Chen, L., Kudla, J., Wang, Y., Han, S., Song, C.-P., & Guo, Y. (2019, 2019/03/11/). The SOS2-SCaBP8 Complex Generates and Fine-Tunes an AtANN4-Dependent Calcium Signature under Salt Stress. *Developmental Cell*, *48*(5), 697-709.e695. <https://doi.org/https://doi.org/10.1016/j.devcel.2019.02.010>
- Magnan, F., Ranty, B., Charpentreau, M., Sotta, B., Galaud, J. P., & Aldon, D. (2008). Mutations in AtCML9, a calmodulin-like protein from Arabidopsis thaliana, alter plant responses to abiotic stress and abscisic acid. *The Plant Journal*, *56*(4), 575-589. <https://doi.org/https://doi.org/10.1111/j.1365-313x.2008.03622.x>
- Mangelsen, E., Kilian, J., Harter, K., Jansson, C., Wanke, D., & Sundberg, E. (2011). Transcriptome analysis of high-temperature stress in developing barley caryopses: early stress responses and effects on storage compound biosynthesis. *Molecular Plant*, *4*(1), 97-115. <https://doi.org/https://doi.org/10.1093/mp/ssq058>
- Manishankar, P., Wang, N., Köster, P., Alatar, A. A., & Kudla, J. (2018). Calcium signaling during salt stress and in the regulation of ion homeostasis. *Journal of Experimental Botany*, *69*(17), 4215-4226. <https://doi.org/https://doi.org/10.1093/jxb/ery201>
- Manzoor, H., Chiltz, A., Madani, S., Vatsa, P., Schoefs, B., Pugin, A., & Garcia-Brugger, A. (2012). Calcium signatures and signaling in cytosol and organelles of tobacco cells induced by plant defense elicitors. *Cell Calcium*, *51*(6), 434-444. <https://doi.org/https://doi.org/10.1016/j.ceca.2012.02.006>

- Marino, D., Dunand, C., Puppo, A., & Pauly, N. (2012). A burst of plant NADPH oxidases. *Trends in Plant Science*, *17*(1), 9-15. <https://doi.org/https://doi.org/10.1016/j.tplants.2011.10.001>
- McAinsh, M. R., Clayton, H., Mansfield, T. A., & Hetherington, A. M. (1996). Changes in stomatal behavior and guard cell cytosolic free calcium in response to oxidative stress. *Plant Physiology*, *111*(4), 1031-1042. <https://doi.org/https://doi.org/10.1104/pp.111.4.1031>
- McAinsh, M. R., & Hetherington, A. M. (1998). Encoding specificity in Ca²⁺ signalling systems. *Trends in Plant Science*, *3*(1), 32-36. [https://doi.org/https://doi.org/10.1016/S1360-1385\(97\)01150-3](https://doi.org/https://doi.org/10.1016/S1360-1385(97)01150-3)
- McCormack, E., & Braam, J. (2003). Calmodulins and related potential calcium sensors of Arabidopsis. *New Phytologist*, *159*(3), 585-598. <https://doi.org/https://doi.org/10.1046/j.1469-8137.2003.00845.x>
- McCormack, E., Tsai, Y.-C., & Braam, J. (2005). Handling calcium signaling: arabidopsis CaMs and CMLs. *Trends in Plant Science*, *10*(8), 383-389. <https://doi.org/https://doi.org/10.1016/j.tplants.2005.07.001>
- Mian, A., Oomen, R. J., Isayenkov, S., Sentenac, H., Maathuis, F. J., & Véry, A. A. (2011). Over-expression of an Na⁺-and K⁺-permeable HKT transporter in barley improves salt tolerance. *The Plant Journal*, *68*(3), 468-479. <https://doi.org/https://doi.org/10.1111/j.1365-313x.2011.04701.x>
- Miernyk, J. A., & Randall, D. D. (1987). Some properties of pea mitochondrial phospho-pyruvate dehydrogenase-phosphatase. *Plant Physiology*, *83*(2), 311-315. <https://doi.org/https://doi.org/10.1111/j.1365-313x.2011.04701.x>
- Miller, R. J., Dumford, S., Koeppe, D., & Hanson, J. (1970). Divalent cation stimulation of substrate oxidation by corn mitochondria. *Plant Physiology*, *45*(6), 649-653. <https://doi.org/https://dx.doi.org/10.1104%2Fpp.45.6.649>
- Møller, I. M. (2001). Plant mitochondria and oxidative stress: electron transport, NADPH turnover, and metabolism of reactive oxygen species. *Annual Review of Plant Biology*, *52*(1), 561-591. <https://doi.org/https://doi.org/10.1146/annurev.arplant.52.1.561>
- Munns, R., Gardner, P. A., Tonnet, M. L., & Rawson, H. (1988). Growth and development in NaCl-treated plants. II. Do Na⁺ or Cl⁻ concentrations in dividing or expanding tissues determine growth in barley? *Functional Plant Biology*, *15*(4), 529-540. <https://doi.org/https://doi.org/10.1071/PP9880529>
- Mwando, E., Angessa, T. T., Han, Y., & Li, C. (2020). Salinity tolerance in barley during germination—homologs and potential genes. *Journal of Zhejiang University-SCIENCE B*, *1*-29. <https://doi.org/https://dx.doi.org/10.1631%2Fjzus.B1900400>
- Nagy, B., Majer, P., Mihály, R., Dudits, D., & Horváth, G. (2011, 01/01). Transient and transgenic approaches for functional testing of candidate genes in barley. *Acta Biologica Szegediensis*, *55*.

- Nelissen, H., Gonzalez, N., & Inze, D. (2016). Leaf growth in dicots and monocots: so different yet so alike. *Current Opinion in Plant Biology*, 33, 72-76. <https://doi.org/https://doi.org/10.1016/j.pbi.2016.06.009>
- O'Neil, K. T., & DeGrado, W. F. (1990). How calmodulin binds its targets: sequence independent recognition of amphiphilic α -helices. *Trends in Biochemical Sciences*, 15(2), 59-64. [https://doi.org/https://doi.org/10.1016/0968-0004\(90\)90177-d](https://doi.org/https://doi.org/10.1016/0968-0004(90)90177-d)
- Oh, S. J., Kwon, C. W., Choi, D. W., Song, S. I., & Kim, J. K. (2007). Expression of barley HvCBF4 enhances tolerance to abiotic stress in transgenic rice. *Plant Biotechnology Journal*, 5(5), 646-656. <https://doi.org/https://doi.org/10.1111/j.1467-7652.2007.00272.x>
- Ordenes, V. R., Moreno, I., Maturana, D., Norambuena, L., Trewavas, A. J., & Orellana, A. (2012). In vivo analysis of the calcium signature in the plant Golgi apparatus reveals unique dynamics. *Cell Calcium*, 52(5), 397-404. <https://doi.org/https://doi.org/10.1016/j.ceca.2012.06.008>
- Ordenes, V. R., Reyes, F. C., Wolff, D., & Orellana, A. (2002). A thapsigargin-sensitive Ca^{2+} pump is present in the pea Golgi apparatus membrane. *Plant Physiology*, 129(4), 1820-1828. <https://doi.org/https://dx.doi.org/10.1104%2Fpp.002055>
- Parvin, N., Carrie, C., Pabst, I., Läufer, A., Laha, D., Paul, M. V., Geigenberger, P., Heermann, R., Jung, K., & Vothknecht, U. C. (2017). TOM9. 2 is a calmodulin-binding protein critical for TOM complex assembly but not for mitochondrial protein import in Arabidopsis thaliana. *Molecular Plant*, 10(4), 575-589. <https://doi.org/https://doi.org/10.1016/j.molp.2016.12.012>
- Pei, Z.-M., Murata, Y., Benning, G., Thomine, S., Klüsener, B., Allen, G. J., Grill, E., & Schroeder, J. I. (2000). Calcium channels activated by hydrogen peroxide mediate abscisic acid signalling in guard cells. *Nature*, 406(6797), 731-734. <https://doi.org/https://doi.org/10.1038/35021067>
- Pirayesh, N., Giridhar, M., Khedher, A. B., Vothknecht, U. C., & Chigri, F. (2021). Organellar Calcium Signaling in Plants: An Update. *Biochimica et Biophysica Acta (BBA)-Molecular Cell Research*, 118948. <https://doi.org/https://doi.org/10.1016/j.bbamcr.2021.118948>
- Price, A. H., Taylor, A., Ripley, S. J., Griffiths, A., Trewavas, A. J., & Knight, M. R. (1994). Oxidative signals in tobacco increase cytosolic calcium. *The Plant Cell*, 6(9), 1301-1310. <https://doi.org/https://doi.org/10.1105/tpc.6.9.1301>
- Prochazkova, D., Sairam, R., Srivastava, G., & Singh, D. (2001). Oxidative stress and antioxidant activity as the basis of senescence in maize leaves. *Plant Science*, 161(4), 765-771. [https://doi.org/https://doi.org/10.1016/S0168-9452\(01\)00462-9](https://doi.org/https://doi.org/10.1016/S0168-9452(01)00462-9)
- Raffaello, A., Mammucari, C., Gherardi, G., & Rizzuto, R. (2016). Calcium at the center of cell signaling: interplay between endoplasmic reticulum, mitochondria, and lysosomes. *Trends in Biochemical Sciences*, 41(12), 1035-1049. <https://doi.org/https://doi.org/10.1016/j.tibs.2016.09.001>
- Ranf, S., Wünnenberg, P., Lee, J., Becker, D., Dunkel, M., Hedrich, R., Scheel, D., & Dietrich, P. (2008). Loss of the vacuolar cation channel, AtTPC1, does not impair Ca^{2+} signals induced

- by abiotic and biotic stresses. *The Plant Journal*, 53(2), 287-299. <https://doi.org/https://doi.org/10.1111/j.1365-313x.2007.03342.x>
- Ranty, B., Aldon, D., & Galaud, J.-P. (2006). Plant calmodulins and calmodulin-related proteins: multifaceted relays to decode calcium signals. *Plant Signaling & Behavior*, 1(3), 96-104. <https://doi.org/https://doi.org/10.4161/psb.1.3.2998>
- Rentel, M. C., & Knight, M. R. (2004). Oxidative stress-induced calcium signaling in Arabidopsis. *Plant Physiology*, 135(3), 1471-1479.
- Roux, S. J., McEntire, K., Slocum, R. D., Cedel, T. E., & Hale, C. C. (1981). Phytochrome induces photoreversible calcium fluxes in a purified mitochondrial fraction from oats. *Proceedings of the National Academy of Sciences*, 78(1), 283-287. <https://doi.org/https://dx.doi.org/10.1073%2Fpnas.78.1.283>
- Rudd, J., & Franklin-Tong, V. (1999). Calcium signaling in plants. *Cellular and Molecular Life Sciences CMLS*, 55(2), 214-232. <https://doi.org/https://doi.org/10.1007/s000180050286>
- Schäfer, K., Künzler, P., Schneider, K., Klingl, A., Eubel, H., & Carrie, C. (2020). The plant mitochondrial TAT pathway is essential for complex III biogenesis. *Current Biology*, 30(5), 840-853. e845. <https://doi.org/https://doi.org/10.1016/j.cub.2020.01.001>
- Schmidt, R., Mieulet, D., Hubberten, H.-M., Obata, T., Hoefgen, R., Fernie, A. R., Fisahn, J., San Segundo, B., Guiderdoni, E., & Schippers, J. H. (2013). SALT-RESPONSIVE ERF1 regulates reactive oxygen species-dependent signaling during the initial response to salt stress in rice. *The Plant Cell*, 25(6), 2115-2131. <https://doi.org/https://doi.org/10.1105/tpc.113.113068>
- Schmöckel, S. M., Garcia, A. F., Berger, B., Tester, M., Webb, A. A. R., & Roy, S. J. (2015). Different NaCl-induced calcium signatures in the Arabidopsis thaliana ecotypes Col-0 and C24. *PLoS One*, 10(2), e0117564-e0117564. <https://doi.org/https://doi.org/10.1371/journal.pone.0117564>
- Schneider, D., & Schmidt, C. L. (2005). Multiple Rieske proteins in prokaryotes: where and why? *Biochimica et Biophysica Acta (BBA)-Bioenergetics*, 1710(1), 1-12. <https://doi.org/https://doi.org/10.1016/j.bbabi.2005.09.003>
- Scholz, S. S., Reichelt, M., Vadassery, J., & Mithöfer, A. (2015). Calmodulin-like protein CML37 is a positive regulator of ABA during drought stress in Arabidopsis. *Plant Signaling & Behavior*, 10(6), e1011951. <https://doi.org/https://dx.doi.org/10.1080%2F15592324.2015.1011951>
- Sello, S., Moscatiello, R., Mehlmer, N., Leonardelli, M., Carraretto, L., Cortese, E., Zanella, F. G., Baldan, B., Szabò, I., & Vothknecht, U. C. (2018). Chloroplast Ca²⁺ fluxes into and across thylakoids revealed by thylakoid-targeted aequorin probes. *Plant Physiology*, 177(1), 38-51. <https://doi.org/https://dx.doi.org/10.1080%2F15592324.2015.1011951>
- Serraj, R., & Sinclair, T. (2002). Osmolyte accumulation: can it really help increase crop yield under drought conditions? *Plant, Cell & Environment*, 25(2), 333-341. <https://doi.org/https://doi.org/10.1046/j.1365-3040.2002.00754.x>

- Shanker, A., & Venkateswarlu, B. (2011). *Abiotic stress in plants: mechanisms and adaptations*. BoD–Books on Demand. <https://doi.org/https://doi.org/10.5772/22248>
- Sharma, P., Jha, A. B., Dubey, R. S., & Pessarakli, M. (2012). Reactive oxygen species, oxidative damage, and antioxidative defense mechanism in plants under stressful conditions. *Journal of Botany*, 2012. <https://doi.org/https://doi.org/10.1155/2012/217037>
- Shimomura, O., Johnson, F. H., & Saiga, Y. (1963). Microdetermination of calcium by aequorin luminescence. *Science*, 140(3573), 1339-1340. <https://doi.org/https://doi.org/10.1126/science.140.3573.1339>
- Slater, E. C., & Cleland, K. (1953). The effect of calcium on the respiratory and phosphorylative activities of heart-muscle sarcosomes. *Biochemical Journal*, 55(4), 566. <https://doi.org/https://dx.doi.org/10.1042%2Fbj0550566>
- Snedden, W. A., & Fromm, H. (2001). Calmodulin as a versatile calcium signal transducer in plants. *New Phytologist*, 151(1), 35-66. <https://doi.org/https://doi.org/10.1046/j.1469-8137.2001.00154.x>
- Søgaard, B., & von Wettstein-Knowles, P. (1987). Barley: genes and chromosomes. *Carlsberg Research Communications*, 52(2), 123-196. <https://doi.org/https://doi.org/10.1007/BF02907531>
- Sorin, A., Rosas, G., & Rao, R. (1997). PMR1, a Ca²⁺-ATPase in yeast Golgi, has properties distinct from sarco/endoplasmic reticulum and plasma membrane calcium pumps. *Journal of Biological Chemistry*, 272(15), 9895-9901. <https://doi.org/https://doi.org/10.1074/jbc.272.15.9895>
- Stael, S., Wurzinger, B., Mair, A., Mehlmer, N., Vothknecht, U. C., & Teige, M. (2012). Plant organellar calcium signalling: an emerging field. *Journal of Experimental Botany*, 63(4), 1525-1542. <https://doi.org/https://doi.org/10.1093/jxb/err394>
- Svensson, J. T., Crosatti, C., Campoli, C., Bassi, R., Stanca, A. M., Close, T. J., & Cattivelli, L. (2006). Transcriptome analysis of cold acclimation in barley Albina and Xantha mutants. *Plant Physiology*, 141(1), 257-270. <https://doi.org/https://doi.org/10.1104/pp.105.072645>
- Takahashi, S., & Badger, M. R. (2011). Photoprotection in plants: a new light on photosystem II damage. *Trends in Plant Science*, 16(1), 53-60. <https://doi.org/https://doi.org/10.1016/j.tplants.2010.10.001>
- Teakle, N. L., & Tyerman, S. D. (2010). Mechanisms of Cl⁻ transport contributing to salt tolerance. *Plant, Cell & Environment*, 33(4), 566-589. <https://doi.org/https://doi.org/10.1111/j.1365-3040.2009.02060.x>
- Tombuloglu, G., Tombuloglu, H., Sakcali, M. S., & Unver, T. (2015). High-throughput transcriptome analysis of barley (*Hordeum vulgare*) exposed to excessive boron. *Gene*, 557(1), 71-81. <https://doi.org/https://doi.org/10.1016/j.gene.2014.12.012>
- Tracy, F. E., Gilliham, M., Dodd, A. N., Webb, A. A., & Tester, M. (2008). NaCl-induced changes in cytosolic free Ca²⁺ in *Arabidopsis thaliana* are heterogeneous and modified by external ionic composition. *Plant, Cell & Environment*, 31(8), 1063-1073. <https://doi.org/https://doi.org/10.1111/j.1365-3040.2008.01817.x>

- Treiman, M., Caspersen, C., & Christensen, S. B. (1998). A tool coming of age: thapsigargin as an inhibitor of sarco-endoplasmic reticulum Ca²⁺-ATPases. *Trends in Pharmacological Sciences*, 19(4), 131-135. [https://doi.org/https://doi.org/10.1016/S0165-6147\(98\)01184-5](https://doi.org/https://doi.org/10.1016/S0165-6147(98)01184-5)
- Trumpower, B., & Edwards, C. A. (1979). Purification of a reconstitutively active iron-sulfur protein (oxidation factor) from succinate. cytochrome c reductase complex of bovine heart mitochondria. *Journal of Biological Chemistry*, 254(17), 8697-8706. [https://doi.org/https://doi.org/10.1016/S0021-9258\(19\)86947-8](https://doi.org/https://doi.org/10.1016/S0021-9258(19)86947-8)
- Trumpower, B. L. (2013). Cytochrome bc1 Complex (Respiratory Chain Complex III). In W. J. Lennarz & M. D. Lane (Eds.), *Encyclopedia of Biological Chemistry (Second Edition)* (pp. 593-598). Academic Press. <https://doi.org/https://doi.org/10.1016/B978-0-12-378630-2.00164-X>
- Ueda, A., Kathiresan, A., Bennett, J., & Takabe, T. (2006). Comparative transcriptome analyses of barley and rice under salt stress. *Theoretical and Applied Genetics*, 112(7), 1286-1294. <https://doi.org/https://doi.org/10.1007/s00122-006-0231-4>
- wa Lwalaba, J. L., Zvobgo, G., Gai, Y., Issaka, J. H., Mwamba, T. M., Louis, L. T., Fu, L., Nazir, M. M., Kirika, B. A., & Tshibangu, A. K. (2021). Transcriptome analysis reveals the tolerant mechanisms to cobalt and copper in barley. *Ecotoxicology and Environmental Safety*, 209, 111761. <https://doi.org/https://doi.org/10.1016/j.ecoenv.2020.111761>
- Waypa, G. B., Marks, J. D., Guzy, R. D., Mungai, P. T., Schriewer, J. M., Dokic, D., Ball, M. K., & Schumacker, P. T. (2013). Superoxide generated at mitochondrial complex III triggers acute responses to hypoxia in the pulmonary circulation. *American Journal of Respiratory and Critical Care Medicine*, 187(4), 424-432. <https://doi.org/https://dx.doi.org/10.1164%2Fccm.201207-1294OC>
- Wiesemann, K., Groß, L. E., Sommer, M., Schleiff, E., & Sommer, M. S. (2013). Self-assembling GFP: A versatile tool for plant (membrane) protein analyses. In *Membrane Biogenesis* (pp. 131-144). Springer. https://doi.org/https://doi.org/10.1007/978-1-62703-487-6_9
- Wu, D., Shen, Q., Qiu, L., Han, Y., Ye, L., Jabeen, Z., Shu, Q., & Zhang, G. (2014). Identification of proteins associated with ion homeostasis and salt tolerance in barley. *Proteomics*, 14(11), 1381-1392. <https://doi.org/https://doi.org/10.1002/pmic.201300221>
- Xia, D., Yu, C.-A., Kim, H., Xia, J.-Z., Kachurin, A. M., Zhang, L., Yu, L., & Deisenhofer, J. (1997). Crystal structure of the cytochrome bc1 complex from bovine heart mitochondria. *Science*, 277(5322), 60-66. <https://doi.org/https://doi.org/10.1126/science.277.5322.60>
- Xiong, T.-C., Bourque, S., Lecourieux, D., Amelot, N., Grat, S., Brière, C., Mazars, C., Pugin, A., & Ranjeva, R. (2006). Calcium signaling in plant cell organelles delimited by a double membrane. *Biochimica et Biophysica Acta (BBA)-Molecular Cell Research*, 1763(11), 1209-1215. <https://doi.org/https://doi.org/10.1016/j.bbamcr.2006.09.024>
- Xiong, X., James, V. A., Zhang, H., & Altpeter, F. (2010). Constitutive expression of the barley HvWRKY38 transcription factor enhances drought tolerance in turf and forage grass (*Paspalum notatum* Flugge). *Molecular Breeding*, 25(3), 419-432. <https://doi.org/http://dx.doi.org/10.1007/s11032-009-9341-4>

- Xu, Z.-S., Ni, Z.-Y., Li, Z.-Y., Li, L.-C., Chen, M., Gao, D.-Y., Yu, X.-D., Liu, P., & Ma, Y.-Z. (2009). Isolation and functional characterization of HvDREB1—a gene encoding a dehydration-responsive element binding protein in *Hordeum vulgare*. *Journal of Plant Research*, 122(1), 121-130. <https://doi.org/https://doi.org/10.1007/s10265-008-0195-3>
- Zhang, G., Liu, Y., Ni, Y., Meng, Z., Lu, T., & Li, T. (2014). Exogenous calcium alleviates low night temperature stress on the photosynthetic apparatus of tomato leaves. *PLoS One*, 9(5), e97322. <https://doi.org/https://doi.org/10.1371/journal.pone.0097322>
- Zhang, J.-L., Flowers, T. J., & Wang, S.-M. (2010). Mechanisms of sodium uptake by roots of higher plants. *Plant and Soil*, 326(1), 45-60. <https://doi.org/https://doi.org/10.1007/s11104-009-0076-0>
- Zhang, Y., Wang, Y., Taylor, J. L., Jiang, Z., Zhang, S., Mei, F., Wu, Y., Wu, P., & Ni, J. (2015). Aequorin-based luminescence imaging reveals differential calcium signalling responses to salt and reactive oxygen species in rice roots. *Journal of Experimental Botany*, 66(9), 2535-2545. <https://doi.org/https://doi.org/10.1093/jxb/erv043>
- Zhang, Z., Huang, L., Shulmeister, V. M., Chi, Y.-I., Kim, K. K., Hung, L.-W., Crofts, A. R., Berry, E. A., & Kim, S.-H. (1998). Electron transfer by domain movement in cytochrome bc 1. *Nature*, 392(6677), 677-684. <https://doi.org/https://doi.org/10.1038/33612>
- Zhu, J., Fan, Y., Shabala, S., Li, C., Lv, C., Guo, B., Xu, R., & Zhou, M. (2020). Understanding mechanisms of salinity tolerance in barley by proteomic and biochemical analysis of near-isogenic lines. *International Journal of Molecular Sciences*, 21(4), 1516. <https://doi.org/https://doi.org/10.3390/ijms21041516>
- Zhu, J. K. (2007). Plant salt stress. *eLS*. <https://doi.org/https://doi.org/10.1002/9780470015902.a0001300.pub2>

Acknowledgment

Firstly, I would like to express my sincere gratitude to my supervisor Prof. Dr. Ute C. Vothknecht for her continuous support, motivation, and guidance throughout my Ph.D. research. Her immense knowledge and enthusiasm helped me at all time points of my academic life. The constant encouragement and advice she gave me to perform better in my oral and written presentations is something that has helped build my confidence level. It was a great privilege and honour to have worked and studied under her leadership.

Secondly, I would like to thank Dr. Fatima Chigri for her supervision, advice, and encouragement during my research period. I am deeply indebted to her for the excellent instructions she gave to carry out my experiments and research.

I express my sincere thanks to the Deutsche Forschungsgemeinschaft (DFG) for granting me the funding for my thesis, the Graduate school (GRK2064), and the IZMB for the valuable criticism, support, and assistance during my research work. Special thanks also go to Prof. Dr. Andreas Meyer whose guidance and feedback have helped me to form a comprehensive and objective critique in my thesis.

Next, I am grateful to my collaborators, Prof Dr. Edgar Peiter and Dr. Bastian Meier from the Department of Agricultural and Nutritional Sciences, located at the Martin Luther University Halle-Wittenberg for the fruitful discussions and practical help during my research. I would also like to thank the NGS Core Facility, the University of Bonn for providing the RNA-Seq service.

My special thanks go to my colleagues and friends, Niloufar Pirayesh and Sakil Mahmud. I was lucky to have worked with such loving, helpful, and knowledgeable colleagues whom I shall continue cherishing for the rest of my life. I would also like to extend my deepest gratitude to Sabarna Bhattacharyya for helping with the Bioinformatics work and to the technical assistants Claudia Heym and Ursula Metbach for their technical support. My thanks also go to the students I supervised during my thesis: Kathrin Pleßner, Sandro Sieger, and Annika Maria Niederberghaus.

Last but not least, I am truly blessed to have the constant support and love from my parents and my husband who has been extremely understanding and caring throughout my thesis. This thesis would not have been possible without them. I dedicate this work to my beloved Grandfather, Late Mr. VNS who encouraged and supported me from the beginning of my research.

Scientific Publications

Pirayesh, N., Giridhar, M., Khedher, A. B., Vothknecht, U. C., & Chigri, F. (2021). Organellar calcium signaling in plants: An update. *Biochimica et Biophysica Acta (BBA)-Molecular Cell Research*, 118948. <https://doi.org/10.1016/j.bbamcr.2021.118948>.

Giridhar, M., Meier, B., Imani, J., Chigri, F., Peiter, E., Vothknecht, U. (2021). Calcium signatures in barley in response to biotic and abiotic stresses (Manuscript preparation).

Giridhar, M., Bhattacharyya, S., Vothknecht, U., Chigri, F. (2021). Transcriptome analysis of barley in response to oxidative stress (Manuscript preparation).